12

INVESTIGATION OF LASER PROPULSION

P. K. Chapman
D. H. Douglas–Hamilton
D. A. Reilly

Avco Everett Research Laboratory, Inc.
Everett, MA. 02149

November 1977

Final Technical Report for Period 1 March 1976 to 15 November 1977
Volume I

Sponsored by

DEFENSE ADVANCED RESEARCH PROJECTS AGENCY
DARPA Order No. 3138

Monitored by

OFFICE OF NAVAL RESEARCH
DEPARTMENT OF THE NAVY
Arlington, VA. 22217

FOREWORD

Contract No.: N00014-76-C-0646

DARPA Order No.: 3138

Program Code No.: 6E20 and 7E20

Short Title of Work: Investigation of Laser Propulsion

Contractor: Avco Everett Research Laboratory, Inc.,
Everett, Massachusetts 02149

Principal Investigator: D. H. Douglas-Hamilton
(617) 389-3000, Ext. 568

Scientific Officer: Director, Physics Program
Physical Sciences Division
Office of Naval Research
800 North Quincy Street
Arlington, Virginia 22217

Effective Date of Contract: 1 March 1976

Contract Expiration Date: 15 November 1977

Amount of Contract: $580,000

UNCLASSIFIED

SECURITY CLASSIFICATION OF THIS PAGE (When Data Entered)

REPORT DOCUMENTATION PAGE	READ INSTRUCTIONS BEFORE COMPLETING FORM
1. REPORT NUMBER	2. GOVT ACCESSION NO. / 3. RECIPIENT'S CATALOG NUMBER
4. TITLE (and Subtitle): INVESTIGATION OF LASER PROPULSION. VOLUME I.	5. TYPE OF REPORT & PERIOD COVERED: Final Technical Report. 1 Mar [redacted]76 - 15 Nov [redacted]77 / 6. PERFORMING ORG. REPORT NUMBER
7. AUTHOR(s): P. K. Chapman, D. H. Douglas-Hamilton [redacted], D. A. Reilly	8. CONTRACT OR GRANT NUMBER(s): N00014-76-C-0646 new / DARPA Order-3138
9. PERFORMING ORGANIZATION NAME AND ADDRESS: Avco Everett Research Laboratory, Inc. 2385 Revere Beach Parkway Everett, Massachusetts 02149	10. PROGRAM ELEMENT, PROJECT, TASK AREA & WORK UNIT NUMBERS: 6E20 7E20
11. CONTROLLING OFFICE NAME AND ADDRESS: Defense Advanced Research Projects Agency DARPA Order No. 3138	12. REPORT DATE: Nov [redacted]77 / 13. NUMBER OF PAGES: 143 (144 p.)
14. MONITORING AGENCY NAME & ADDRESS (if different from Controlling Office): Office of Naval Research Department of the Navy Arlington, Virginia 22217	15. SECURITY CLASS. (of this report): Unclassified / 15a. DECLASSIFICATION/DOWNGRADING SCHEDULE

16. DISTRIBUTION STATEMENT (of this Report)

Approved for public release; distribution unlimited.

17. DISTRIBUTION STATEMENT (of the abstract entered in Block 20, if different from Report)

NH

18. SUPPLEMENTARY NOTES

19. KEY WORDS (Continue on reverse side if necessary and identify by block number)

Laser
Rocket Engine
Propulsion

20. ABSTRACT (Continue on reverse side if necessary and identify by block number)

The use of large ground based lasers to radiate power into a rocket engine allows arbitrary choice of propellant and specific impulse. The case of launch of one ton payload from near ground to geosynchronous transfer ellipse appears to be feasible using stacked carbon dioxide repetitive pulse lasers. Atmospheric propagation is enhanced by bleaching out CO_2 absorption and using phase correction of the thermal blooming generated, ~~we expect that~~ 1 microradian beam spreading can be achieved. The use of pulsed lasers permits an engine based on the laser detonation wave, in which laser energy

DD FORM 1 JAN 73 1473 EDITION OF 1 NOV 65 IS OBSOLETE

UNCLASSIFIED

SECURITY CLASSIFICATION OF THIS PAGE (When Data Entered)

048 450

20. Abstract (Continued)

is efficiently absorbed by inverse Bremsstrahlung in the propellant, which then expands out of the engine and provides thrust. Continuous use costs in the order of $20/lb to GEO are anticipated.

TABLE OF CONTENTS

VOLUME I

LIST OF ILLUSTRATIONS

VOLUME I

SECTION I

INTRODUCTION

The concept that spacecraft propulsion can be powered by means external to the spacecraft has long been an attractive but remote possibility. The use of solar radiation to provide the energy required is compromised by the low energy density of the radiation available at Earth orbit, thus requiring gigantic focussing mirrors which could not be transported through the atmosphere. Similarly, powering the spacecraft propulsion system by microwave radiation requires very large ground-based transmitters and correspondingly large receiving antennae on the spacecraft, with the same attendant difficulties. Such suggestions have generally been relegated to the genre of science fiction.

The advent of the high-power laser forced a re-evaluation of the externally powered propulsion system. The collimated laser beam virtually eliminates the requirement for large collectors, and the concept of stacking a number of moderate powered units in parallel allows one to achieve the power level of 1 GW required for launching from Earth to orbit.

This report covers analysis undertaken at Avco Everett Research Laboratory, Inc. of the problems associated with the laser propulsion concept. In Section II the trajectories of laser propelled rockets are discussed, and it is shown that the most promising application of this system is to launching rockets directly from Earth to geosynchronous orbit. A laser providing 10^9 W would be capable of launching a brennschluss weight of 1 ton to synchronous orbit. In Section III the concept and

properties of the pulsed laser detonation wave engine are discussed. This extremely important invention opens up the possibility of using pulsed lasers, with their attendant advantages in electrical efficiency and atmospheric beam propagation. Its relative insensitivity to beam-thrust angle is an important benefit, and the potential of using solid or liquid propellant greatly increases system flexibility. Although not strongly wavelength dependent, we have discussed the breakdown phenomena of this engine in the context of the CO_2 laser, our preferred embodiment. The laser facility and equipment required is discussed in Section IV, and potentially interesting CW engines in Section V. In Section VI the propagation of CO_2 laser radiation through the atmosphere and the rocket engine plume is analysed, and it is shown that using phase corrections, a 1 GW beam at $\lambda = 10.6\ \mu m$ is expected to propagate through the atmosphere essentially undistorted. The CO_2 laser is considered here since it is the least expensive high-power laser. Furthermore the bleaching of the CO_2 absorption component in the atmosphere is shown to be very significant for the pulsed CO_2 laser. Plume absorption in the high-altitude and mid-altitude cases turns out to be negligible for an H_2O plume; in the low altitude case its magnitude depends upon the disputed H_2O absorptance at elevated temperatures for 10.6 μm radiation. In Section VII the economic considerations giving promise to the laser propulsion concept are outlined.

SECTION II

POTENTIAL PERFORMANCE OF LASER-POWERED LAUNCH VEHICLES

1. BOOST TRAJECTORY ANALYSIS

A laser-powered launch vehicle presents a set of performance capabilities and constraints which are quite different to those familiar in chemical booster design. Because a laser-powered rocket engine (LPRE) is not limited by the relatively low enthalpies per unit mass of working fluid which are attainable in combustion, it may be possible to tailor the specific impulse to the mission under consideration. It may also be possible to vary the specific impulse during boost: in some engines, this may require only variation of the mass flow rate, and in some other cases it may even be possible to vary the specific impulse from the ground, by control of the output characteristics (pulse repetition frequency and energy per pulse) of the laser.

On the other hand, boost must be accomplished while the vehicle is within a range of the laser station which is determined by the laser beam-spread (due to diffraction and atmospheric effects) and the size of the collecting optics aboard the vehicle. Atmospheric absorption of the laser beam may also dictate that the boost trajectory be confined within a specified zenith angle, as seen from the laser station. Vehicle and engine design considerations may impose restrictions on the angle between the line of sight from the laser station (i. e., the laser beam) and the vehicle thrust axis, or on variations in this angle during boost. Finally, because the launching laser is a capital intensive system (see Section VII) in

which many of the costs are dependent on the laser output power, there is a strong motivation to choose both the trajectory and the design parameters of the vehicle so as to minimize the power required to meet a given mission objective with a payload of given mass.

At this early stage in the development of the laser launching system, the objectives of boost trajectory analysis are:

1) To update classical analyses of the satellite launching problems by incorporation of the new constraints.
2) To demonstrate the potential mission performance capabilities of a launching laser, on the assumption that efficient and economical engines can be developed.
3) To provide inputs to engine design studies, by specification of the power, mass flow rates, specific inpulse, angles between the laser beam and the thrust axis, etc., which are required to meet given mission objectives.
4) To determine the performance penalties associated with various constraints which may be imposed to simplify engine design.
5) To supply data needed for decisions concerning competing approaches to system design and to allow tradeoffs between capital and operational costs as a function of the launch traffic.

The missions to be discussed in this section are:

a) Vertical ascent to escape velocity. This case, being relatively simple, provides a good introduction to the power and range-limited boost problem. As will be seen, this trajectory may prove useful for some applications.

b) Injection to an escape hyperbola at minimum power.

c) Injection to a transfer ellipse to geosynchronous orbit (GSO).

Other possible missions for laser propulsion systems (e. g. , launch to low Earth orbit (LEO), orbit-to-orbit transfer, etc.) and mission-related issues (e. g. , techniques for circularization of a transfer ellipse at GSO, etc.) are discussed briefly here and will be considered in more detail in a future report. Direct ascent to GSO was given priority for study because (1) this orbital location is essential or highly desirable for many military and civilian applications, but present transportation costs are very high ($20,000/kg[1]); and (2) as compared with laser-powered launch to LEO, the specific impulse required is higher but it may be possible to maintain collinearity of the laser beam and the thrust axis of the vehicle. The mission thus lends itself to the design of a simple engine of high performance, providing suitable goals for laboratory demonstration in the present phase of engine development.

Since we are here concerned with broad performance objectives rather than with precision guidance, it is unnecessary as yet to carry out trajectory calculations in the most painstaking detail. Nevertheless, the question of trajectory optimization has been addressed for each of the above cases. Finding the optimal performance subject only to physical constraints is important not only in terms of the ultimate performance of the system, but because it provides a reference against which the costs of engineering constraints may be judged. Furthermore, optimization reduces the degrees of freedom in the general trajectory problem and may result in a simpler computation. When engineering constraints are added (e. g. , constant exhaust velocity), trajectory calculations often

involve two-point boundary value problems in which the differential equations can be integrated only by numerical means, leading to tedious and not necessarily convergent iterative computations. In such cases, it is very helpful to have available rough values of some parameters, obtained from previous analytic optimization calculations.

Unless otherwise indicated, in this section most quantities in the equations are normalized by using the units listed in Table 1. For future reference, the values of the units for the moon as well as the Earth are included in this table. The normalization procedure may in some cases prevent dimensional checks of the equations, but it avoids cluttering them with unnecessary symbols and provides an immediate indication of one relative significance of various terms.

TABLE 1. UNITS

Unit of	Name	Symbol	Value	
			Earth	Moon
distance	planetary radius	r_o	6378 km	1738 km
velocity	low orbit velocity	v_{co}	7.909 km/sec	1.67 km/sec
acceleration	surface gravity	g_o	9.806 m/sec^2	1.62 m/sec^2
time	schuler period/2π	$\sqrt{r_o/g_o}$	13^m 26.5^s	17^m 16^s
power/unit mass	———	$g_o v_{co}$	77.56 MW/ton	2.72 MW/ton
energy/unit mass	surface escape energy	$g_o r_o$		

2. BASIC RELATIONSHIPS

It is assumed that the LPRE exhaust is well matched to ambient pressure and that relatively little enthalpy is carried away from the vehicle by the exhaust stream. In this ideal case, the exhaust power is given by

$$P = -\frac{1}{2}\dot{m}c^2 \tag{1}$$

where $\dot{m}$ is the rate of change of mass of the vehicle (so $-\dot{m}$ is the mass flow rate through the engine) and c is the exhaust velocity.

The thrust produced is then

$$F = ma = -\dot{m}c = \frac{2P}{c} \tag{2}$$

where m is the instantaneous mass of the vehicle and a is the specific thrust (or "acceleration due to thrust").

The specific exhaust power (i.e., the exhaust power per unit burnout mass) is given by Eq. (2) as

$$\frac{P}{m_1} = \frac{1}{2} a_1 c_1 \tag{3}$$

where m_1, and a_1 and c_1 are the vehicle mass, the specific thrust and the exhaust velocity just before burnout. An alternative expression may be obtained by eliminating c in Eqs. (1) and (2) which gives

$$2\dot{m}P = -m^2 a^2 \tag{4}$$

or

$$\frac{d}{dt}\left(\frac{P}{m}\right) = \frac{1}{2} a^2 \tag{5}$$

Integration gives

$$\frac{P}{m_1} = \frac{1}{2} \frac{R}{R-1} \int_0^\tau a^2 dt \tag{6}$$

where τ is the duration of boost and

$$R = m_o/m_1 \tag{7}$$

is the mass ratio, with m_o the initial vehicle mass.

3. RECTILINEAR BOOST IN FREE SPACE

The specific exhaust energy (i.e., the total energy exhausted during boost, divided by the burnout mass) is given simply by

$$E/m_1 = \frac{P}{M_1}\ \tau \tag{8}$$

In designing a laser launcher, a suitable compromise must be found between:

a) The power needed to boost a given payload to the desired mission velocity. In the early stages of buildup of a launching laser facility, minimizing the specific power will allow the smallest possible laser to be used to launch a given payload, and hence will minimize the initial capital costs. As the facility grows, operation at minimum specific power maximizes the payload which the laser can launch in a single throw; this may become particularly important if propagation effects limit the ultimate laser power which can be transmitted through the atmosphere.

b) The specific impulse required of the engine. In general, minimizing the exhaust velocity reduces the enthalpy per unit mass in the thrust chamber and exhaust stream, which will normally simplify engine design, especially with respect to heat transfer problems.

c) The mass ratio of the vehicle. For probable propellants, the fuel cost is likely to be a small component of overall launch costs (cf Section VIII) but it is nonetheless desirable to minimize the fuel load because this reduces the structural sophistication and hence the cost of the vehicle itself. When gravity losses are taken into account, the required mass ratio is trajectory-dependent and hence is not uniquely fixed by the choice of exhaust velocity.

d) The energy consumed during boost. The direct energy costs are expected to be quite significant in high throughput operations (cf Section VIII). Moreover, the maximum rate at which mass can be injected into the desired orbit is clearly m_1/τ, so that the maximum throughput of a given laser may be increased by minimizing the quantity of Eq. (8). This performance criterion will become important only if and when the traffic builds to a level which taxes the annual capacity of the launching laser, and it is, therefore, given a lower priority in most of our present analyses.

The simplest case which can be considered is rectilinear boost from rest to a velocity v_1 in a distance y_1 in field-free space, with constant exhaust velocity. The acceleration is then

$$\dot{v} = a = - \frac{\dot{m}}{m} c = \frac{2P}{mc} \tag{9}$$

which gives the rocket equation

$$m = m_o e^{v/c} \tag{10}$$

In particular, the mass ratio required for boost is

$$R = m_o/m_1 = e^{v_1/c} \tag{11}$$

For this case, the specific exhaust power is found most readily by direct integration of the equation of motion, using Eq. (10):

$$\int_o^v e^{-v/c}\, v dv = c^2 \left[1 - (1 + \frac{v_1}{c}) e^{-v_1/c}\right] = \frac{2P}{m_o c}\, y_1 \tag{12}$$

With Eq. (10), the specific exhaust power is then

$$\begin{aligned} \frac{P}{m_1} &= \frac{1}{2}\, \frac{c^3}{y_1} (e^{v_1/c} - v_1/c - v_1/c - 1) \\ &= \frac{1}{2}\, \frac{v^3 1}{y_1}\, \frac{(R - \ln R - 1)}{\ln^3 R} \end{aligned} \tag{13}$$

The specific power, normalized by dividing by $(1/2\, v_1^3/y_1)$, is shown as a function of the mass ration R in Figure 1. (In the curve labelled "negligible tank mass".)

The burnout mass may be written

$$m_1 = m_t\, m_2 \tag{14}$$

where m_t is the mass of the propellant tanks and m_2 the mass of payload plus engines, pumps, and other vehicle structure; these masses are lumped together for this preliminary analysis because their relative magnitudes differ markedly for the different types of LPRE to be discussed in later sections.

For pump-fed engines (i.e., tanks at relatively low pressure), the tankage mass may be approximated by a semi-empirical formula

$$m_t = A_t\, m_p/\rho_p^{2/3} \tag{15}$$

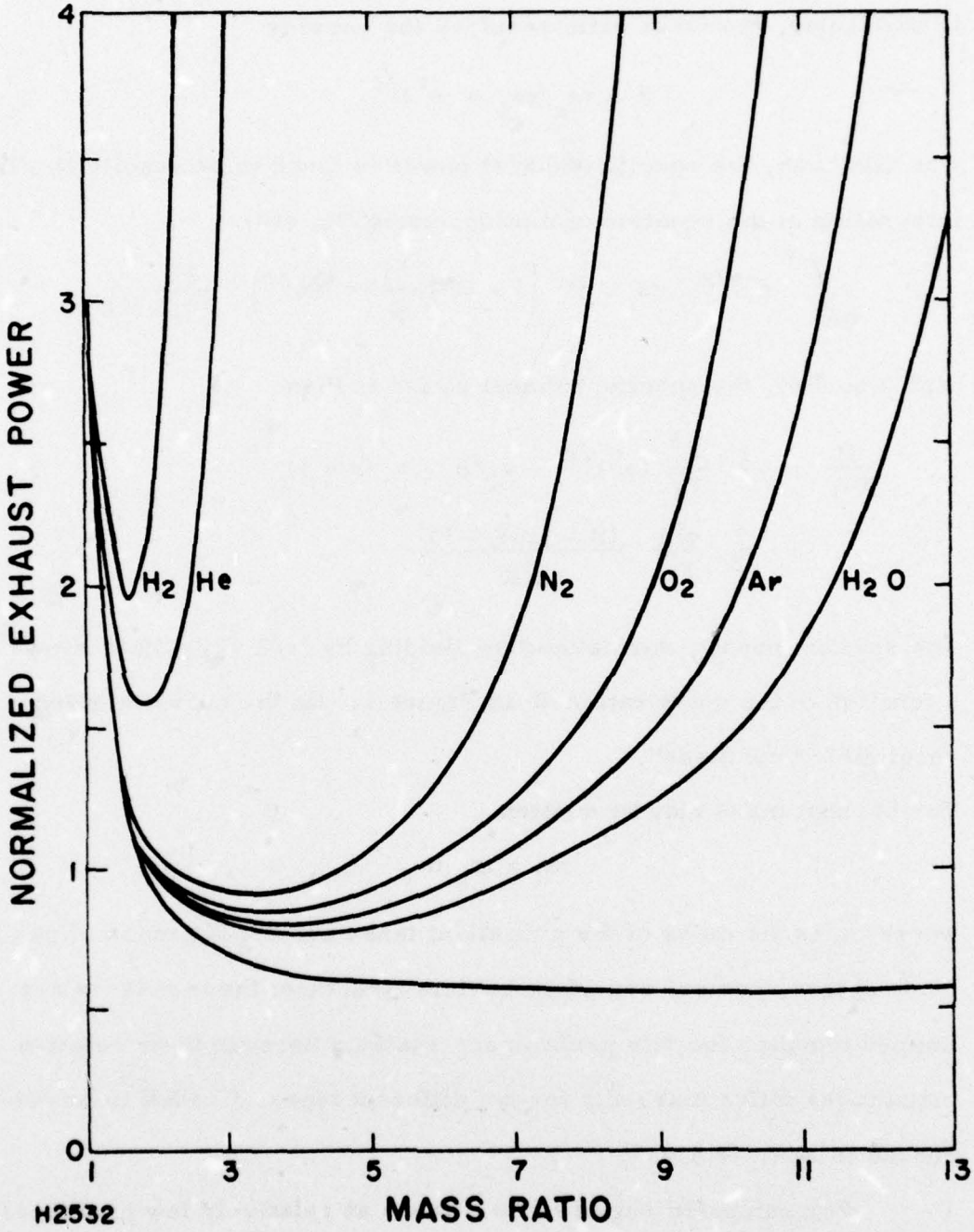

Figure 1 Boost Power Requirements with Different Propellants

where ρ_p is the density of the propellant in the tank

m_p is the mass of propellant

A_t is a numerical factor determined by the tank material and tank pressure. A typical value for balloon tank is $7\ (kg/m^3)^{2/3}$

The propellant mass is

$$m_p = m_o - m_1 = (R - 1)m_1 \tag{16}$$

Thus,

$$m_1 = m_2 / (1 - A_t(R - 1)/\rho_p^{2/3} \tag{17}$$

and, from Eq. (13),

$$\frac{P}{m_2} = \frac{1}{2} \frac{v^3}{y_1} \frac{(R - \ln R - 1)}{\ln^3 R \left(1 - A_t(R - 1)/\rho_p^{2/3}\right)} \tag{18}$$

The mass ratio dependence of this equation is also shown in Figure 1, for the propellants listed in Table 2. For the cryogenic liquids, the value $A_t \simeq 10\ (kg/m^3)^{2/3}$ has been used, to allow for required insulation.

TABLE 2. CANDIDATE PROPELLANTS

Propellant	Density in Liquid Phase (kg/m^3)	Boiling Point (^oK)
hydrogen	70	20.7
helium	122	4.6
nitrogen	808	77.4
water	1000	373.0
oxygen	1140	90.2
argon	1402	87.5

While the details of these curves depend on the techniques used for tank fabrication, it is clearly desirable to use a propellant which has a high density in the liquid phase. As discussed in Section VIII, the launch costs for this system are sufficiently low so that construction costs for the propellant tanks can be significant, and this may require the use of relatively unsophisticated and heavy materials and designs.

In order to minimize the exhaust power (and hence the laser output power) which is required for a given mission, it appears that mass ratios in the range 2.5 to perhaps 7 (depending on the propellant) should be used. In field-free space, the corresponding exhaust velocities range from about the mission velocity down to about half that value*.

The energy consumed during boost may be calculated simply from Eq. (8). For constant exhaust velocity and constant power the mass flow rate is

$$-\dot{m} = \frac{2P}{c^2} = \text{constant} \tag{19}$$

from Eq. (1), so the mass of the vehicle at time t is

$$m = m_o - \frac{2P}{c^2} t \tag{20}$$

In particular, the duration of boost is

$$\tau = \frac{c^2}{2P} (m_o - m_1) = \frac{1}{2} (R - 1)c^2 \frac{m_1}{P} \equiv \frac{1}{2} v^2 \frac{(R-1}{\ln^2 R} \frac{m_1}{P} \tag{21}$$

from Eq. (11). Thus, from Eq. (8),

$$\frac{E}{m_1} = \frac{1}{2} v^2 \frac{(R-1)}{\ln^2 R} \tag{22}$$

*These figures will require modification when gravity losses are taken into account, in the following sections.

The effect of propellant tankage may be taken into account by replacing m_1 by m_2 from Eq. (17), as in the power calculation above, to obtain

$$\frac{E}{m_2} \equiv \frac{1}{2} v^2 \frac{R - 1}{\ln^2 R} \left(1 - A_t (R - 1) \rho_\rho^{2/3}\right) \tag{23}$$

This expression, normalized by dividing by the kinetic energy $1/2\ v^2$ per unit mass m_2, is plotted in Figure 2 for the candidate propellants of Table 2. Comparison with Figure 1 shows that maximizing energy efficiency requires generally lower mass ratios than does minimizing power requirements. A good compromise is a mass ratio near 3.

The implications of these results for engine design are considered in Section III.

4. VERTICAL ASCENT TO ESCAPE

The problem to be considered here is that of vertical, rectilinear boost from rest at the laser station to escape velocity at an altitude y_1 above the planetary surface. Aerodynamic effects and planetary rotation are neglected.

Vertical ascent is not the power-optimal trajectory for escape missions (and certainly not for insertion into lower orbits). It is however, the only trajectory in which it is possible for both the beam/thrust angle to be zero and the laser beam stationary. If slewing of the beam is not required to avoid atmospheric thermal blooming (cf Section VI), these characteristics of the vertical trajectory may allow simplifications in the engine design and in the laser pointing and tracking systems which, in terms of costs, offset the slightly higher laser power level requirements. One long-range application in which these trajectory may be of

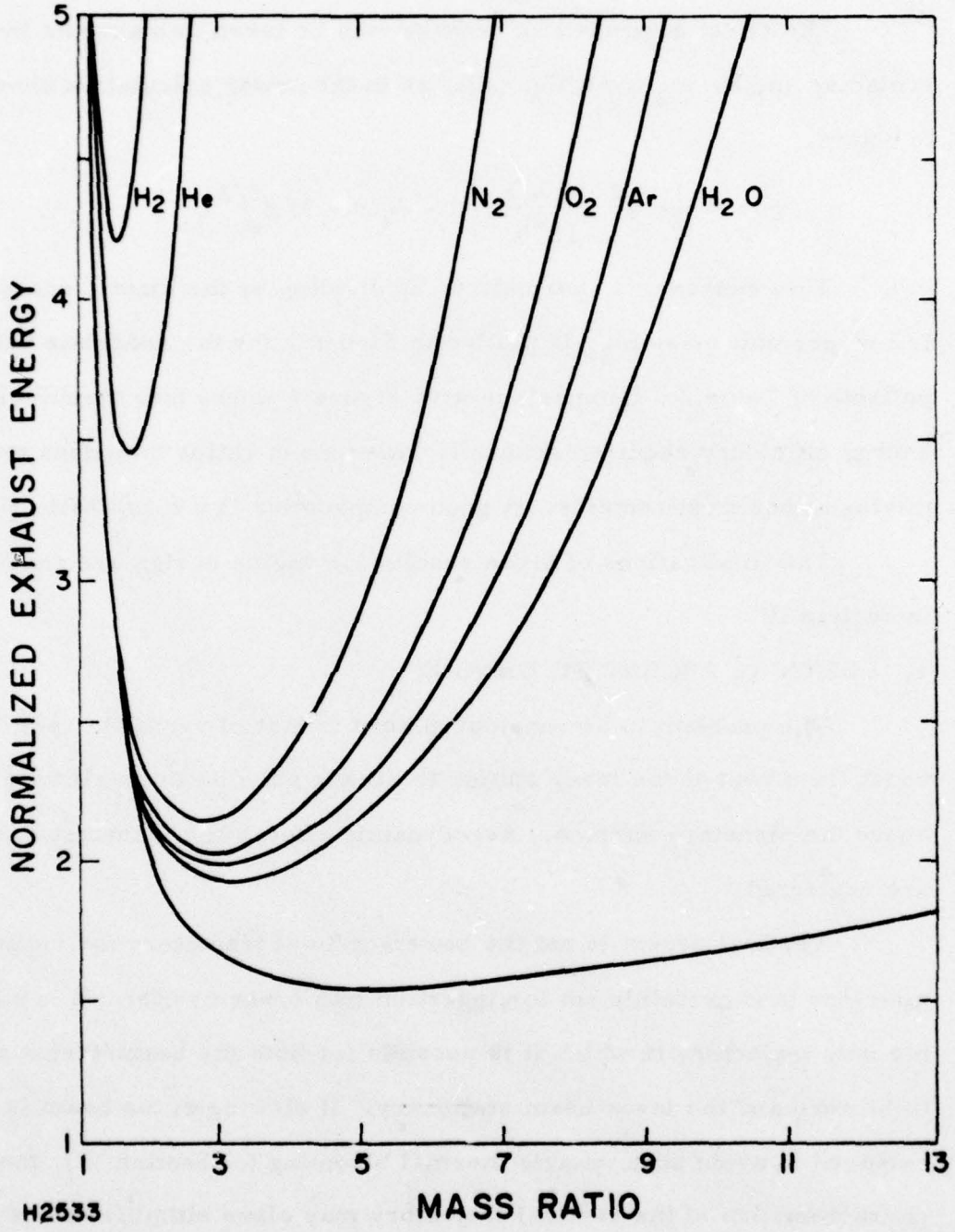

Figure 2 Boost Energy Requirements

interest is the use of a laser station on the moon to provide power for routine traffic to and from the laser surface, allowing economical exploitation of lunar resources when space industrialization is well under way.

In any case, the vertical trajectory is the simplest case in which it is possible to take realistic account of gravity losses during ascent. Some useful conclusions can be drawn and the analysis provides an introduction to the techniques needed in discussing trajectories which may have broader operational utility.

a. Power-Optimal Vertical Ascent

We first consider how the thrust of the LPRE should be varied so as to minimize the peak exhaust power required to boost a given payload m_1 to escape velocity at an altitude y_1. It should be clear that boost should be at constant power if peak power is to be minimized, and this condition will be assumed without further discussion (it can, of course, be demonstrated rigorously).

This problem can be solved by elementary techniques of the calculus of variations. However, having in mind more complicated trajectories which will be considered in later sections, optimal vertical ascent will be set up formally as a problem of Mayer in variational calculus. For convenience in following the argument, a slightly simplified general formulation of the problem of Mayer and of the technique for solution is set forth in Derivation Summary 1.

The equations of motion for vertical ascent and the power condition (Eq. (4)) are written as first order differential constraints:

$$\phi_1 = \dot{y} - v = 0 \tag{24a}$$

$$\phi_2 = \dot{v} - g - a = 0 \tag{24b}$$

$$\phi_3 = \dot{m} + \frac{m^2 a^2}{2P} = 0 \tag{24c}$$

where, in the units of Table 1, the gravitational field is

$$g = -1/(1 + y)^2 \tag{25}$$

The initial conditions are

$$\begin{aligned} t = 0; \quad & y = 0 \\ & v = 0 \end{aligned} \tag{26}$$

DERIVATION SUMMARY 1: THE PROBLEM OF MAYER

Consider the class of functions

$$Z_k(t) \qquad k = 1, \ldots\ldots, n$$

satisfying the constraints

$$\phi_j(t, Z_k, Z,) = 0 \quad j = 1, \ldots\ldots, p < n$$

which allow $f \equiv n\text{-}p$ degrees of freedom. Assuming that these functions must be consistent with the initial conditions*

$$\omega_r(o, Z_k) = 0 \quad r = 1, \ldots\ldots, q \tag{27}$$

and the terminal conditions

$$\omega_r(\tau, Z_{k1}) = 0 \quad r = q + 1, \ldots\ldots, s \leq 2n + 2 \tag{28}$$

find that special set which minimizes the pay-off function

$$\psi = \left[G(t, Z_k)\right]\Big|_0^I \tag{29}$$

*The subscripts 0 and 1 refer to initial and terminal points, respectively.

To solve this problem introduce a set of variable Lagrange multipliers $\lambda_j(t)$ and form the augmented function

$$F = \sum_{j=1}^{P} \lambda_j \phi_j \tag{30}$$

The extremal arc (i.e., the curve in Z_k - space which gives an extremal value to ψ) must satisfy, not only the constraints (28), but also the Euler-Lagrange equations

$$\frac{d}{dt}\left(\frac{\partial F}{\partial \dot{Z}_k}\right) = \frac{\partial F}{\partial Z_k} \quad k = 1, \ldots\ldots, n \tag{31}$$

Equations (28) and (31) constitute n + p equations, allowing (in principle) the simultaneous determination of the n dependent variables Z_k and the p Lagrange multipliers λ_j.

If the augmented function F is formally independent of t, a first integral of the Euler-Lagrange equations is available

$$C = \sum_{k=1}^{n} \frac{\partial F}{\partial \dot{Z}_k} \dot{Z}_k = \text{constant} \tag{32}$$

The system of Eqs. (28) and (31) are subjected to 2n + 2 boundary conditions, of which s are supplied by Eqs. (27) and (28) and 2n + 2 - s by the transversality condition, which (for F formally independent of t) reads

$$\left[dG - Cdt + \sum_{k=1}^{n} \frac{\partial F}{\partial \dot{Z}_k} dZ_k\right]\Bigg|_0^1 \equiv 0 \tag{33}$$

This condition at the initial and terminal points is to be satisfied identically for all infinitesimal displacements which are consistent with Eqs. (27) and (28).

It sometimes happens that the solution to this variational problem involves points along the extremal arc (called corners) where some of the $\dot{Z}_k$ exhibit jump discontinuities. In such cases, the extremal arc may be pieced together from the segments between corners (called subarcs) by making use of the Erdman-Weierstrass corner conditions, which state that the first integral C should have a constant value throughout the extremal arc and that

$$\frac{\partial F}{\partial \dot{Z}_k} \qquad k = 1, \ldots\ldots, n \tag{34}$$

should be continuous across each corner.

The escape velocity at the specified burnout altitude y_1 (see Appendix A) gives the terminal conditions

$$\begin{aligned} y &= y_1 \\ v &= v_1 = \sqrt{\frac{2}{1 + y_1}} \end{aligned} \tag{35}$$

The variational problem may now be formally stated as follows: Among t the four functions y(t), v(t), a(t) and m(t) which are consistant with the three constraints (24) and with the boundary conditions (26) and (35), find the set which minimizes

$$\Delta G = G_1 - G_o \tag{36}$$

where

$$G = P/M \tag{37}$$

so

$$\Delta G = \frac{P}{m_1} - \frac{P}{m_o} = \frac{P}{m_1}\left(\frac{R - 1}{R}\right) \tag{38}$$

For a given mass ration, minimizing G is thus equivalent to minimizing the specific exhaust power. Comparison with (6) shows that

$$\Delta G = \frac{1}{2} \int_o^\tau a^2 dt \tag{39}$$

We introduce Lagrange multipliers λ_1, λ_2, λ_3, and set up the augmented function

$$F = \lambda_1 (\dot{y} - v) + \lambda_2 (\dot{v} - g - a) + \lambda_3 \left(\dot{m} + \frac{1}{2} \frac{m^2 a^2}{P} \right) \tag{40}$$

and derive, according to (31), the Euler-Lagrange equations

$$\dot{\lambda}_1 = -\lambda_2 \frac{dg}{dy} \tag{41a}$$

$$\dot{\lambda}_2 = -\lambda_1 \tag{41b}$$

$$\dot{\lambda}_3 = \lambda_3 \frac{m^2 a}{P} \tag{41c}$$

$$o = -\lambda_2 + \lambda_3 \frac{m^2 a}{P} \tag{41d}$$

Since (40) is formally independent of time, a first integral of these equations is given by the formula (39):

$$C = \lambda_1 v + \lambda_2 \dot{v} - \frac{1}{2} \lambda_3 \frac{m^2 a^2}{P} = \text{constant} \tag{42}$$

The transversality condition (33) reads

$$\left[-\frac{P}{m^2} dm - C dt + \lambda_1 dy + \lambda_2 dv + \lambda_3 dm \right] \Bigg|_o^1 = o \tag{43}$$

Since y and v at the initial and terminal points are fixed, this reduces to

$$\left[\left(\lambda_3 - \frac{P}{m^2} \right) dm - C dt \right] \Bigg|_o^1 = o \tag{44}$$

which implies

$$C = 0 \tag{45}$$

$$\lambda_3 = \frac{P}{m^2} \quad \text{at } t = \tau \text{ and } t = o \tag{46}$$

Using Eq. (24c) in Eq. (41c) gives

$$\frac{\dot{\lambda}_3}{\lambda_3} = - \frac{2\dot{m}}{m} \tag{47}$$

whose solution, meeting the boundary condition (46), is

$$\lambda_3 = \frac{P}{m^2} \tag{48}$$

with this result, (41d) gives

$$\lambda_2 = a \tag{49}$$

and (41b) and (41a) then gives

$$\ddot{a} - \ddot{\lambda}_2 = - \dot{\lambda}_1 = \lambda_2 \frac{dy}{dy} = a \frac{dg}{dy} \tag{50}$$

The first integral (42) now yields

$$a\dot{v} - \dot{a}v = \frac{1}{2} a^2 \tag{51}$$

At $t = o$, for $v = o$, gives

$$\dot{v}_o = \frac{1}{2} a_o \tag{52}$$

and the equation of motion (24b) reads

$$\frac{1}{2} a_o - g_o - a_o = 0$$

or

$$a_o = - 2g_o = 2 \tag{53}$$

The vehicle thus departs with an initial upward acceleration v_o which is equal in magnitude to the local acceleration of gravity.

Equation (51) may be integrated again, by writing it in the form

$$\frac{1}{a^2}\,(a\dot{v} - \dot{a}v) = \frac{d}{dt}\left(\frac{v}{a}\right) = \frac{1}{2} \tag{54}$$

with solution, meeting the initial condition $v_o = o$,

$$\dot{v} = \frac{1}{2}\,at \tag{55}$$

The equation of motion (24b) may now be written

$$\dot{v} - \frac{2v}{t} = g \tag{56}$$

or

$$\frac{d}{dt}\left(\frac{v}{t^2}\right) = \frac{g}{t^2} \tag{57}$$

Numerical integration of this equation is inconvenient, because (as may be seen from (53) and (55)) v/t^2 is infinite at the origin. We, therefore, introduce a new variable q in place of a, by the relation

$$a = 2(1 + qt) \tag{58}$$

which automatically gives the correct initiated value (53). Equation (55) then becomes

$$\dot{y} = v = \frac{1}{2}\,at = t + qt^2 \tag{59}$$

and the equation of motion yields

$$\begin{aligned} \dot{v} - a &= 1 + 2qt \quad \dot{q}t^2 - 2 - 2qt \\ &= \dot{q}t^2 - 1 = g \end{aligned} \tag{60}$$

The equations to be integrated are now

$$\dot{q} = (1 + g)/t^2 \tag{61a}$$

$$y = t + qt^2 \tag{61b}$$

with the initial conditions $y = \dot{y} = o$ at $t = o$. The initial value chosen for q will set the altitude at which escape velocity is reached.

1) Constant Gravitational Field

If the gravitational field may be taken as constant

$$g = g_o = -1 \tag{62}$$

the (61a) shows q is constant and

$$\dot{y} = t \quad q_o t^2 \tag{63}$$

with solution

$$y = \frac{1}{2} t^2 + \frac{1}{3} q_o t^3 \tag{64}$$

At the burnout time τ, we require, from (35) and (63)

$$v_1 = \sqrt{\frac{2}{1 + y}} = \tau + q_o \tau^2 \tag{65}$$

so that

$$q_o = (v_1 - \tau)/\tau^2 \tag{66}$$

substituting this in (64) gives

$$\frac{1}{6} \tau^2 + \frac{1}{3} \tau \sqrt{\frac{2}{1 + y_1}} - y_1 = 0 \tag{67}$$

which may be solved to give the duration of boost as a function of the range at burnout.

The specific exhaust power is given for this case by (6) and (58) as

$$\frac{P}{m_1} = \frac{1}{2} \frac{R}{R-1} \int_o^\tau a^2 dt$$

$$= \frac{2R}{R-1} \int_0^{\tau} (1 + q_o t)^2 \, dt$$

$$= \frac{2}{3} \frac{R}{R-1} \frac{1}{q_o} \left[(1 + q_o \tau)^3 - 1 \right]$$

$$= \frac{2}{3} \frac{R}{R-1} \frac{\tau^2}{v_1 - \tau} \left(\left(\frac{v_1}{\tau} \right) - 1 \right) \qquad (68)$$

$$= \frac{2}{3} \frac{R}{R-1} \frac{1}{\tau} \left(\frac{v_1^3 - \tau^3}{v_1 - \tau} \right)$$

$$= \frac{2}{3} \frac{R}{R-1} \frac{1}{\tau} (v_1^2 + v_{1\tau} + \tau^2)$$

The results are shown in Figure 3, for R = 3.

2) Linear g

As a next approximation, we retain the linear term in a Taylor expansion of the gravitational field (25) about the origin

$$g = -1 + 2y + \ldots \qquad (69)$$

This case may also be handled without numerical integration. The Eq. (50) for the optimum specific thrust program reads

$$\ddot{a} - 2a = 0 \qquad (70)$$

with the solution, satisfying the initial condition (53),

$$a = 2 \cos h \sqrt{2}t + B \sin h \sqrt{2}t \qquad (71)$$

where b is a constant, to be determined. The equation of motion may now be written

$$\ddot{y} = g + a$$

$$= -1 + 2y + 2 \cos h \sqrt{2}t + B \sin h \sqrt{2}t$$

or

$$\ddot{y} - 2y = -1 + 2 \cos h \sqrt{2}t + B \sin h \sqrt{2}t \qquad (72)$$

with the solution, meeting the initial conditions

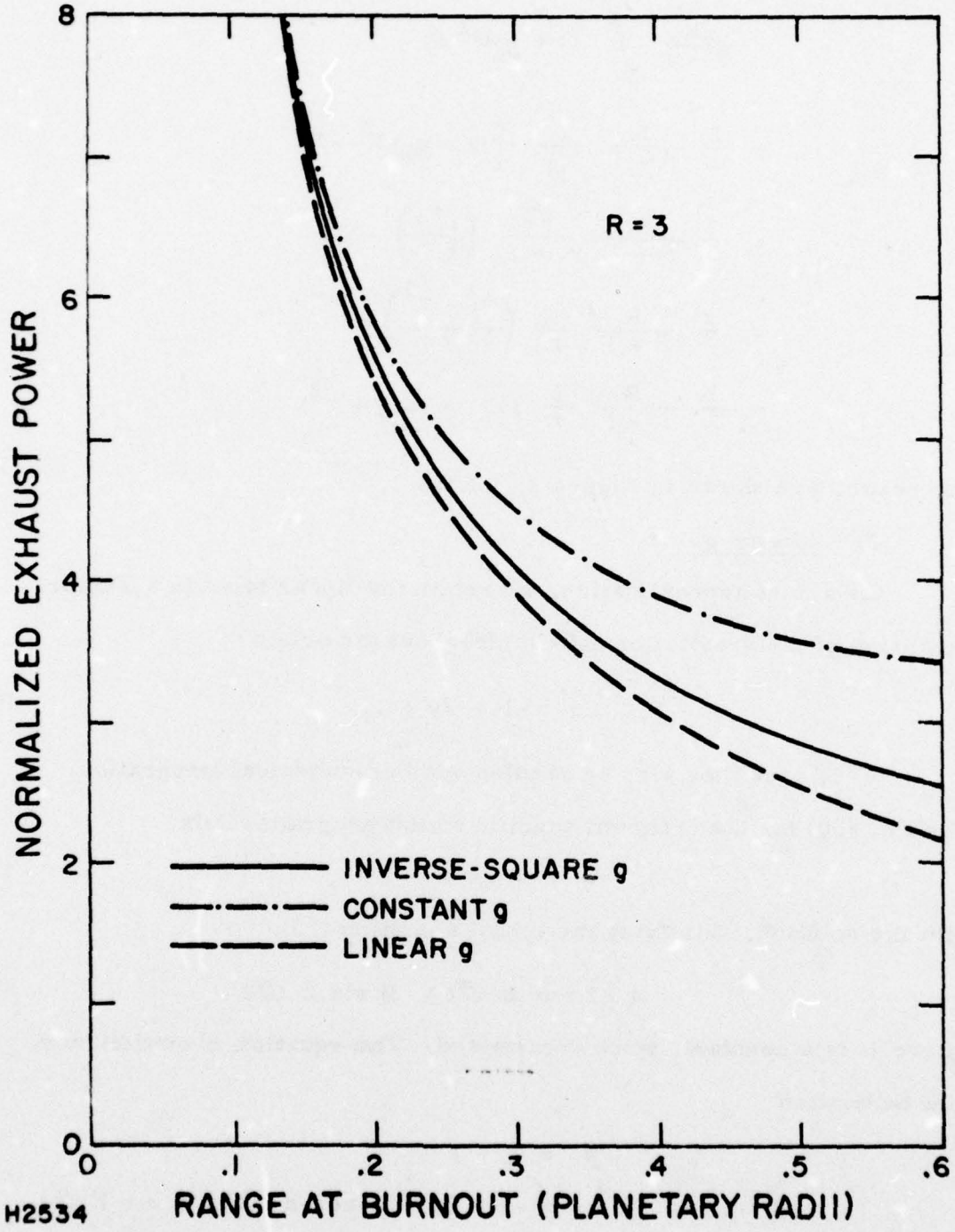

Figure 3 Power Required for Optimal Vertical Ascent to Escape

$$y = \frac{1}{2}(1 - \cos h\ \sqrt{2}\,t) + \frac{1}{\sqrt{2}}\,t\ \sin \sqrt{2}t - \frac{1}{4}B(\sin h\sqrt{2}\,t - \cos h\ \sqrt{2}\,t) \tag{73}$$

The velocity is given by (55) or by differentiation of (2.71) as

$$\dot{y} = t \cos h\ \ \sqrt{2}\,t + \frac{1}{2}B\,t \sin h\ \sqrt{2}\,t \tag{74}$$

Eliminating B from these equations at $t = \tau$ gives

$$y_1 = \frac{1}{2}(1 - \cos h\ \sqrt{2}\tau) + \frac{1}{\sqrt{2}}\tau \sin h\sqrt{2}\tau - \frac{1}{2}$$

$$\frac{(\sin h\ \sqrt{2}\tau - \sqrt{2}\tau\ \cos h\sqrt{2}\tau)\,(v_1 - \tau \cos h\sqrt{2}\tau}{\tau \sin h\ \sqrt{2}\tau}$$

$$= \frac{1}{2 \sin h\ \sqrt{2}\tau}\ \left[\sin h\ \sqrt{2}\tau - \sqrt{2}\tau - v_1\left(\frac{1}{\tau}\ \sin h\sqrt{2}\tau\right.\right. \tag{75}$$

$$\left.\left. - \sqrt{2} \cos h\ \sqrt{2}\tau\right)\right]$$

where $v_1 = \sqrt{\frac{2}{1\ y_1}}$. This equation may be solved numerically to give the boost duration as a function of the range at burnout. We also have

$$B = \frac{2(v_1 - \tau \cos h\sqrt{2}\tau)}{\tau \sin h\sqrt{2}\tau} \tag{76}$$

The specific exhaust power is now obtained from (71)

$$P/m_1 = \frac{1}{2}\ \frac{R}{R-1} \int_0^\tau a^2 dt = \frac{1}{2}\ \frac{R}{R-1} \int_0^\tau [4 \cos h^2 \sqrt{2}\tau$$

$$+ 2B \sin h\ 2\ \sqrt{2}\tau + B^2 \sin h^2\ \sqrt{2}\tau]\ dt \tag{77}$$

$$= \frac{1}{2\sqrt{2}}\ \frac{R}{R-1}\ [\sin h\ 2\sqrt{2}\tau + 2\sqrt{2}\tau + B\ (\cos h\ 2\sqrt{2}\tau - 1)$$

$$+ \frac{1}{4}\ B^2\ (\sin h\ 2\sqrt{2}\tau - 2\sqrt{2}\tau)]$$

The results of this calculation are also plotted in Figure 3, for $R \cong 3$.

3) Inverse - Square g

Finally Eq. (61) may be integrated numerically, using the expressions (25) for g. The range at burnout and the boost duration corresponding to a chosen initial value of q may thus be calculated. The corresponding specific exhuast power is found by numerical integration from (6):

$$P/m_1 = \frac{1}{2} \frac{R}{R-1} \int_0^\tau a^2 dt = \frac{2R}{R-1} \int_0^\tau (1+qt)^2 dt \qquad (78)$$

The results are shown in Figure 4, for $R = 3$. As one would expect, the linear-g model is a more accurate approximation than the constant-g model and will be used most frequently in the calculations which follow.

For launch from the Earth, it is not expected that ranges at burnout in excess of about 0.25 radii (~1600 km) will be practical, because of laser beamspread due to diffraction and atmospheric effects. For the baseline vehicle, with a payload of about one ton, a burnout range of 1000 km (~ 153 radii) has in fact generally been used in studies to date. For launch from the moon, however, boost out to ranges in excess of 0.5 radii (~ 870 km) is optically possible, although other limitations may be encountered (see Sec. II.4.b.)

Multiplying the value of specific exhaust power obtained from Figure 3 by the appropriate value of $g_o v_{co}$ from Table 1 will give the power requirements in megawatts per ton of payload. The laser output power will then be obtained by taking into account the efficiency of the engine and the transmission losses to the vehicle.

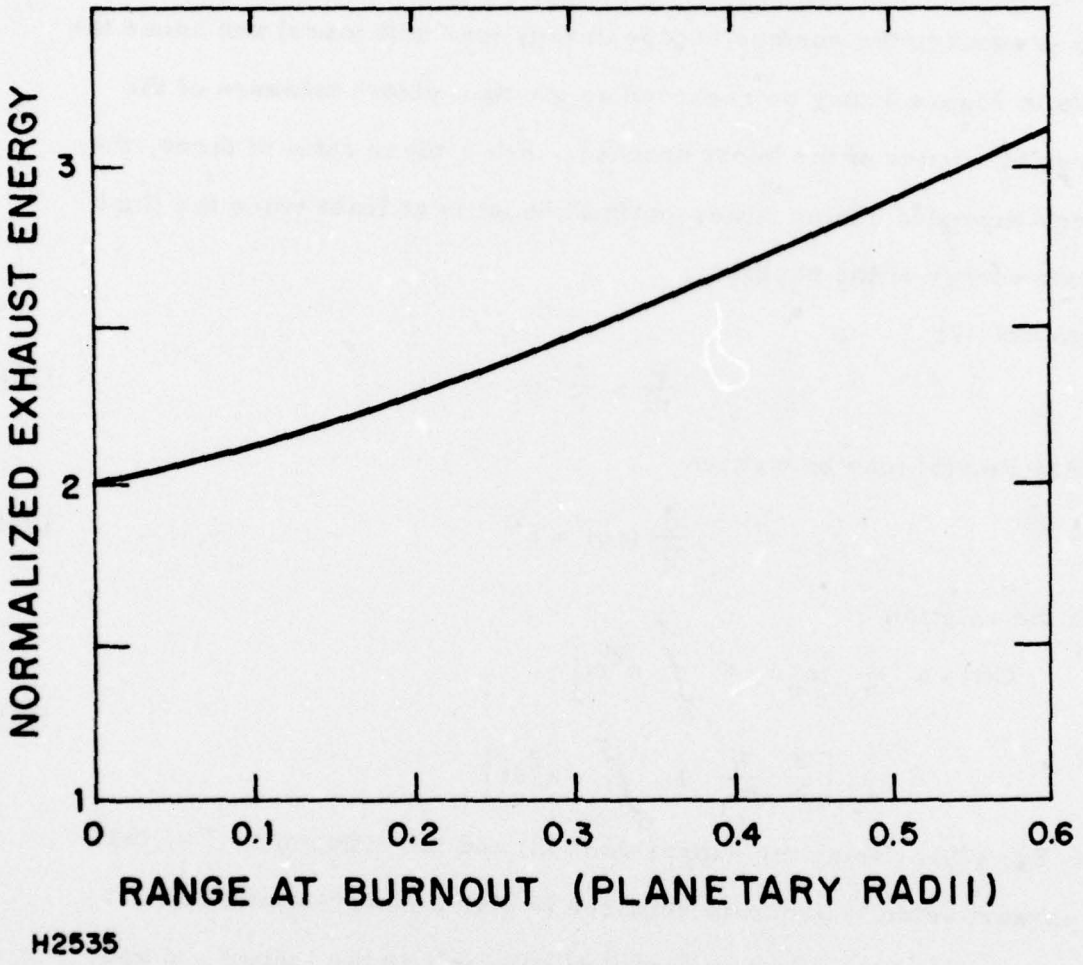

Figure 4 Exhaust Energy vs Range

The total exhaust energy expended during boost, per unit payload, may be calculated simply as the product of the specific exhaust power and the boost duration. As listed in Table 1, the unit of energy used here is equal to the surface escape energy (per unit mass) and hence the curve in Figure 4 may be regarded as giving a direct measure of the energy efficiency of the boost process. For a mass ratio of three, the energy expended during power-optimal boost is at least twice the final kinetic energy of the payload.

From Eq. (2)

$$\frac{P}{m} = \frac{1}{2} ac \tag{79}$$

so that Eq. (5) may be written

$$\frac{d}{dt} (ac) = a^2 \tag{80}$$

with the solution

$$\begin{aligned} C(t) &= \frac{1}{a} \left[a_o c_o + \int_o^\tau a^2 dt \right] \\ &= \frac{1}{a} \left[\frac{2}{R} \frac{P}{m_1} + \int_o^\tau a^2 dt \right] \end{aligned} \tag{81}$$

from Eq. (79). Using the expression (58) and the differential Eq. (61), the exhaust velocity program required to give a power-optimal thrust history may now be calculated (analytically only in the instant - g and linear - g approximations).

Using Eq. (53), the initial exhaust velocity is found from Eq. (79) to be simply

$$\begin{aligned} c_o &= \frac{2}{a_o} \frac{P}{m_o} = \frac{1}{R l g_o l} \frac{P}{m_1} \\ &= \frac{1}{R l g_o l} \frac{P}{m_1} \end{aligned} \tag{82}$$

so that, for constant mass ratio R, its dependence on the burnout range is similar to that for the normalized exhaust power, shown in Figure 4.

When the calculation represented by Eq. (81) is carried out, it is found that, during boost to short burnout ranges, the required exhaust velocity starts at a high value, decreases to a minimum, and then rises to a final value which is less than that at lift-off. As the burnout range is increased, the initial exhaust velocity decreases, the final exhaust velocity increases, and the minimum shifts to an earlier time in the boost, until eventually the exhaust velocity becomes a monotonic increasing function of time. This behavior is summarized in Figure 5 which shows (in linear-g approximation) the initial, final and minimum exhaust velocities as functions of the range at burnout. The cross-hatched area gives the range of exhaust velocities of which the engine must be capable, in order to allow power-optimal vertical ascent to escape, with a mass ratio of 3. It appears that both the maximum required exhaust velocity and the variability in the exhaust velocity may be minimized by choosing a burnout range of about 0.22 planetary radii (for the Earth, e. 1400 km).

The principal disadvantages of power-optimal vertical ascent are (i) the relatively high and variable exhaust velocity which is required; and (ii) the energy inefficiency of the process, as shown in Figure 4. As will be shown, the power (and hence capital cost) savings from power optimal vertical ascent, as compared to operation at constant exhaust velocity, are insufficient to offset these disadvantages.

b. Vertical Ascent to Escape at Constant Exhaust Velocity

With c constant, Eq. (2) gives

$$ma = m_o a_o \quad ; \quad -\dot{m}c = \frac{2P}{c} = \text{constant} \tag{83}$$

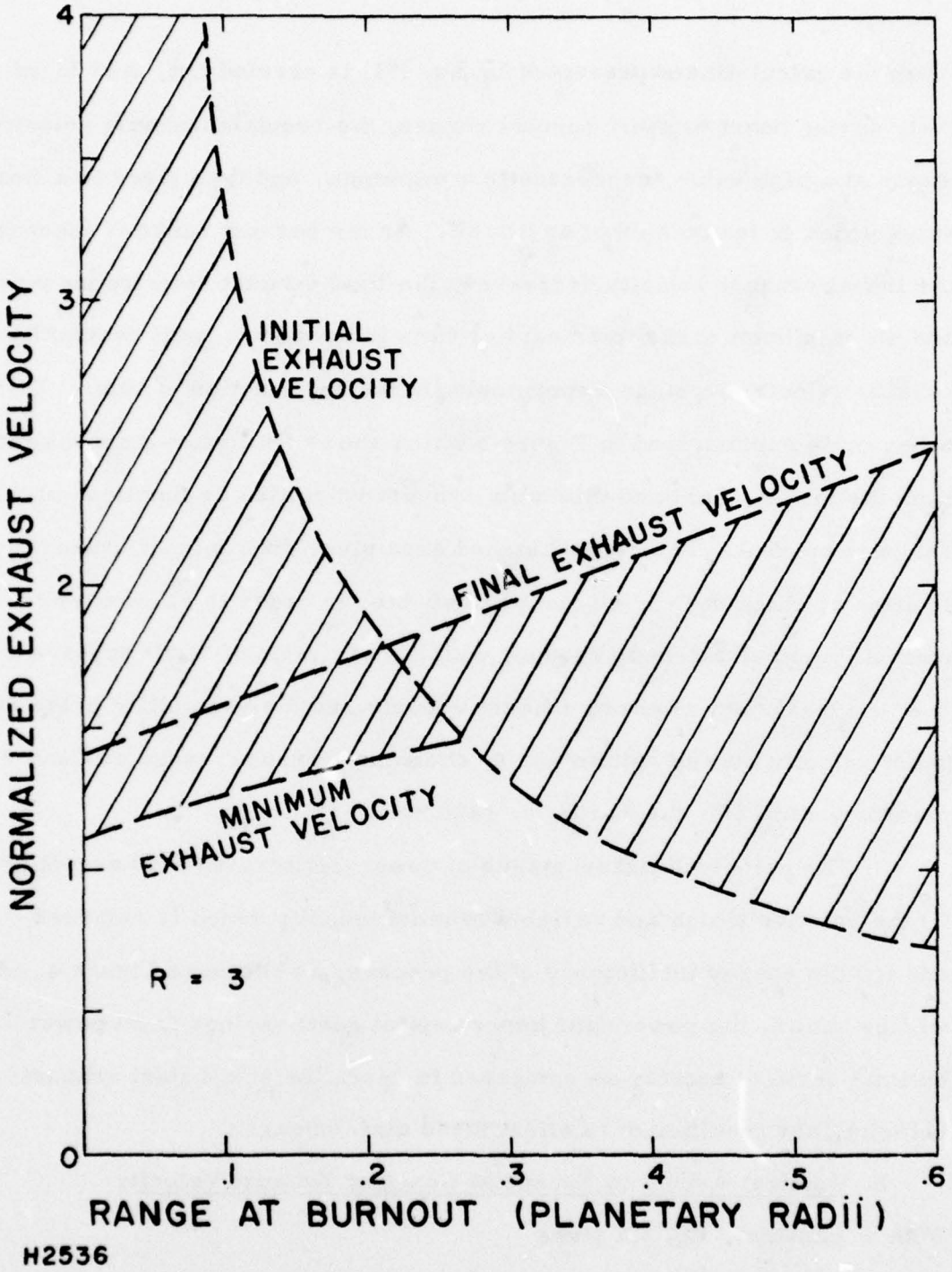

Figure 5 Exhaust Velocities for Optimal Vertical Ascent

so

$$\dot{m} = - m_o a_o / c = \text{constant} \tag{84}$$

and

$$\begin{aligned} m &= m_o + \dot{m} t \\ &= m_o (1 - t/\tau_o) \end{aligned} \tag{85}$$

where

$$\tau_o = -m_o/\dot{m} = c/a_o \tag{86}$$

Then Eq. (83) gives

$$a = \frac{m_o a_o}{m} = \frac{a_o}{1 - t/\tau_o} \tag{87}$$

The thrust program is thus determined by a_o and τ_o, or, equivalently, by choice of the exhaust velocity and the lift-off acceleration.

The mass ratio is found from Eq. (85) at burnout ($t = \tau$) to be

$$R = \frac{m_o}{m_1} = \frac{1}{1 - \tau/\tau_o} = \frac{a_1}{a_o} \tag{88}$$

The boost duration is thus determined if R and τ_o are specified.

The specific exhaust power is found most simply from Eq. (83) at $t = \tau$ as

$$\begin{aligned} \frac{P}{m_1} &= \frac{1}{2} a_1 c \\ &= \frac{1}{2} R a_o^2 \tau_o \end{aligned} \tag{89}$$

from Eqs. (86) and (88)

The problem is to choose the parameters a_o and τ_o so that (i) escape velocity is reached at a specified burnout range y_1; and (ii) the mass ratio has a specified value. This, of course, requires integration of the equations of motion, which are

$$\begin{aligned} \ddot{y} &= g\, a \\ &= - \frac{1}{(1\ y)^2} \frac{a_o}{1 - t/\tau_o} \end{aligned} \tag{90}$$

Once again, we consider three approximations to the gravitation field:

1) Constant Gravitational Field

The equation of motion is now

$$\ddot{y} = -1 + a_o/(1 - t/\tau_o) \tag{91}$$

which, with the initial conditions $y = \dot{y} = o$ at $t = o$, integrates immediately to give

$$\dot{y} = -t - a_o\tau_o \ln(1 - t/\tau_o \tag{92}$$

and integrates again to give

$$\begin{aligned} y &= -\frac{1}{2}t^2 + a_o\tau_o^2 \left[(1 - t/\tau_o)(\ln(1 - t/\tau_o) - 1) + 1\right] \\ &= -\frac{1}{2}t^2 + a_o\tau_o^2 \left[(1 - t/\tau_o)\ln(1 - t/\tau_o) + t/\tau_o\right] \end{aligned} \tag{93}$$

At $t = \tau$, these become, using Eq. (88)

$$v_1 = \tau_o \left[a_o \ln R - 1 + \frac{1}{R}\right] \tag{94}$$

$$y_1 = \tau_o^2 \left[\frac{a_o}{R}(R - \ln R - 1) - \frac{1}{2}\left(\frac{R - 1}{R}\right)^2\right] \tag{95}$$

Eliminating a_o betwen these equations gives

$$\begin{aligned} y_1 &= \tau_o^2 \frac{(R - 1)}{R^2} \left[\frac{R - \ln R - 1}{\ln R} - \frac{1}{2}(R - 1)\right] \\ &\quad + \tau_o v_1 \frac{(R - \ln R - 1}{R \ln R} \end{aligned} \tag{96}$$

With the escape velocity v_1 given as a function of the burnout altitude y_1, this quadratic equation may be solved for τ_o. Equation (94) then gives a_o and Eq. (89) the specific exhaust power. The results are shown in Figure 6.

As the burnout range increases, the initial acceleration decreases. The curve shown terminates when $a_o = 1$ (lift-off limit).

2) Linear and Inverse-Square Gravitational Field

In the linear-g case, the equation of motion becomes

$$\ddot{y} - 2y = -1 + a_o/(1 - t/\tau_o) \tag{97}$$

While this equation may readily be reduced to quandratures, the particular integral contains exponential integrals, of the form $\frac{e^{\sqrt{2}t}}{t}\,dt$, which cannot be expressed in terms of elementary functions. Since numerical integration of the euqation of motion is required in any case in the inverse-square case, it is simpler to write it as

$$\ddot{y} = g + a_o/(1 - t/\tau_o) \tag{98}$$

and, in the Runge-Kutta integration procedure, merely put

$$g = -1 + 2y \tag{99a}$$

or

$$g = -\frac{1}{(1 + y)^2} \tag{99b}$$

to cover the two cases.

In order to meet the desired terminal conditions (achievement of escape velocity at a specified range and mass ratio), an iterative procedure is required in order to correct assumed values of a_o and τ_o in the integration of Eq. (98). The constant - g analysis, above, can, however, provide good approximate starting values for these parameters.

For the purpose of plotting the specific exhaust power as a function of burnout range, the problem may be simplified by choosing values of τ_o a priori, on the basis of the constant - g calculation, since it is

not necessary to specify in advance the exact burnout ranges at which the data points are obtained. The problem then reduces to choosing the appropriate value of a_o.

Once τ_o is chosen the Runge-Kutta integration may be carried out to a fixed time

$$\tau = \tau_o \left(\frac{R - 1}{R}\right) \tag{100}$$

from Eq. (88), using an assumed a_o. In general, the calculated velocity at this time will not be euqal to the escape velocity at the calculated altitude.

In order to find a correction for a_o, it is sufficient to use the constant - g analysis. According to Eqs. (94) and (95), the effect of a change Δa_o in a_o on the terminal velocity and altitude is

$$\Delta v_1 = \tau_o \ln R \, \Delta a_o \tag{101a}$$

$$\Delta y_1 = \tau_o^2 \frac{(R - \ln R - 1)}{R} \Delta a_o \tag{101b}$$

At the end of the integration, the error in the calculated velocity is

$$\epsilon = v_1 - \sqrt{\frac{2}{1 y_1}} \tag{102}$$

where v_1 and y_1 are the calculated values. If we change a_o, the change in E will be,

$$\Delta \epsilon = \Delta v_1 + \frac{1}{\sqrt{2}} \frac{1}{(1 + y_1)^{3/2}} \Delta y_1 \tag{103}$$

$$= \left[\tau_o \ln R \frac{1}{\sqrt{2}} \frac{1}{(1 + y_1)^{3/2}} \tau_o^2 \frac{(R - \ln R - 1)}{R} \Delta a_o\right]$$

In order to reduce ϵ to zero, we, therefore, choose

$$\Delta a_o = \left(\sqrt{\frac{2}{1+y_1}} - v_1\right) \Big/ \left[\tau_o \ln R \, \frac{1}{\sqrt{2}} \, \frac{1}{(1+y_1)^{3/2}} \, \tau_o^2 \, \frac{(R - \ln R - 1)}{R}\right] \quad (104)$$

The results of the calculations are also shown in Figure 6, the curves again terminating when $a_o = 1$. It is interesting to observe that, in order to have a positive acceleration at lift-off, the maximum burnout range which can be used is about 0.45 planetary radii (obtained from the inverse-square calculation). To use longer ranges, if that were desired, it would be necessary to change the exhaust velocity in the early stages of boost, or perhaps to use a small chemical rocket to get the stage moving.

Figure 7 shows a comparison of the power curves calculated for optimal and constant-c vertical ascent to escape, using the accurate (inverse square) expression for the gravitational field. The important result which has been obtained is that the power savings effected by the power-optimal thrust program are quite negligible, at least for this mission. It is much more important to maximize the range at burnout than to use the power-optimal ascent profile.

The curves given can of course be converted from the normalized units to conventional units by multiplying the abscissa by to, the planetary radius, and the ordinate by $g_o v_{co}$. Figure 8 shows the power requirements for vertical ascent to escape (with R = 3) as a function of the range at burnout for the Earth, Mars and the Moon, the curves terminating at the lift-off limits. It is interesting to obeerve that a launching laser for use on the Moon, with a vehicle of constant exhaust velocity, can use a range of only up to about 750 km. At this range, the power requirements are only

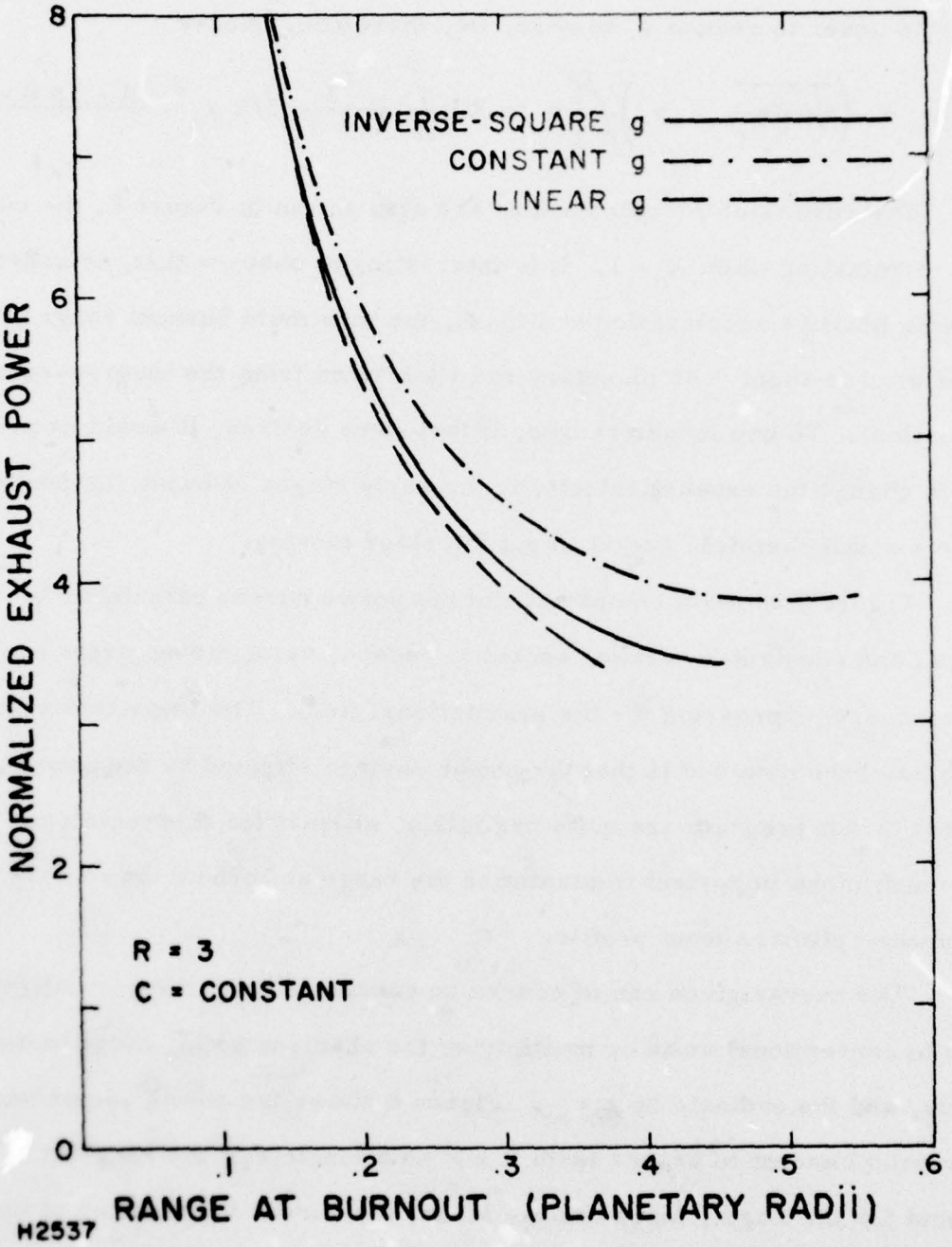

Figure 6 Power Required for Vertical Ascent to Escape at Constant Exhaust Velocity

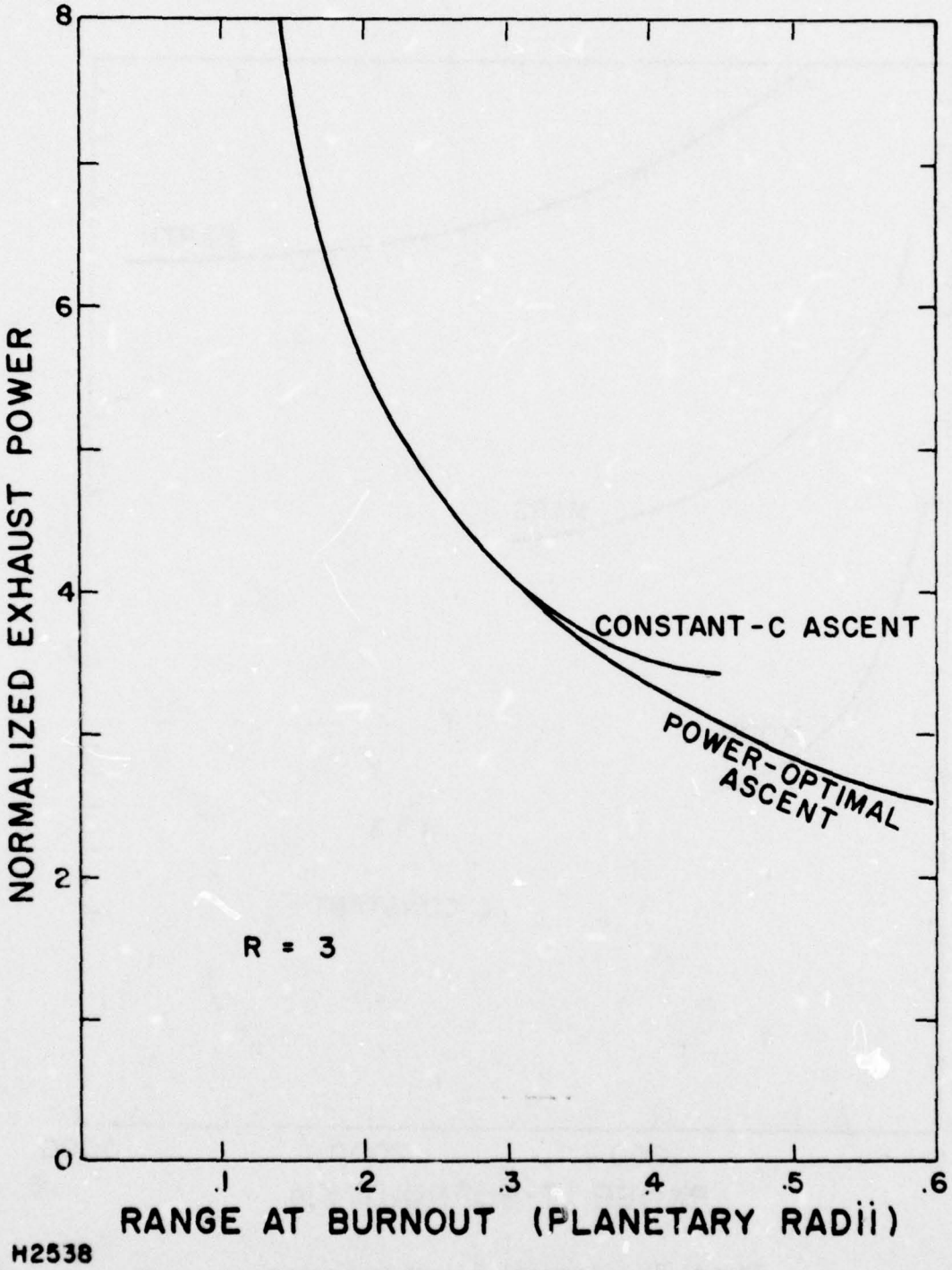

Figure 7 Comparison of Vertical Ascent Power Requirements

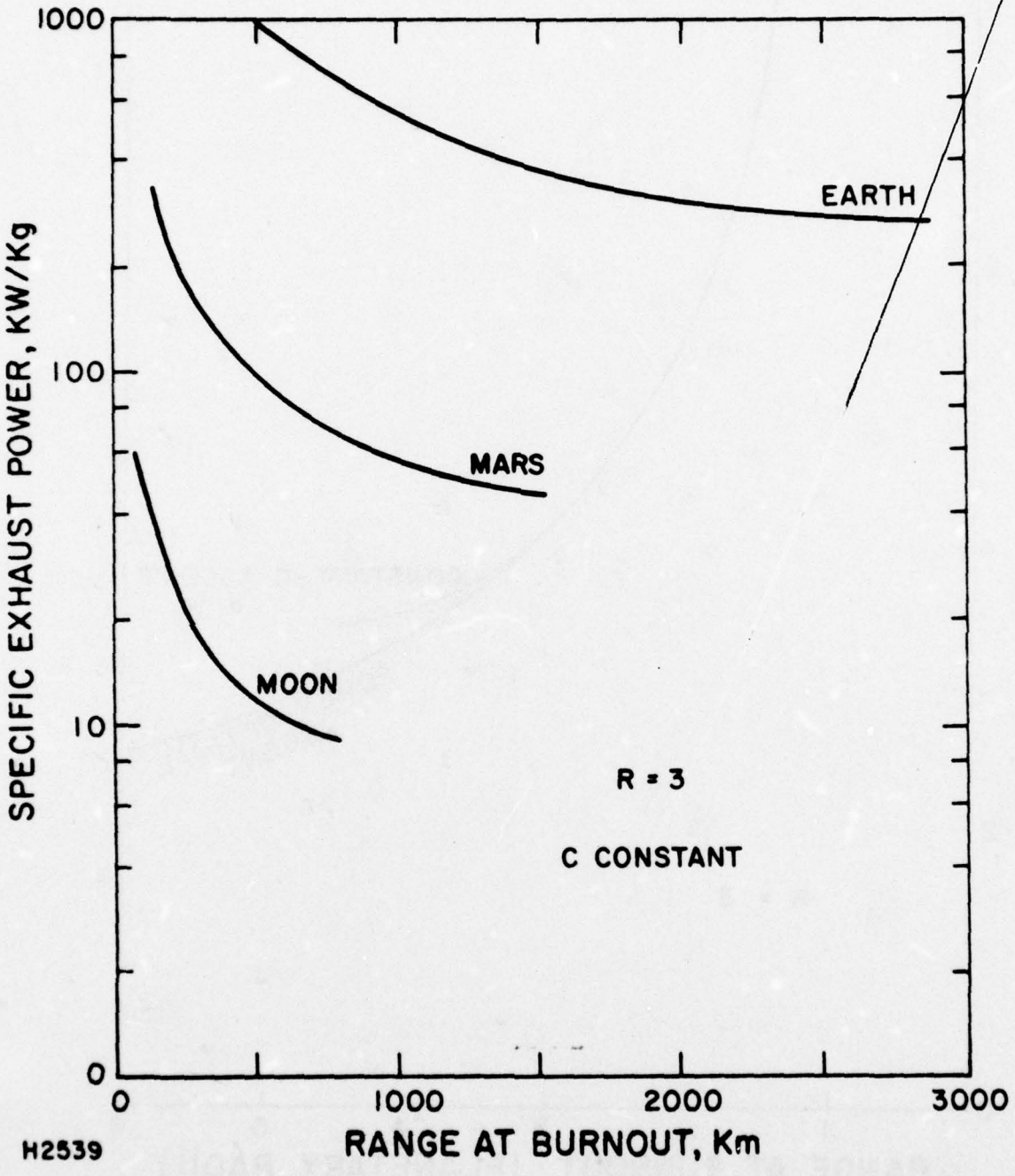

Figure 8 Vertical Ascent to Escape

about 10 MW/ton, two orders of magnitude less than for launch from the Earth with a similar burnout range.

The exhaust velocities required to achieve the performance of Figure 9 may, of course, be calculated from τ_o and a_o. The results are shown in Figure 9. The values obtained are always considerably less (by 20% or more) than the peak exhaust velocities required for optimal ascent, as shown in Figure 5. Nevertheless, for the Earth, vertical ascent to escape, with a mass ratio of 3, requires that the engine delivers a specific impulse in the range 1000 ~1300 sec.

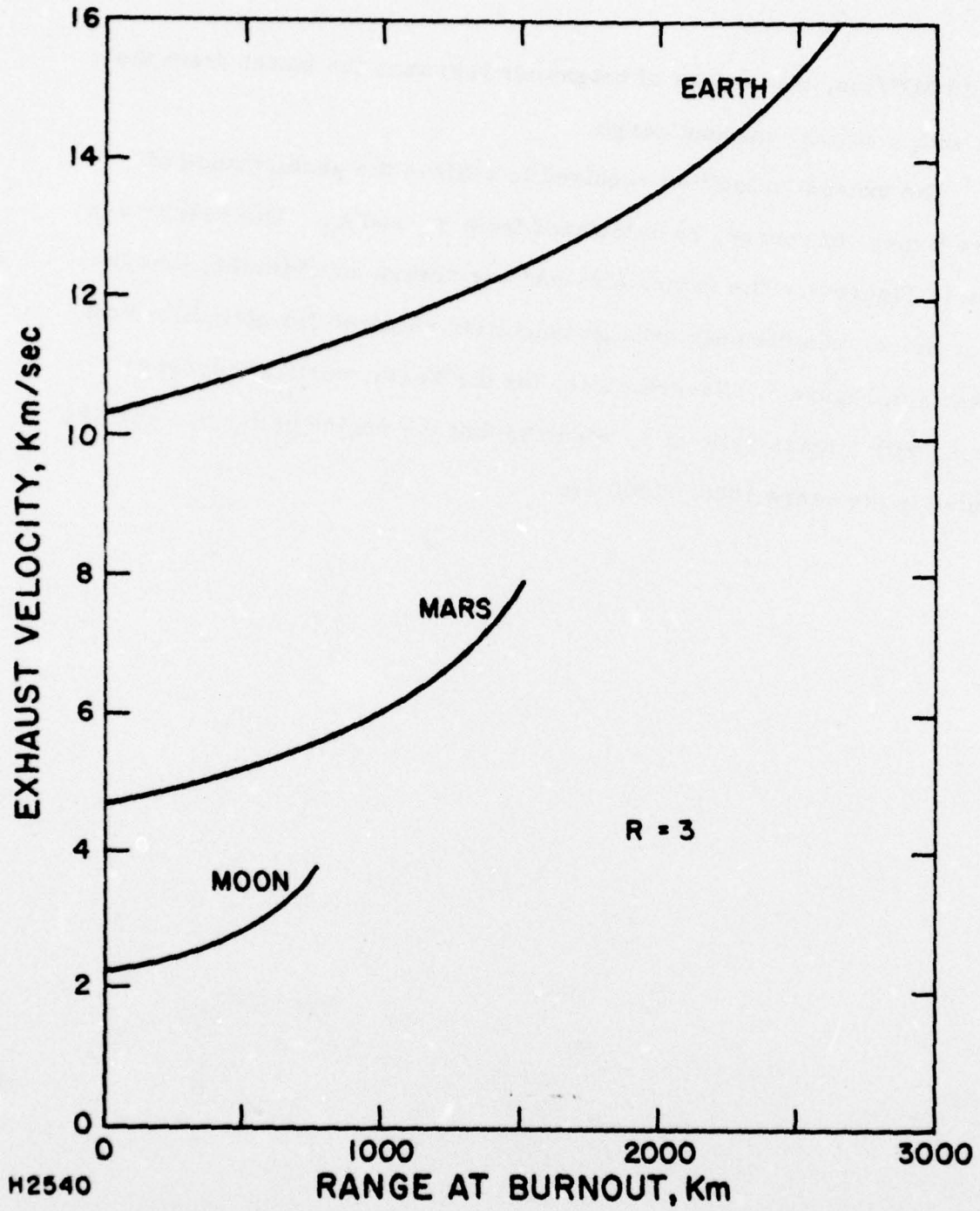

Figure 9 Vertical Ascent to Escape

5. POWER-OPTIMAL ASCENT TRAJECTORIES

This section presents an investigation of the problem of range-limited, laser-powered boost from a launch site on the planetary surface, so as to achieve desired orbit injection conditions while minimizing exhaust power (and hence laser power requirements). The assumptions on which the analysis is based are as follows:

1) The launch site is immediately adjacent to the launching laser.
2) At boost initiation, the launch vehicle has zero velocity.
3) The ascent trajectory lies in a vertical plane through the laser station.
4) Because of laser propagation limitations, the boost trajectory must be contained within zenith angles Θ_1 and range ρ_1 from the laser station. Within this fan-shaped area, attenuation of the laser beam by absorption, beamspread, etc., may be neglected.

The present analysis is limited to cases in which the mission objectives are such that it is not necessary to specify in advance the flight path angle at burnout. In particular, the following missions are considered in detail:

Mission A: Injection to an Escape Parabola

The velocity required at burnout for escape is given (in the units of Table 1) by (see Appendix A)

$$V_1^2 = \frac{2}{r_1} \tag{105}$$

where r_1 is the geocentric radius at burnout, given in turn by

$$r_1^2 = 1 + \rho_1^2 + 2\rho_1 \cos \Theta_1 \tag{106}$$

Any flight path angle at burnout (at least in the range $-\frac{\pi}{2} < \gamma_1 < \frac{\pi}{2}$ is acceptable for this mission. The optimization procedure will select that value of γ_1 for which the required specific exhaust power is minimized.

Mission B: Injection to a Transfer Ellipse to Geosynchronous Orbit

For this preliminary analysis, it is assumed for simplicity that the launch site is equatorial. Furthermore, the chosen transfer ellipse is contangential with GSO at apogee - this is the simplest, but not necessarily the optimal transfer orbit. As shown in the Appendix, the required injection velocity is given by

$$V_1^2 = 2\left(\frac{1}{r_1} - \frac{1}{r_a}\right)/\left[1 - \left(\frac{r_1}{r_a}\right)^2 \sin^2(\gamma_p - \delta_1)\right] \tag{107}$$

where

$r_a = 6.625$ is the radius of GSO

δ_1 is the geocentric angle traversed during boost, given by $\tan \delta_1 = \rho_1 \sin \theta_1/(1 + \rho_1 \cos \theta_p)$ (108)

For the ranges at burnout considered here, the velocity given by Eq. (107) varies by only about 1.5% as γ_1 is varied through all possible values. As γ_1 is not specified a priori, it is sufficient to start with the approximation

$$V_1^2 \approx 2\left(\frac{1}{r_1} - \frac{1}{r_a}\right) \tag{109}$$

A trajectory calculated on this basis will yield a value of γ_1, which can then be used to correct V_1.

Notice that Mission B reduces to Mission A if we put $r_a = \infty$.

The optimization procedure will select that transfer ellipse for which the required exhaust power during boost is a minimum. In practice,

it may be necessary to impose additional constraints on the transfer trajectory - for example, it may be required that the transfer ellipse have an exoatmospheric perigee, to avoid impacting the Earth if in the event of a failure to circularize the orbit at geosynchronous altitude. Such constraints will generally lead to specification in advance of the flight path angle at burnout.

Another example of a mission in which the flight path angle is specified is, of course, injection to circular orbit at the burnout altitude.

These and other possible missions for laser propulsion systems are discussed briefly, and will be considered in detail in a later report.

It should also be noted that the optimization procedure for Mission B which is presented here minimizes the exhaust power per unit mass at burnout. Whether or not this minimizes the laser power required to inject a given payload into geosynchronous orbit depends on the technique used to circularize the transfer ellipse at apogee. If a chemical kick stage is used for this purpose, the mass ratio for circularization depends strongly on the velocity at apogee, which is given by (see Appendix)

$$v_a^2 = \frac{2r_p}{r_a (r_p + r_a)} \tag{110}$$

where r_p is the perigee of the transfer ellipse. The problem of minimizing the laser power per unit payload in this case is also beyond the scope of the present analysis. Other technique for circularization will, however, be briefly considered below.

a. The Optimization Problem

The problem under consideration may be stated as follows: Given the desired range ρ_1 and zenith angle θ_1 at burnout, together with the

injection conditions listed above for specific missions, find the thrust vector control low (and hence the ascent trajectory) which minimizes the (constant) exhaust power required for a specified burnout mass m_1 and boost mass ratio R.

As in Section II.4.a, the calculation may be set up as a problem of Mayer in variational calculus. Choosing the Cartesian coordinate system shown in Figure 10, with origin at the laser station, the x_2-axis vertical and the x_1-axis in the trajectory plane, the equations of motion are first written as first-order differential constraints:

$$\phi_1 = v_1 - \dot{x}_1 = 0 \tag{111a}$$

$$\phi_2 = v_2 - \dot{x}_2 = 0 \tag{111b}$$

$$\phi_3 = \dot{v}_1 - g_1 - a_1 = 0 \tag{111c}$$

$$\phi_4 = \dot{v}_2 - g_2 - a_2 = 0 \tag{111d}$$

where

g_1, g_2 are the components of gravitation

a_1, a_2 are the specified thrust components.

In addition, we have the power condition (4):

$$\phi_5 = m^2 a^2 \, 2\dot{m}P = m^2(a_1^2 \, a_2^2) \, 2\dot{m}P = 0 \tag{111e}$$

In all cases, the initial conditions are

$$x_1 = x_2 = v_1 = v_2 = 0 \text{ at } \tau = 0 \tag{112}$$

The final conditions depend on the specific mission. If only the burnout velocity $\sqrt{1}$ (and not the flight path angle) is specified, as in Missions A and B, then we have

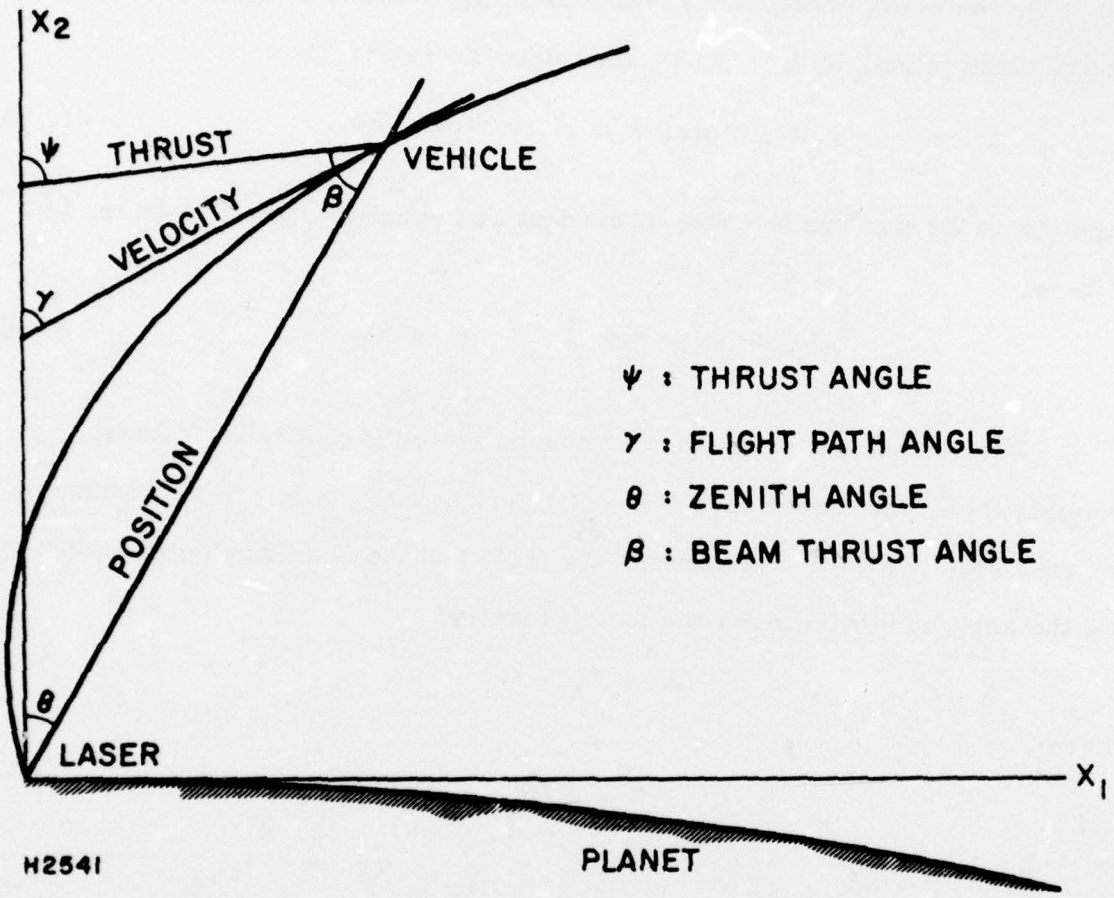

Figure 10 Ascent Trajectory Geometry

$$v_1^2 \; v_2^2 = \sqrt{T}^2 \tag{113}$$

at $t = \tau$, the boost duration. Variations in the velocity components at burnout are allowed but, by Eq. (113), they must be related by

$$v_1 dv_1 \; v_2 dv_2 = 0 \qquad (t = \tau) \tag{114a, b}$$

Since the range and zenith angle at burnout are specified, we also have, in all cases

$$d\chi_1 = d\chi_2 = 0 \qquad (t = \tau) \tag{115}$$

The variational problem may now be stated formally as follows: Amongst the seven functions $\chi_1(t)$, $\chi_2(t)$, $v_1(t)$, $v_2(t)$, $a_1(t)$, $m(t)$ which are consistent with the five constraints (111) and the boundary conditions, find the set which minimizes the payoff function

$$\Delta G = G_f - G_o \tag{116}$$

where

$$G = P/m \tag{117}$$

so

$$\Delta G = P/m_1 \left(\frac{R - 1}{R}\right) \tag{118}$$

As in Section III. 3. a, we introduce variable Lagrange multipliers λ_1 (i = 1, 2, 3, 4, 5) and form the augmented function

$$\begin{aligned} F = {} & \lambda_1(v_1 - \dot{\chi}_1) \; \lambda_2(v_2 - \dot{\chi}_2) \; \lambda_3(\dot{v}_1 - g_1 - a_1) \\ & \lambda_4(\dot{v}_2 - g_2 - a_2) \; \lambda_5(m^2(a_1^2 \; a_2^2) \; 2\dot{m}P) \end{aligned} \tag{119}$$

The Euler-Lagrange equations of the problem are obtained of the problem are obtained by applying the formula (31), to obtain

$$\dot{\lambda_1} = \lambda_3 g_{1,\ 1} \quad \lambda_4 g_{2,\ 1} \tag{120a}$$

$$\dot{\lambda_2} = \lambda_3 g_{1,\ 2} \quad \lambda_4 g_{2,\ 2} \tag{120b}$$

$$\dot{\lambda_3} = \lambda_1 \tag{120c}$$

$$\dot{\lambda_4} = \lambda_2 \tag{120d}$$

$$0 = - \lambda_3 \quad 2a_1 m^2 \lambda_5 \tag{120e}$$

$$0 = - \lambda_4 \quad 2a_2 m^2 \lambda_5 \tag{120f}$$

$$2P\dot{\lambda_5} = 2m(a_1^{\ 2} \ a_2^{\ 2})\ \lambda_5 = 2ma^2 \lambda_5 \tag{120g}$$

where

$$g_{1,\ 2} = \frac{\partial g_1}{\partial \chi_2}, \text{ etc.}$$

Since Eq. (119) is formally independent of time, a first integral of these equations is given by the formual (32):

$$C = - \lambda_1 v_1 - \lambda_2 v_2 \ \lambda_3 v_1 \ \lambda_4 v_2 - \lambda_5 m^2 a^2 \tag{121}$$

The transversality condition (33) gives, with Eq. (117).

$$- \frac{P}{m^2}\, dm - Cdt - \lambda_1 dx_1 - \lambda_2 dx_2 \ \lambda_3 dv_1 \ \lambda_4 dv_2$$

$$2P\lambda_5 \, dm \Big|_o^F = 0 \tag{122}$$

In all cases, this yields

$$C = 0 \tag{123}$$

$$\lambda_5 = - \frac{1}{2m^2} \qquad (t = \tau) \tag{124}$$

For missions where the burnout flight path angle is unspecified, Eq. (114a, b) gives an additional boundary condition from Eq. (122):

$$\lambda_3 v_2 - \lambda_4 v_1 = 0 \qquad (t = \tau) \tag{125a, b}$$

Using Eq. (1113), Eq. (120g) may be written

$$m\dot{\lambda}_5 + 2\dot{m}\lambda_5 = 0 \tag{126}$$

with solution, meeting the boundary condition (2.120),

$$\lambda_5 = \frac{1}{2m^2} \tag{127}$$

Then Eqs. (120e) and (120f) give

$$\lambda_3 = a_1 \tag{128a}$$

$$\lambda_4 = a_2 \tag{128b}$$

This result allows Eqs. (120e) thru (120d) to be consolidated in tensor rotation as

$$\ddot{a}_j = g_{j,i} a_i \tag{129}$$

where the suffixes take on the values 1, 2 and repeated suffixes are summed.

If the gravity gradients $g_{j,i}$ may be neglected (i.e., in constant-g approximation), the solution to Eq. (129) is

$$a_i = A_{oi} + A_{1i} t \tag{130}$$

where A_{oi}, A_{1i} are constants. The angle between the thrust vector and the laser-station vertical is then given by

$$\tan \psi = a_1/a_2 = \frac{A_{o1} + A_{11} t}{A_{o2} + A_{12} t} \tag{131}$$

which is the well-known optimal thrust-steering law of Lawden.

In the general case, we have now found expressions for all of the λ_i in terms of the variables of the problem. They are collected here for future reference, followed in parentheses by the equation numbers where these results were obtained:

$$\lambda_1 = \dot{a}_1 \qquad (120c),\ (128a) \qquad (132a)$$

$$\lambda_2 = a_2 \qquad (120d),\ (128b) \qquad (132b)$$

$$\lambda_3 = a_1 \qquad (128a) \qquad (132c)$$

$$\lambda_4 = a_2 \qquad (128b) \qquad (132d)$$

$$\lambda_5 = \frac{1}{2m^2} \qquad (129) \qquad (132e)$$

With Eq. (123), the first integral (121) may now be written

$$a_1\dot{v}_1 - \dot{a}_1 v_1 + a_2\dot{v}_2 - \dot{a}_2 v_2 - \tfrac{1}{2}a^2 = 0 \qquad (133)$$

It will sometimes be useful to write this in vector notation, as

$$\tfrac{1}{2}a^2 = \underline{a} \cdot \dot{\underline{v}} - \dot{\underline{a}} \cdot \underline{v} \qquad (133a)$$

The equations of motion (111c) and (111d) are, in this notation,

$$\dot{\underline{v}} = \underline{g} + \underline{a} \qquad (134)$$

Substituting this in Eq. (133a) yields

$$\tfrac{1}{2}a^2 + \underline{a} \cdot \underline{g} - \dot{\underline{a}} \cdot \underline{v} = 0 \qquad (135)$$

At lift-off, when $\underline{v} = 0$, this yields the important result

$$a^2 = -\underline{a} \cdot \underline{g} \qquad (t = 0) \qquad (136)$$

or

$$a_o = a\left|g_o\right|\cos\psi_o \qquad (137)$$

where ψ_o is the initial thrust angle. In other words, the initial specific thrust is equal in magnitude to twice the component of gravitation along the initial thrust direction.

Since $a^2 = a_1^2 a_2^2$, the first integral (133) may also be written

$$a_1^2 \left(\frac{d}{dt}\left(\frac{v_1}{a_1}\right) - \frac{1}{2}\right) a_2^2 \left(\frac{d}{dt}\left(\frac{v_2}{a_2}\right) - \frac{1}{2}\right) = 0 \qquad (138)$$

Sufficient (but not clearly necessary) conditions for the validity of the first integral are thus

$$\frac{d}{dt}\left(\frac{v_1}{a_1}\right) = \frac{1}{2} \qquad (139a)$$

$$\frac{d}{dt}\left(\frac{v_2}{a_2}\right) = \frac{1}{2} \qquad (139b)$$

with the solutions

$$v_1 = \left(\frac{1}{2} t + c_1\right) a_1 \qquad (140a)$$

$$v_2 = \left(\frac{1}{2} t + c_2\right) a_2 \qquad (140b)$$

where c_1, c_2 are constants.

The boundary condition (125a, b) which is specific to the present case, in which the flight path angle at burnout is not constrained a priori may be written

$$a_1 v_2 = a_2 v_1 \qquad (t = \tau) \qquad (141a, b)$$

Note that this states that the thrust vector is parallel to the velocity vector - i.e., tangential to the trajectory - just before burnout. Inserting Eq. (140) in Eq. (141) gives

$$(\tfrac{1}{2}\tau + c_2)\, a_1 a_2 = (\tfrac{1}{2}\tau + c_1)\, a_1 a_2$$

or

$$c_1 = c_2 \tag{142}$$

so that Eq. (140) becomes

$$\underline{v} = (\tfrac{1}{2} t + c_1)\, \underline{a} \tag{143}$$

At lift-off ($t = 0$), $\underline{v} = 0$, so

$$c_1 \underline{a}_o = 0 \tag{144}$$

Comparison with Eq. (137) shows that (unless the initial thrust vector is horizontal), $c_1 = 0$. We thus obtain the optimal specific thrust program

$$a = \frac{2}{t}\, \underline{v} \tag{145}$$

so that the thrust is tangential to the trajectory throughout boost, not just at burnout. The trajectory is thus flown at zero angle of attack. This result may be compared to the law (55) found for optimal vertical ascent.

The equation of motion (134) may now be written

$$\underline{v} - \frac{2}{t}\, \underline{v} = t^2 \frac{d}{dt} (\frac{1}{t^2}\, \underline{v}) = \underline{g} \tag{146}$$

Near lift-off, where $\underline{g}$ g_o, this equation may be solved explicitly:

$$\underline{v} = - \underline{g}_o t + \underline{q}_o t^2 \tag{147}$$

where $\underline{q}_o$ is a constant vector. From Eq. (145), the thrust program is then

$$a = - 2\underline{g}_o + 2\underline{q}_o t \tag{148}$$

In particular at lift-off,

$$a = - 2\underline{g}_o \tag{149}$$

so that the lift-off is vertical, with an initial net upward acceleration of 1 g. Note that this is a special case of Eq. (137).

According to Eq. (145), the optimal thrust is always parallel to the vehicle velocity. Since the lift-off is vertical, this may seem to imply that no thrust can develop in the χ_1 - direction, but it is clear from Eq. (148) that this is not true if $\underline{q}_o$ has an χ_1 - component.

The optimal trajectory problem is now readily solved in the constant-g approximation - i.e., if we write

$$g^o{}_i = \begin{bmatrix} 0 \\ \\ -1 \end{bmatrix} \tag{150}$$

At burnout, the vehicle velocity is given by

$$V_1^2 = v_1^2 + v_2^2 = q_{01}^2 \tau^4 + (\tau\, q_{02} \tau^2)^2 \tag{151}$$

from Eq. (147). Integration of Eq. (147) gives

$$\underline{c} = -\frac{1}{2} g_o \tau^2 + \frac{1}{3} q_o t^3 \tag{152}$$

or, at burnout,

$$\rho_1 \sin \theta_1 = \frac{1}{3} q_{o1} \tau^3 \tag{153a}$$

$$\rho_1 \cos \theta_1 = \frac{1}{2} \quad ^2 + \frac{1}{3} q_{02} \tau^3 \tag{153b}$$

Given the required burnout position and the magnitude of the required burnout velocity, Eqs. (151) and (153) may be solved to yield the boost duration τ and the components q_{01} and q_{02} of $\underline{q}_0$. The required specific exhaust power may then be found from Eq. (6), with a^2 obtained from Eq. (148).

Instead of carrying through their calculation, we turn to the liner-gravity approximation, which, in the vertical ascent case, was found to give appreciably more accurate results.

b. The Linear-Gravity Approximation

The gravitational field may be expanded in a vector Taylor series about the origin:

$$g_i = g_i^o + g_{i,j}\chi_j + \ldots \tag{154}$$

where g_i^o is given by Eq. (150) and $g_{i,j}^o$ is the gravity-gradient tensor, evaluated at the origin. In general, the gravitational field may also be written

$$g_i = -(r^2)^{-3/2} r_i \tag{155}$$

where

$$r_i = \begin{bmatrix} \chi_1 \\ 1 + \chi_2 \end{bmatrix}$$

is the geocentric position vector. Since it is clear from this that $dr_i = d\chi_i$, the gravity-gradient tensor may be calculated as follows, from Eq. (155):

$$\begin{aligned} g_{i,j} &= -(r^2)^{-3/2}\delta_{ij} + \frac{3}{2}(r^2)^{-5/2} r_i \frac{2r^2}{2r_j} \\ &= -r^{-3}\delta_{ij} + \frac{3}{2} r^{-5} r_i \frac{\partial}{\partial r_j}(r_k r_k) \\ &= -r^3\delta_{ij} + 3r^{-5} r_i r_k \delta_{jk} \\ &= -r^3\left[\delta_{ij} - 3r^{-2} r_i r_j\right] \end{aligned} \tag{157}$$

where δ_{ij} is the two-dimensional kronecker delta. Evaluating this expression at the origin $(\chi_1 = \chi_2 = 0)_1$ we find the simple form

$$g^{o}_{i,j} = \begin{bmatrix} -1 & 0 \\ 0 & 2 \end{bmatrix} \tag{158}$$

and the expansion of the gravitational field (2.150) is, in components,

$$g_1 = x_1 + \ldots\ldots \tag{159a}$$

$$g_2 = -1 + 2x_2 + \ldots \tag{159b}$$

The equations of motion (2.142) may now be written

$$x_1 - \frac{2}{t} x_1 + x_1 = 0 \tag{160a}$$

$$x_2 - \frac{2}{t} x_2 - 2x_2 \equiv -1 \tag{160b}$$

Instead of attempting to solve this pair of differential equations with time-varying coefficients, it proves simpler in this case to return to the fundamental Eq. (129) for the optimal thrust program. In the linear approximation, the gravity gradients are constants, given by Eq. (158), so Eq. (129) becomes

$$a_1 + a_1 \equiv 0 \tag{161a}$$

$$a_2 - 2a_2 \equiv 0 \tag{161b}$$

The solutions of these equations, meeting the initial condition (149) for $\underline{a}$, are

$$a_1 \equiv B_{11} \sin t \tag{162a}$$

$$a_2 \equiv 2 \cos h \sqrt{2}\, t + \frac{1}{\sqrt{2}} B_{21} \sin h \sqrt{2}\, t \tag{162b}$$

This expression for $\underline{a}$ could now be used in the equations of motion in the form (134), using (159) for $\underline{g}$. However, having already carried out a general first integration of the equations of motion, we may instead use (145), which now gives

$$x_1 = v_1 = \frac{1}{2} t a_1 \approx {}_2 B_{11} t \sin t \tag{163a}$$

$$x_2 = v_2 = {}_2 t a_2 = t \cos h \sqrt{2}\, t \frac{1}{2\sqrt{2}} B_{21} t \sin h \sqrt{2}\, t \tag{163b}$$

so that

$$x_1 = \frac{1}{2} B_{11} \int_0^\tau t \sin t \, dt = \frac{1}{2} B_{11} (\sin t - t \cos t) \tag{164a}$$

$$x_2 = \int_0^\tau t \cos \sqrt{2}\, t \, dt + \frac{1}{2\sqrt{2}} B_{21} \int_0^\tau t \sin h \sqrt{2}\, t \, dt$$

$$= \frac{1}{2} \left[\sqrt{2}\, t \sin h \sqrt{2}\, t - \cos h \sqrt{2}\, t + 1\right] \tag{164b}$$

$$+ \frac{1}{4\sqrt{2}} B_{21} \left[\sqrt{2}\, t \cos h \sqrt{2}\, t - \sin h \sqrt{2}\, t\right]$$

In the linear-g approximation, Eqs. (163) replace Eq. (147), and Eqs. (164) replace Eq. (152) of the constant-g case.

At burnout, Eq. (164) gives

$$B_{11} = \frac{2x_1}{\sin \tau - \tau \cos \tau} \tag{165}$$

$$B_{21} \equiv \frac{2\sqrt{2}\, 2x_2 - 1 \cos h \sqrt{2}\tau - \sqrt{2}\tau \sin h \sqrt{2}\tau}{\sqrt{2}\tau \cos h \sqrt{2}\tau - \sin h \sqrt{2}\tau} \tag{166}$$

and the burnout components of velocity Eqs. (163) are then, after some algebraic reduction,

$$v_1(\tau) \equiv \frac{x_1 \tau}{1 - \tau \cos \tau} \tag{167a}$$

$$v_2(\tau) \equiv \frac{\tau\, (2x_2 - 1) \sin h\, \tau\, 2\, \tau\, \sqrt{2}\, \tau}{\sqrt{2}\tau \cos h \sqrt{2} - \sin h \sqrt{2}} \tag{167b}$$

Squaring and adding these equations gives the magnitude of the burnout velocity as

$$V_1^2 \equiv \tau^2 \frac{x_1^2}{(1 - \tau \cot \tau)^2} \frac{((2x_2 - 1) \sinh \sqrt{2}\tau \sqrt{2}\tau)^2}{(\sqrt{2}\tau \cosh \sqrt{2}\tau - \sinh \sqrt{2}\tau)^2} \tag{168}$$

Given the burnout position (x_1, x_2) and the mission velocity (105), (107) or (109), this equation may be solved numerically for the boost duration τ. The flight path angle at burnout may also be found in this calculation from the ratio of (167a) to (167b) and used to correct (107) and (109), if required. The specific exhaust power may then be calculated from Eq. (6) and Eq. (162) as

$$P/m_1 \equiv \frac{1}{2} \frac{R}{R-1} \int_0^\tau a^2 \, dt$$

$$\equiv \frac{1}{2} \frac{R}{R-1} \int_0^\tau \left[B_{11}^2 \sin^2 t \left(\frac{1}{\sqrt{2}} B_{21} \sinh \sqrt{2}\, t \, 2 \cosh \sqrt{2}\, t\right)^2 \right] dt$$

$$\equiv \frac{R}{R-1} \left[\frac{1}{8} B_{11}^2 (2\tau - \sin 2\tau) \frac{1}{2\sqrt{2}} (1 \tfrac{1}{8} B_{21}^2) \right. \tag{169}$$

$$\left. \sinh 2\sqrt{2}\tau + \frac{1}{4} B_{21} (\cosh 2\sqrt{2}\tau - 1) + (1 - \tfrac{1}{8} B_{21}^2) \tau \right]$$

With the constants B_{11}, B_{21} given by Eq. (171).

The calculation leading to Eq. (81) is valid in this case also: the exhaust velocity program required to give the optimal thrust history is given by

$$c(t) \equiv \frac{1}{a} \frac{2}{R} \frac{P}{m_1} + \int a^2 \, dt \tag{170}$$

where now a is obtained from Eqs. (162). The thrust vector steering law is

$$\tan \psi \equiv \frac{a_1}{a_2}$$

$$\equiv \frac{B_{11} \sin t}{2 \cos h \sqrt{2}\tau + \frac{1}{\sqrt{2}} B_{21} \sin h \sqrt{2}\, t} \qquad (171)$$

$$\equiv \tan \gamma$$

c. Power-Optimal Boost Trajectories for High Orbit or Escape

Using the mission velocities (2.103A) and (2.103B), the theory presented in the previous Section was first used to compute the specific exhaust power during power-optimal boost, in the linear-gravity approximation, as a function of the burnout zenith angle, for a boost mass ratio R = 3 and for several burnout ranges. The results are shown in Figure 11 for ascent to an escape parabola and in Figure 12 for injection to a transfer ellipse to geosynchronous orbit. To facilitate comparison with previous results and (in the case of escape missions*) to allow application to extraterrestrial bodies, the data are given in the normalized units of Table 1. Data in conventional units is given later.

For both missions, the optimal exhaust power per unit burnout mass is almost independent of the burnout zenith angle. For launch to GSO, however, the mass at burnout is that injected to the transfer ellipse: a "kick in the apogee" is required to circularize the orbit at synchronous altitude. It is shown in Appendix A that the ΔV for circularization is given by

$$\Delta V_k = V_c - V_1 \left(\frac{r_1}{r_a}\right) \sin (\gamma_1 - \delta) \qquad (172)$$

where $V_c = r_a^{-1/2}$ is the geosynchronous circular velocity.

* The radius r_a of synchronous orbit of a planet obviously depends on its rotation rate and hence is specific to a planet, even when measured in normalized units. The data given here thus apply to synchronous orbit about the Earth only.

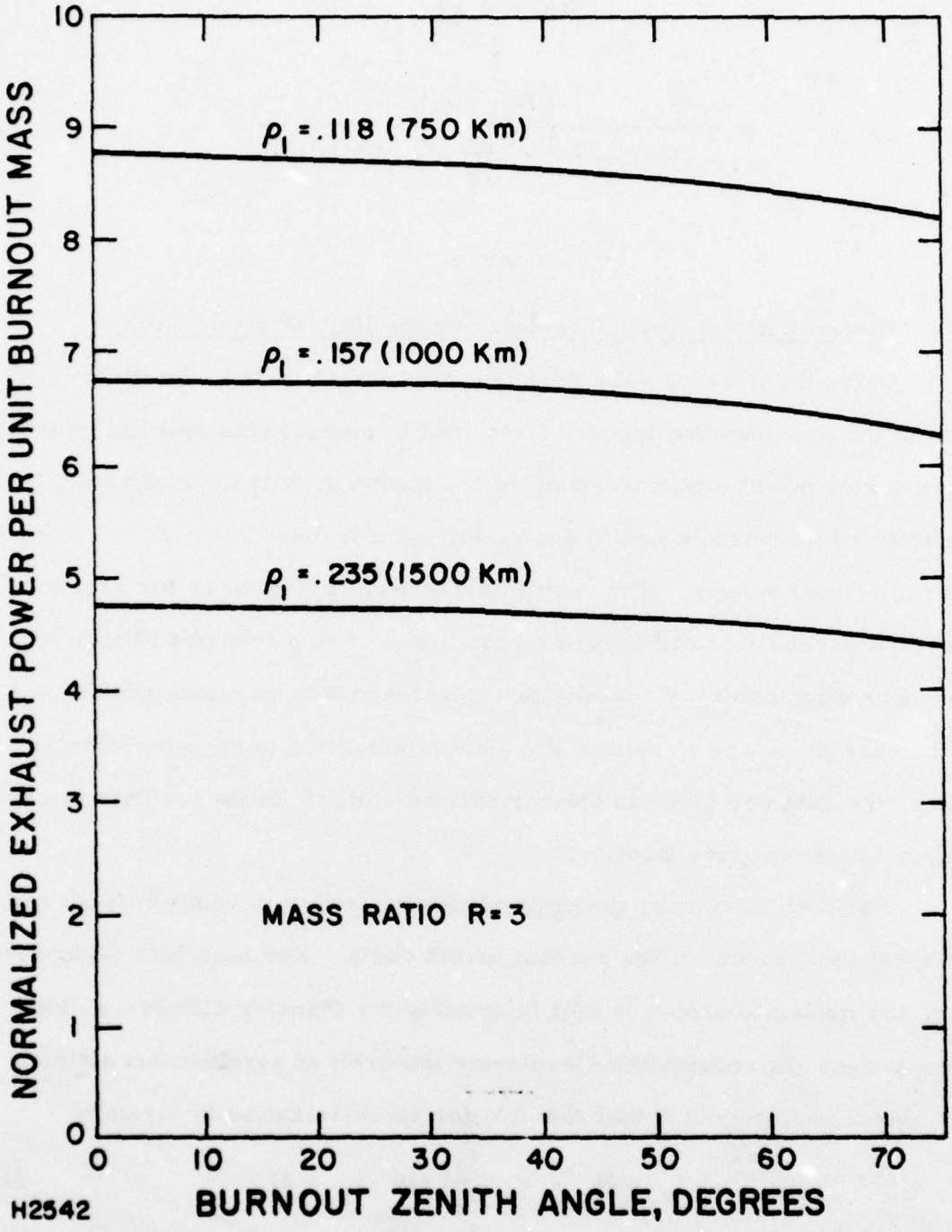

Figure 11 Power vs Burnout Zenith Angle for Optimum Ascent to Escape

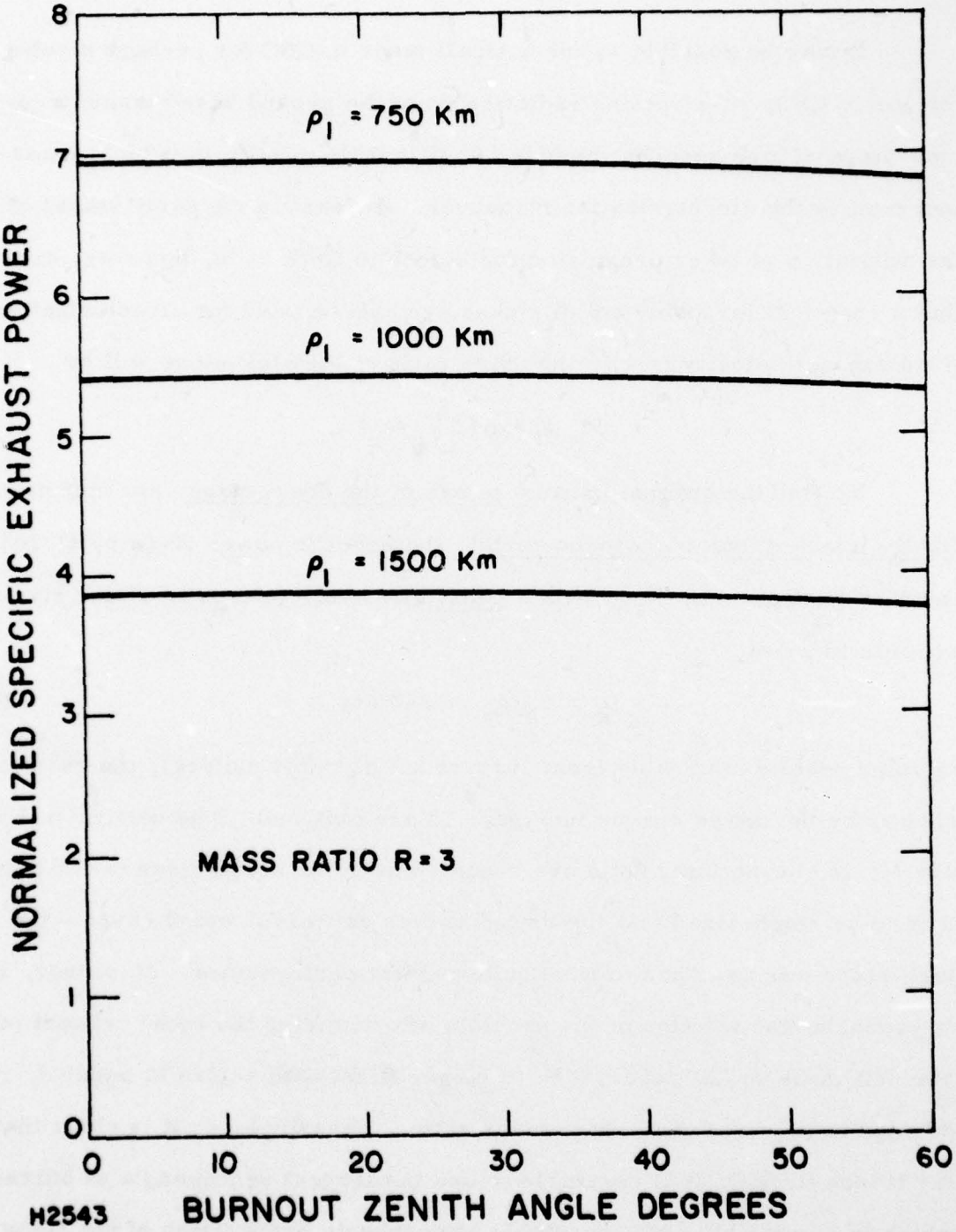

Figure 12 Exhaust Power vs Zenith Angle

It may be possible to use a small laser in GSO (or perhaps a relay mirror in GSO, re-directing radiation from the ground based laser) to power kick-stage of high specific impulse, so that little penalty in vehicle mass is incurred by the circularization maneuver. At least is the early stages of the utilization of laser propulsion for launch to GSO, it is, however, expected that a chemical (probably solid) kick-stage will be used for circularization. If its exhaust velocity is c_k, the mass ratio of the kick-stage will be

$$R_k = \exp(\Delta V_k / c_k) \tag{173}$$

To find the optimal exhaust power of the boost stage, per unit mass finally injected into synchronous orbit, the specific power given by (2.165) must be multiplied by R_k. With a boost mass ratio of 3, and a kick stage specific impulse

$$I_k = c_k / g_o \approx 240 \text{ sec} \tag{174}$$

(a value readily obtainable from current solid rocket motors), the results shown, by the dotted curves in Figure 13 are obtained. The data from Figure 12, *in conventional units* are repeated here for comparison (solid curves). It is to be emphasized that the dotted curves represent worst cases - the kick-stage was assumed to have quite modest performance. Moreover, it is probable that solution of the problem of optimizing the boost exhaust power per unit mass in GSO would lead to larger flight path angles at burnout, reducing the required kick-stage mass ratio. Nevertheless, it is clear that, for launch to GSO, it is desirable to use the largest zenith angle at burnout which is compatible with acceptable atmospheric propagation of the laser beam.

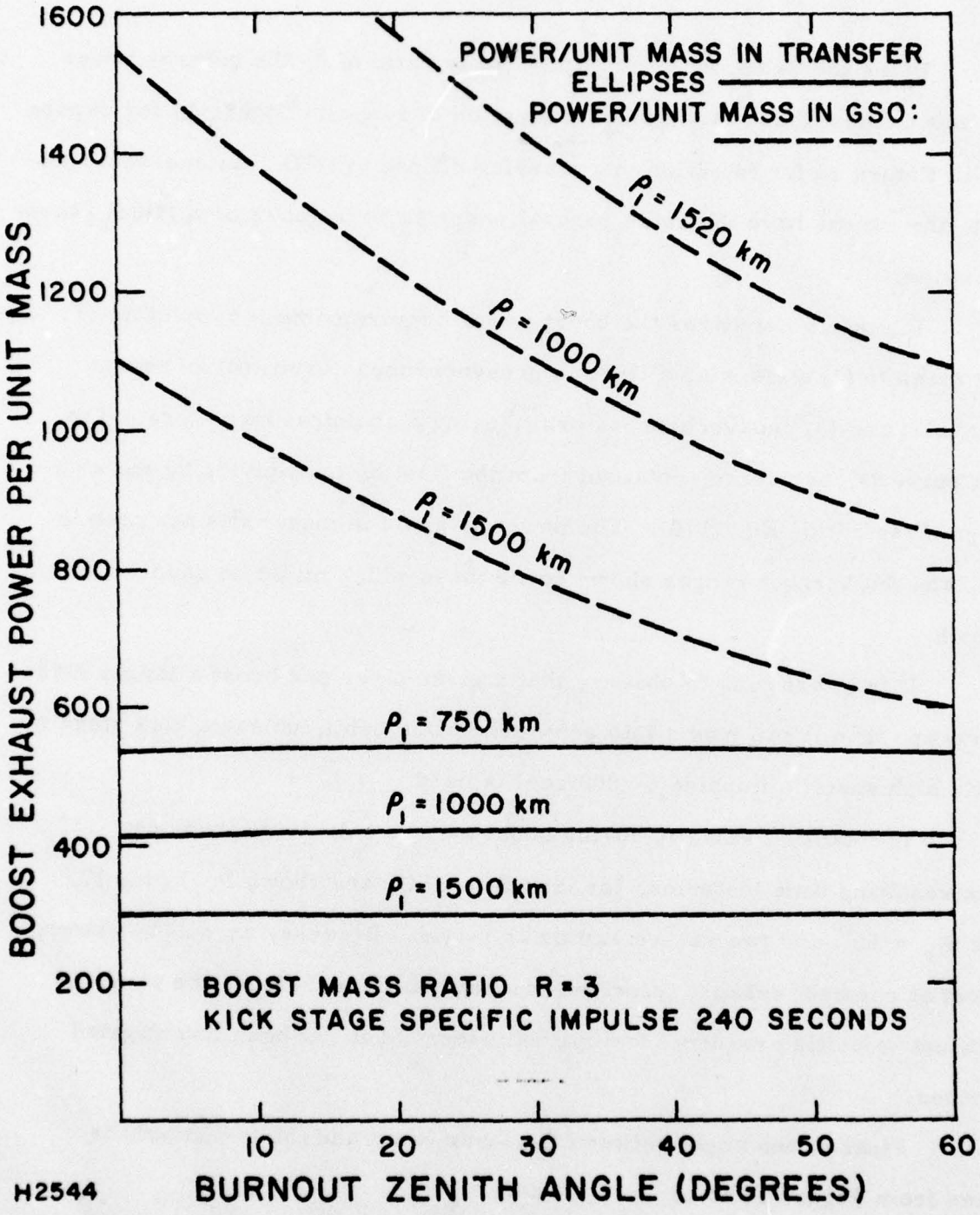

Figure 13 Exhaust Power per Unit Mass vs Zenith Angle

Using the value $\Theta_1 = 60^\circ$ and a mass ratio of 3, the exhaust power per unit burnout mass is shown as a function of range in Figure 14 for escape and in Figure 15 for injection to a transfer ellipse to GSO. As one would expect, the curves have the same general shape as in the case of vertical ascent to escape.

Figure 16 compares the boost power requirements for injection of unit mass to (1) a transfer ellipse to geosynchronous orbit; (2) an escape parabola; and (3) geosynchronous orbit, using a chemical kick stage. The last curve is, ov course, obtained from the first by multiplying by the kick-stage mass ratio, Eq. (173). The power is given in megawatts per metric ton, and the burnout ranges shown cover these which might be used for Earth launch.

It is interesting to observe that a given laser can boost a larger mass to escape than it can insert into geosynchronous orbit, unless a kick stage of quite high specific impulse (~ 800 sec) is used.

The exhaust velocity during boost may be calculated from Eq. (170). The resulting time histories, for launch to GSO, are shown in Figure 17, for $\Theta_1 = 60^\circ$ and two ranges and mass ratios. Because, as will be shown, boost at constant exhaust velocity is an acceptable technique, the range of exhaust velocities required for optimal ascent have not been investigated further.

Finally, the angle between the laser beam and the thrust axis is seen from Figure 10 to be

$$B = \psi - o \tag{175}$$

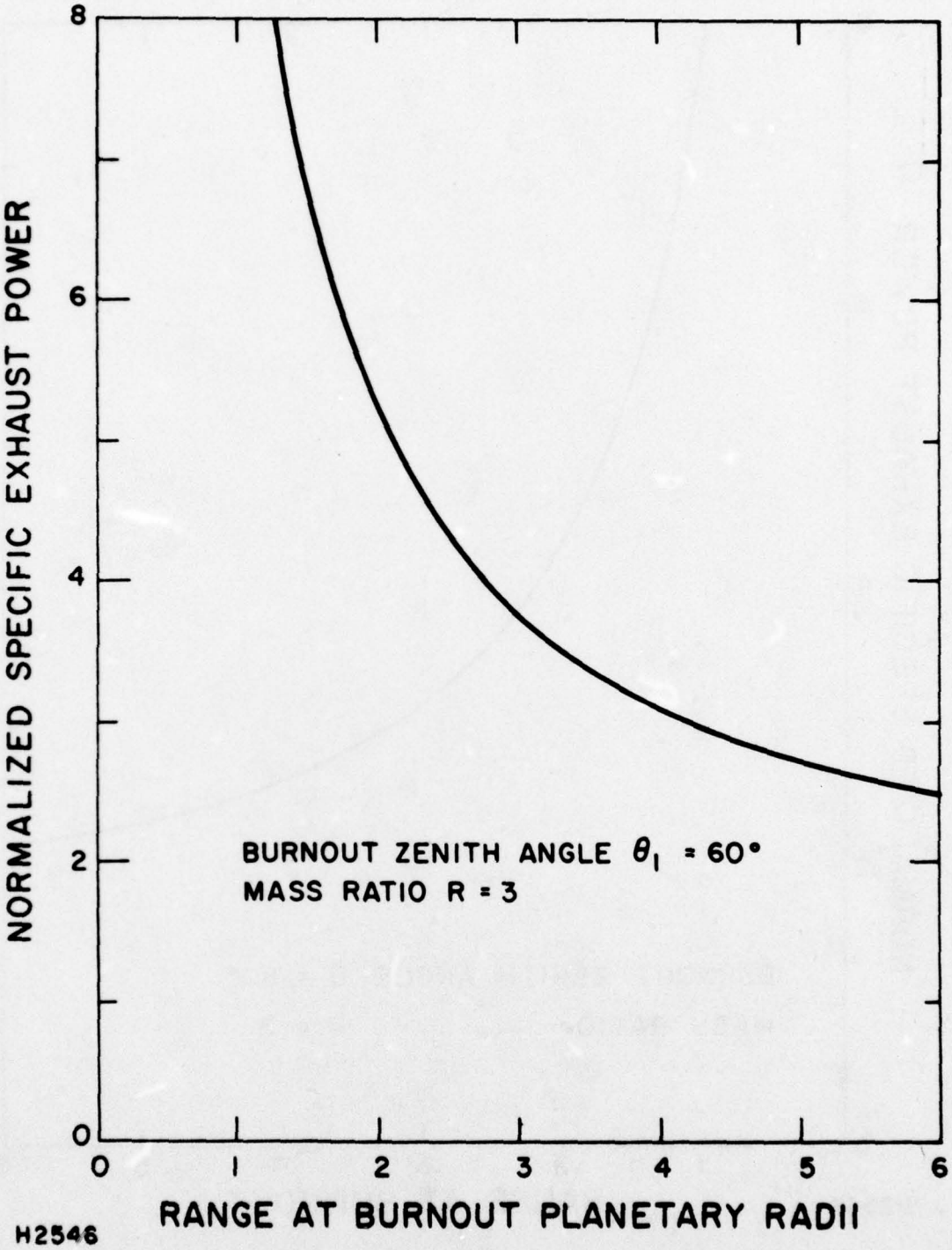

Figure 14 Specific Exhaust Power vs Range

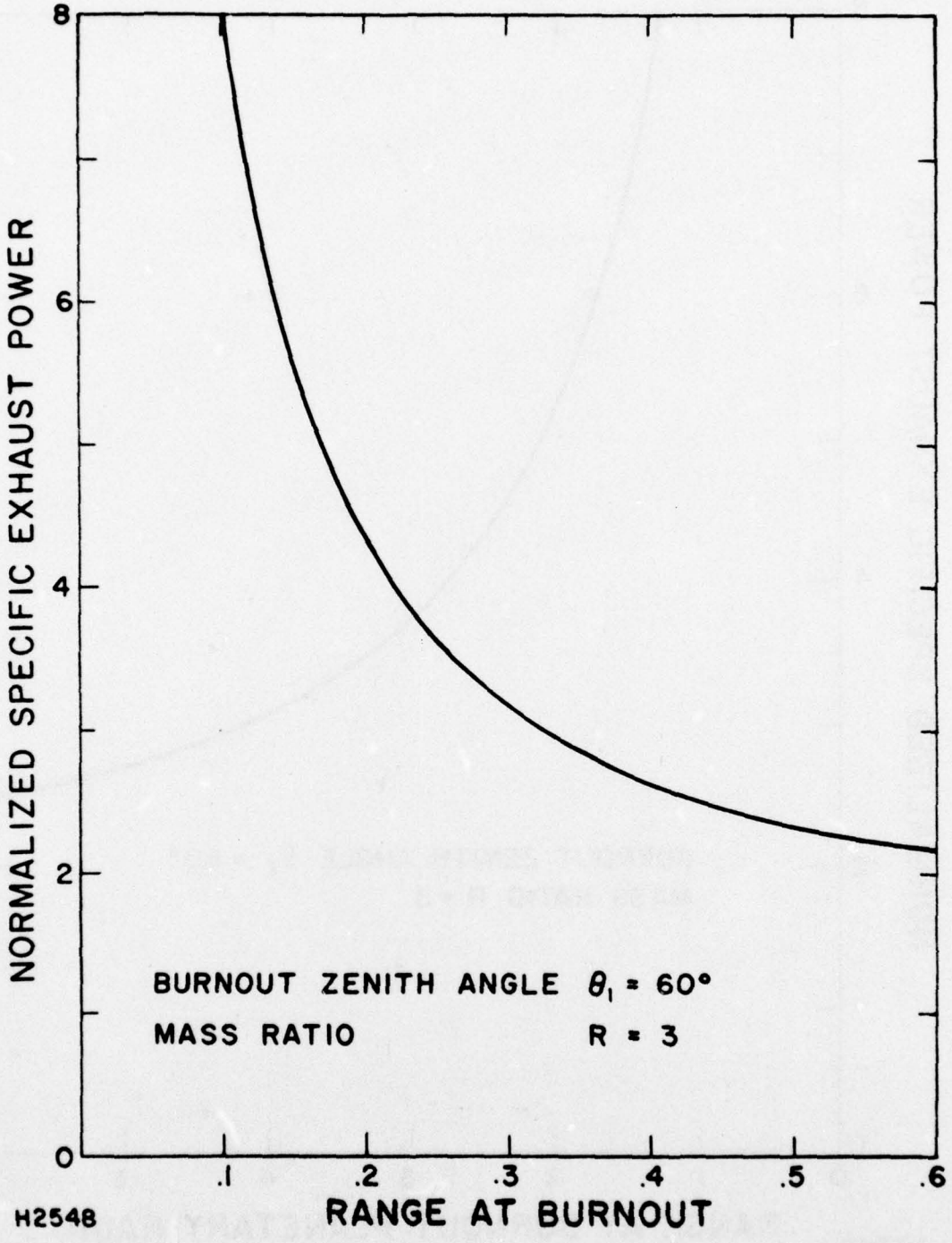

Figure 15 Specific Exhaust Power vs Range

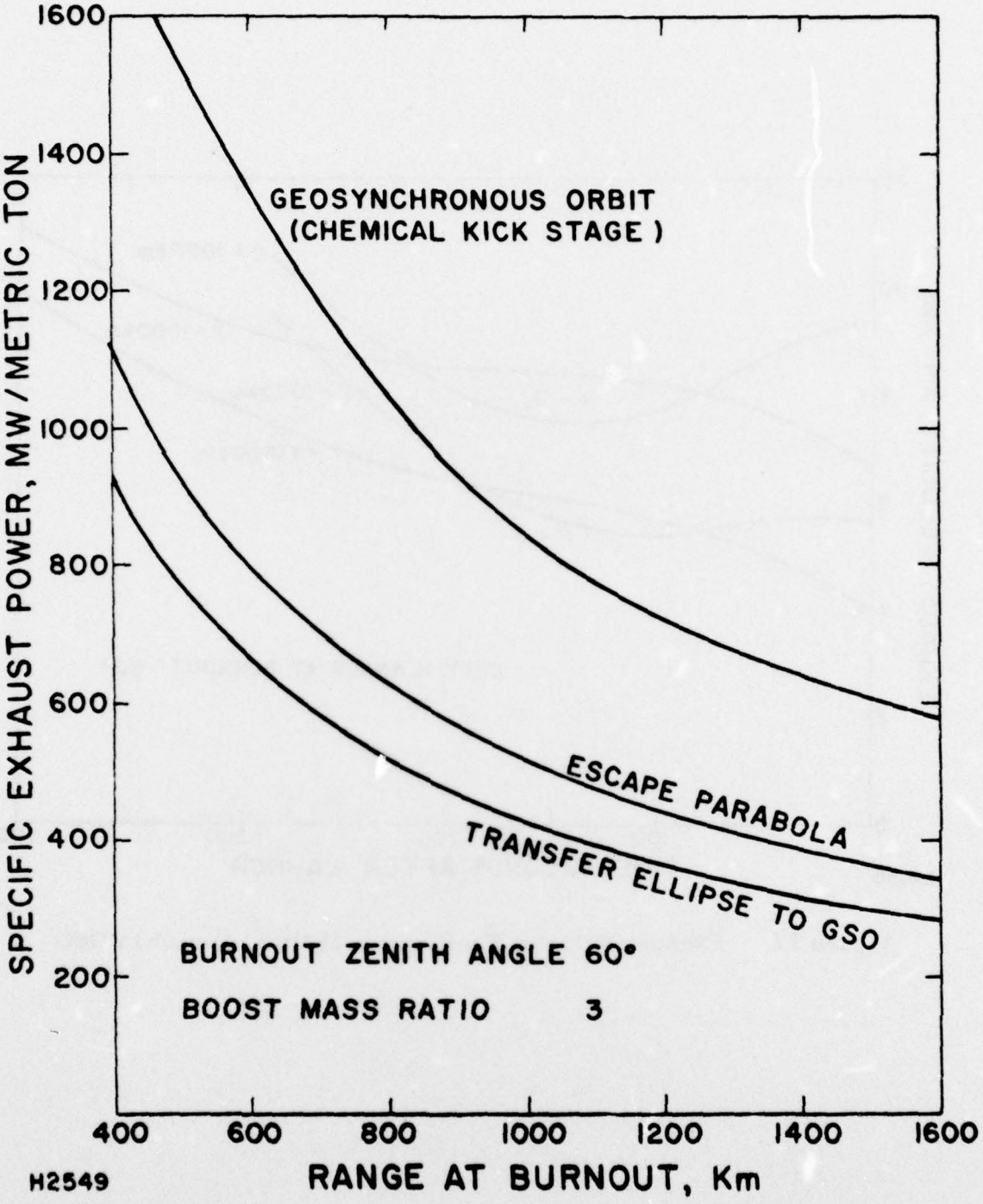

Figure 16 Specific Exhaust Power vs Range

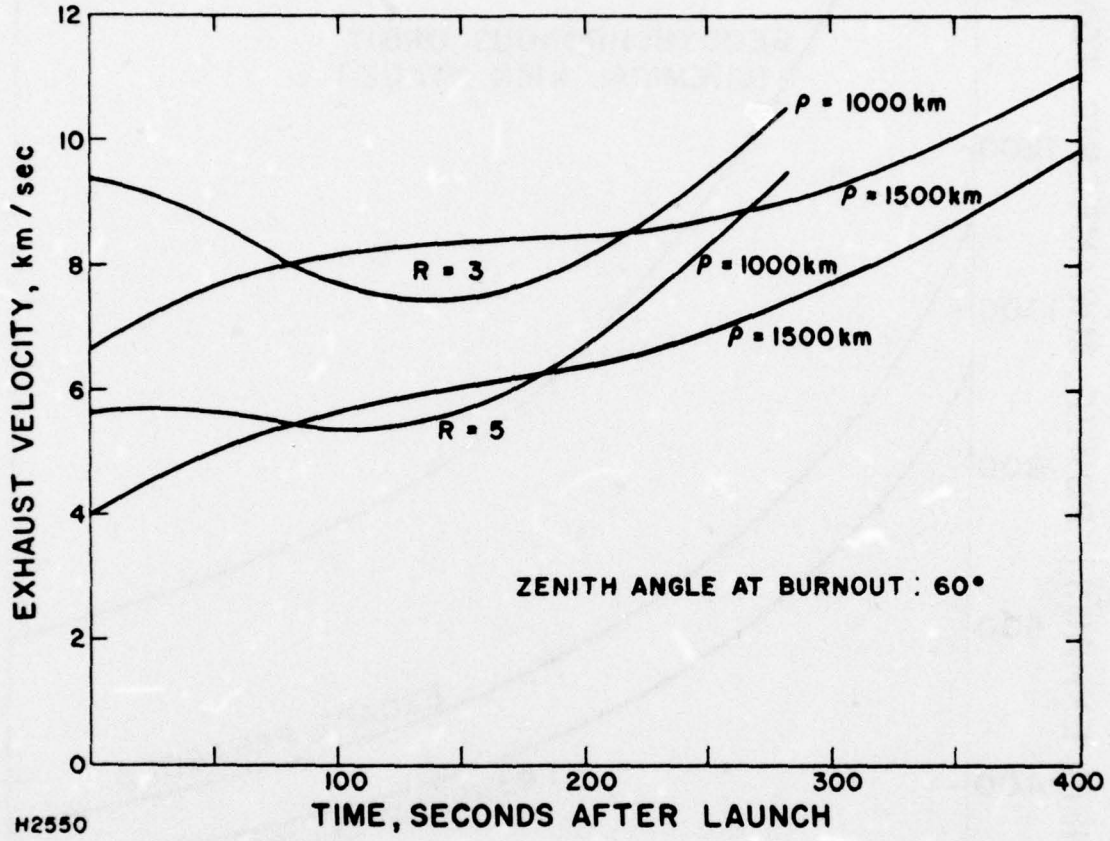

Figure 17 Exhaust Velocity Profiles for Optimal Launch to GSO

where

$$\tan \psi = a_1/a_2 \tag{176}$$

and is given by Eq. (171) and

$$\tan \Theta = x_1/x_2 \tag{177}$$

and may be calculated from Eqs. (164). The variation of the beam thrust angle during boost to a GSO transfer ellipse (with $\Theta_1 = 60^\circ$) is shown in Figure 18, for two ranges at burnout. The excursions of the thrust vector, relative to the laser beam, are relatively small, and could most probably be accomodated in a single-port laser powered rocket engine design.

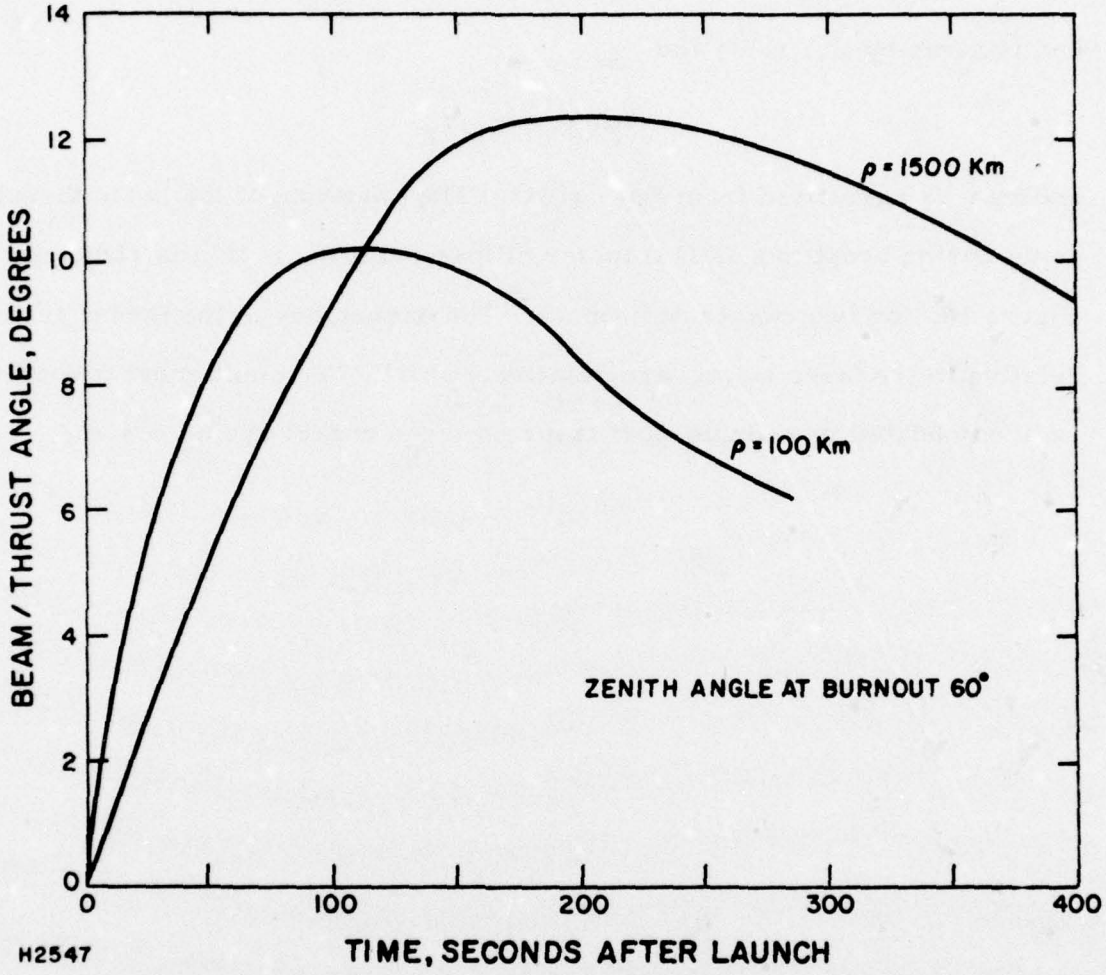

Figure 18 Beam/Thrust Angle History

6. RADIAL-THRUST ASCENT AT CONSTANT EXHAUST VELOCITY

As in the discussion of vertical ascent, it is desirable to investigate the power penalties associated with boost at constant exhaust velocity, as this mode of operation may allow simplifications in engine design. For ascent to high orbit or escape, the relatively small beam/thrust angles found in the previous section suggest that a further simplification may be possible, constraining the thrust axis of the vehicle so that it is always directed radially towards the laser station (i. e., so that the beam/thrust angle remains zero). This mode, which is here called radial-thrust ascent, would permit the simplest possible engine design.

With constant power and exhaust velocity, the relations between specific thrust, mass ratio and boost duration are as obtained in Section II. 4. b. The results are repeated here for convenience

$$a = \frac{a_o}{1 - t/\tau^*} = \frac{C}{\tau^* - t} \tag{178}$$

where

$$\tau^* = c/a \tag{179}$$

$$\tau = \left(\frac{R - 1}{R}\right) \tau^* \tag{180}$$

The equations of motion

$$\ddot{x}_i - a_i - g_i = 0 \tag{181}$$

May be integrated numerically, with the thrust angle ψ taken equal to the instantaneous zenigh angle Θ, so as to satisfy the radial-thrust condition. To facilitate comparison with the optimal ascent calculations of the previous section, only the linear terms in the expansion (2. 115) for the gravitational field are retained in this integration.

It is desirable to plot the results of this calculation with the mass ratio rather than the exhaust velocity as a constant parameter. Successive values of τ^* may be chosen a priori, thereby determining the range at burnout, but it is necessary to choose the exhaust velocity c and the initial direction of thrust ψ_o so that:

1) burnout occurs at the specified zenith angle Θ_f:
2) the vehicle has the injection velocity at burnout given by Eq. (79) for excape or by Eq. (80) for ascent to GSO; and
3) the mass ratio R has a specified value at burnout.

A systematic iterative procedure is essential for solving this two-point boundary value problem. Once R and τ^* are specified, the time step in the Runge-Kutta integration procedure may be chosen as a submultiple of the boost duration, from Eq. (180), ensuring that the routine terminates at the correct time, but the parameters c and ψ_o must be modified in successive integrations. In deriving expressions for corrections to the parameters, in terms of the results of successive integrations of the equations of motion, it is sufficient to use the constant approximation to the gravitational field. We write the equations of motion

$$\ddot{x}_1 - \delta - a \sin \psi = 0 \tag{182a}$$

$$\ddot{x}_2 + 1 - a \cos \psi = 0 \tag{182b}$$

where, for reasons which will appear, we have allowed for a constant component δ of the gravitational field in the x_1-direction. These equations may be converted to integral expressions by introducing a pair of adjoint functions λ_i, as yet unspecified except that they have continuous second derivations with respect to time. Whatever form is given to the λ_i, it is clear that, along the trajectory specified by Eqs. (182), we have

$$\int_0^\tau \left[\lambda_1(\ddot{x}_1 - \delta - a \sin\psi) + \lambda_2(\ddot{x}_2 + 1 - a\cos\psi)\right] dt = 0 \tag{183}$$

Integration by parts of the terms in $\ddot{x}_i$ gives

$$\int_0^{\left[\dot{\lambda}_1 x_\pi + \dot{\lambda}_2 x_2 - a(\lambda_1 \sin\psi \;\; \lambda_2 \cos\psi) - \lambda_1\delta\;\lambda_2\right]} dt$$

$$\left[\lambda_1 v_1 - \dot{\lambda}_1 x_1 \lambda_2 v_2 - \dot{\lambda}_2 x_2\right]\Big|_0^\tau = 0 \tag{184}$$

If now we choose the λ_1 so that they satisfy the simple adjoint equations

$$\ddot{\lambda}_i = 0 \tag{185}$$

then

$$\left[\lambda_i v_1 - \lambda_1 x_1 + \lambda_2 v_2 - \lambda_2 x_2\right]_0^\tau = \int_0^\tau \left[a(\lambda_1 \sin\psi + \lambda_2 \cos\psi) + \lambda_1\delta - \lambda_2\, dt\right] \tag{186}$$

By choice of functions λ_i, satisfying Eq. (185), we may now obtain integral expressions for the burnout values of the components of position and velocity of the vehicle, using the initial conditions $x_i = v_i = o$. With

$$\begin{aligned} \lambda_1 &= \tau - t \\ \lambda_2 &= 0 \end{aligned} \tag{187}$$

we obtain

$$x_1(\tau) = \frac{1}{2}\,\tau^2 + \int_0^\tau a(\tau - t)\sin\psi\, dt \tag{188a}$$

With

$$\begin{aligned} \lambda_1 &= 0 \\ \lambda_2 &= \tau - t \end{aligned} \tag{189}$$

$$x_2(\tau) = -\frac{1}{2}\tau^2 + \int_0^\tau a(\tau - t)\cos\psi \, dt \tag{188b}$$

With

$$\begin{aligned} \lambda_1 &= 1 \\ \lambda_2 &= 0 \end{aligned} \tag{190}$$

$$v_1(\tau) = \delta_\tau + \int_0^\tau a \sin\psi \, dt \tag{191a}$$

With

$$\begin{aligned} \lambda_1 &= 0 \\ \lambda_2 &= 1 \end{aligned} \tag{192}$$

$$v_{2\,1}(\tau) = -\tau + \int_0^\tau a \cos\psi \, dt \tag{191b}$$

The Eqs. (191) for the velocity components at burnout may also be obtained by differentiation of Eq. (188) with respect to τ, or by direct formal integration of the equations of motion (182).

These integral expressions are, of course, valid for any thrust steering law $\psi(t)$. For radial thrust ascent, with given values of c, τ^* and ψ_o, and with $\delta = o$, we have

$$x_1(\tau) = \int_0^\tau a(\tau - t)\sin \quad dt \tag{193a}$$

$$x_2(\tau) = -\frac{1}{2}\tau^2 + \int_0^\tau A(\tau - t)\cos \quad dt \tag{193b}$$

$$v_1(\tau) = \int_0^\tau a \sin\Theta \, dt \tag{194a}$$

$$v_2(\tau) = -\tau + \int_0^\tau a \cos \Theta \, dt \tag{194b}$$

Let us first consider the effect on these terminal quantities of an increase $\Delta\psi_o$ in the initial thrust angle. If we also rotate the coordinate system about the origin by an angle $\Delta\psi_o$, the new trajectory problem, in the new coordinate system, will be physically equivalent to that in the original problem, except that the gravitational field will be transferred to

$$g_i = \begin{bmatrix} \Delta\psi_o \\ -1 \end{bmatrix} \tag{195}$$

to first order in $\Delta\psi_o$. To obtain the first order effect, we may thus write, in Eqs. (188) and (191), $\psi = \Theta + \Delta\psi_o$, to account for the geometric rotation of the trajectory, and $\delta = \Delta\psi_o$, to account for the change in the orientation of the trajectory with respect to the gravitational field. The changes in the terminal position are thus found to be

$$\begin{aligned} \Delta_\psi x_1(\tau) &= \tfrac{1}{2} \Delta\psi_o \tau^2 + \int_0^\tau a(\tau - t) \left[\sin(\Theta + \Delta\psi_o) - \sin\Theta\right] dt \\ &= \Delta\psi_o \left(\tfrac{1}{2}\tau^2 + \int_0^\tau a\,(\tau - t) \cos\Theta \, dt\right) \\ &= \Delta\psi_o \left(\tau^2 + x_2(\tau)\right) \end{aligned} \tag{196a}$$

$$\begin{aligned} \Delta_\psi x_2(\tau) &= \int_0^\tau a\,(\tau - t) \left[\cos(\Theta + \Delta\psi_o) - \cos\Theta\right] dt \\ &= -\Delta\psi_o \int_0^\tau a\,(\tau - t) \sin\Theta \, dt \\ &= -\Delta\psi_o \, x_1(\tau) \end{aligned} \tag{196b}$$

The changes in the velocity components at burnout may similarly be calculated as

$$\Delta\psi v_1(\tau) = \Delta\psi_o \left[\tau + \int_o^\tau a \cos\Theta \, dt\right]$$
$$= \Delta\psi_o \left[2\tau + v_2(\tau)\right] \tag{197a}$$

$$\Delta_\psi v_2(\tau) = -\Delta\psi_o \int_o^\tau a \sin\Theta \, dt$$
$$= -\Delta\psi_o \, v_1(\tau) \tag{197b}$$

The changes in the terminal conditions due to a change ΔC in the exhaust velocity may be calculated simply from Eqs. (193) and (194). For example, sin using Eq. (178) in Eq. (193a), we have immediately

$$\Delta_c x_1(\tau) = \Delta c \int_o^\tau \frac{\tau - t}{\tau^* - t} \sin\Theta \, dt$$

$$= \frac{\Delta c}{c} \int_o^\tau a\,(\tau - t) \sin\Theta \, dt \tag{198a}$$

$$= \frac{\Delta c}{c} \, x_1(\tau)$$

Similarly

$$\Delta_c x_2(\tau) = \frac{\Delta c}{c} \, \frac{1}{2} \, \tau^2 + x_2(\tau) \tag{198b}$$

$$\Delta c v_1(\tau) = \frac{\Delta c}{c} \, v_1(\tau) \tag{199a}$$

$$\Delta_c v_1(\tau) = \frac{\Delta c}{c} \, (\tau + v_2(\tau)) \tag{199b}$$

Adding together the changes in the components of terminal position and velocity due to changes in the initial thrust angle ψ_o and the exhaust velocity c, we find

$$\Delta x_1(\tau) = \Delta\psi_o\,(\tau^2 + x_2(\tau)) + \frac{\Delta c}{c}\,x_1(\tau) \tag{200a}$$

$$\Delta x_2(\tau) = -\Delta\psi_o\,x_1(\tau) + \frac{\Delta c}{c}\,(\tfrac{1}{2}\,\tau^2 + x_2(\tau)) \tag{200b}$$

$$\Delta v_1(\tau) = \Delta\psi_o\,(2\tau + v_2(\tau)) + \frac{\Delta c}{c}\,v_1(\tau) \tag{200c}$$

$$\Delta v_2(\tau) = -\Delta\psi_o\,v_1(\tau) + \frac{\Delta c}{c}\,(\tau + v_2(\tau)) \tag{200d}$$

In order to find an iteration procedure to ensure that, at the burnout time τ (given by Eq. (180)) the vehicle is at the specified zenith angle Θ, and has the specified velocity V_1, we must find expressions for the changes in these quantities with changes in the components of position and velocity at burnout.

Since

$$\tan\Theta(\tau) = x_1(\tau)/x_2(\tau) \tag{201}$$

$$\Delta\Theta(\tau) = \frac{1}{\rho(\tau)}\left[\cos\Theta\,\Delta x_1 - \sin\Theta\,\Delta x_2\right]$$

$$= \Delta\psi_o\left[\frac{\tau^2\cos\Theta_1}{\rho_1}\;\frac{x_2\cos\Theta_1}{\rho_1}\;\frac{x_1\sin\Theta}{\rho_1}\right]$$

$$\frac{\Delta c}{c}\left[\frac{x_1}{\rho_1}\cos\Theta - \frac{1}{2}\,\frac{\tau^2}{\rho_1}\sin\Theta - \frac{x_2\sin\Theta}{\rho_1}\right] \tag{202}$$

$$\Delta\psi_o\left[1 + \frac{\tau^2\cos\Theta_1}{\rho_1}\right] - \frac{\Delta c}{2c}\,\frac{\tau^2}{\rho_1}\sin\Theta_1$$

since

$$x_1(\tau) = \rho_1\sin\Theta_1, \text{ etc.}$$

since

$$V_x^2(\tau) = v_1^2(\tau) + v_2^2(\tau) \tag{203}$$

$$\begin{aligned}\Delta V(\tau) &= \Delta v_1(\tau) \sin\gamma(\tau) + \Delta v_2(\tau) \cos\gamma(\tau) \\ &= \Delta\psi_o (2\tau \sin\gamma_1 + v_2 \sin\gamma_1 - v_1 \cos\gamma_1) \\ &\quad \frac{\Delta c}{c} (v_1 \sin\gamma_1 + \tau\cos\gamma_1 - v_2 \cos\gamma_1) \\ &= \Delta\psi_o (2\tau \sin\gamma_1) + \frac{\Delta c}{c} (V_1 - \cos\gamma_1)\end{aligned} \tag{204}$$

since

$$v_1(\tau) = V(\tau) \sin\gamma(\tau), \text{ etc.}$$

We have thus finally found the changes in the burnout zenith angle and velocity, which may be summarized in the equation

$$\begin{bmatrix} \Delta\Theta(\tau) \\ \Delta V(\tau) \end{bmatrix} = \begin{bmatrix} 1 + \frac{\tau^2}{\rho}\cos\Theta & \frac{-\tau^2}{2\rho c}\sin\Theta \\ 2\tau \sin\gamma & \frac{1}{c}(V + \tau\cos\gamma \end{bmatrix} \begin{bmatrix} \Delta\psi_o \\ \Delta c \end{bmatrix} \tag{205}$$

The integration of the equations of motion now proceeds as follows:

1) The value of R and the burnout zenith angle Θ, are specified.

2) A value of τ^* is chosen. This will fix the range at burnout, which is not know a priori.

3) The boost duration τ is calculated from Eq. (180).

4) A preliminary guess is made for the values of c and ψ_o.

5) The equations of motion

$$\begin{aligned} x_1 &= a \sin\Theta \\ x_2 &= a\cos\Theta - 1 \end{aligned} \tag{206a}$$

are integrated by the 4th order Runge-Kutta method, using a fairly large step size h which is a submultiple of τ; the integration terminates when $t = \tau$.

6) The values of range and flight path angle found at the termination of the integration are used to calculate an estimate of the desired mission velocity V_1, using Eq. (105) or Eq. (106). The difference between this and the actual velocity computed in the integration gives ΔV, on the left hand side of Eq. (205), and the difference between the chosen Θ_1 and the terminal zenith angle found in the integration gives $\Delta\Theta$.

7) The matrix of coefficients in Eq. (205) is calculated using the desired value of Θ, the boost duration found in step 3), the estimate of the mission velocity V_1 from step 6), and the values of ρ and γ found in the integration.

8) The Eqs. (205) are inverted to give corrections to c and ψ_o.

9) The process is repeated until the errors in Θ_1 and V_1 are as small as desired. The step-size in the Runge-Kutta integration is reduced in later iterations to give increasing accuracy, while keeping it a submultiple of τ.

This iteration process has generally been found to be convergent. In cases where it is not, the initial guesses for c and ψ_o can usually be improved by inspection of the integration results, sufficiently to reach estimates from which the calculation converges.

a. Radial-Thrust Ascent to a Transfer Ellipse to GSO

Once the equations of motion have been integrated, the specific exhaust power is found most readily from Eqs. (3) and (178) as

$$P/m_1 = \frac{1}{2} a_1 c = \frac{1}{2} \frac{c^2}{(\tau^* - t)} \tag{207}$$

The integration program has to date only been carried through for the case of launch to a transfer ellipse to GSO. With a mass ratio of 3 and a burnout zenith angle of 60^{o}, the calculated exhaust power per unit burnout mass for this case varies with range at burnout as shown in Figure 19. Also shown in the figure is the optimal specific exhaust power, from Figure 16.

It appears that radial thrust ascent to a transfer ellipse to GSO exacts quite insignificant laser power penalties, compared to the power optimal case. This result may have very significant implications for the simplified design of laser-powered rocket engines for this class of mission.

The power penalties arising from the need to boost a kick-stage for circularization at geosynchronous altitude will of course, be the same for radial-thrust ascent as for the power optimal case, so the discussion leading to Figure 16 is not repeated here.

The exhaust velocity required to give a specified mass ratio, as a function of the range at burnout, is also obtained in the integration routine. The results are shown in Figure 20, for mass ratios of 3 and 5.

It was shown in Section II. 3 that, when the mass of propellant tankage is taken into account, the exhaust power per unit payload is minimized by using a mass ratio in the range 3 to 5, at least for acceleration in field-free space (Figure 1). Minimization of the boost energy requirements (Figure 2) requires slightly lower mass ratios. It appears that a mass ratio of 3 is a good compromise.

It would be useful to compute curves of specific exhaust power vs mass ratio (including the tankage effects) for specific missions, taking into account gravity losses. An example would be a set of curves analogous to Figure 1 for launch to a transfer ellipse to GSO, with a burnout range of

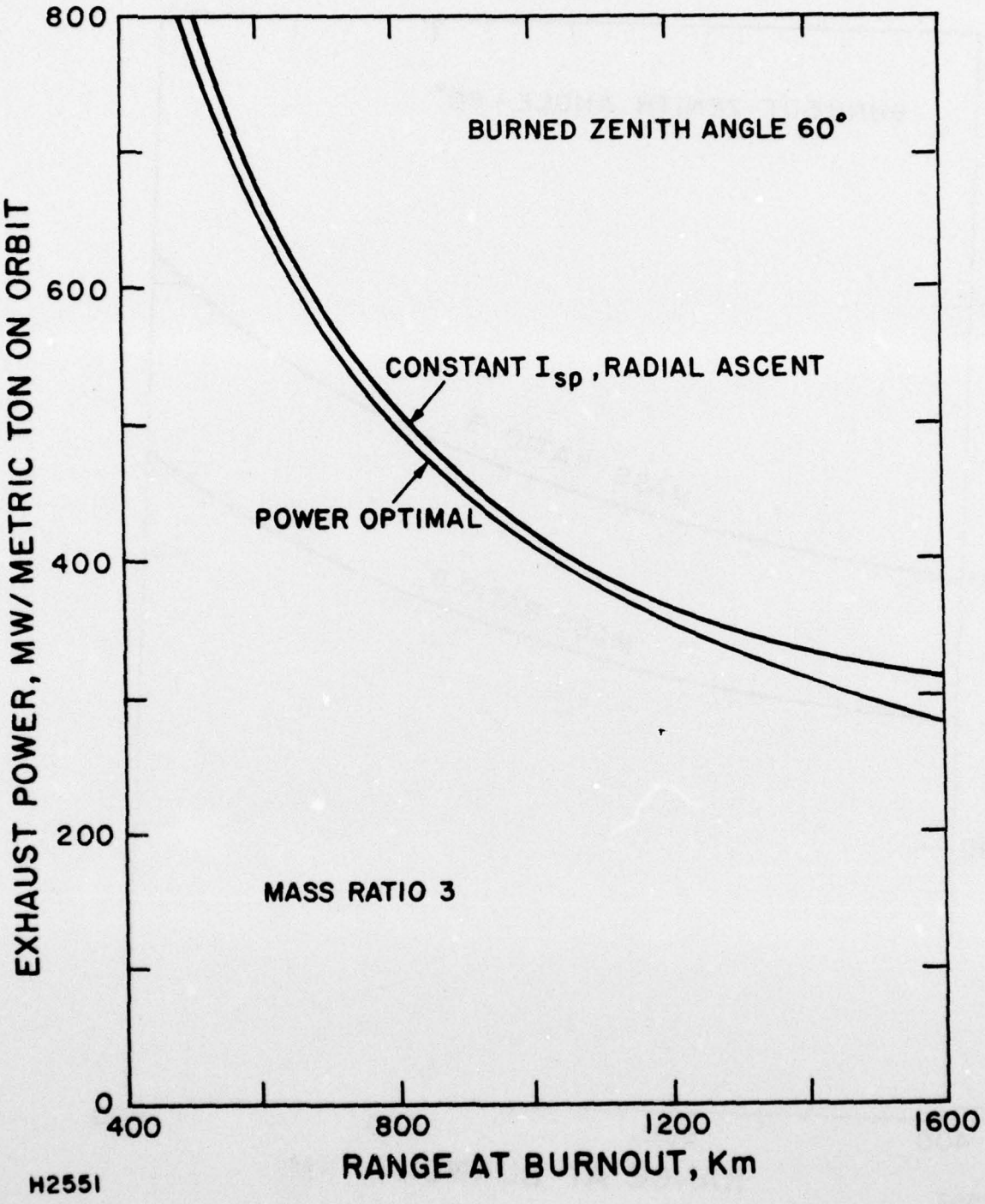

Figure 19 Power Required for Launch to GSO

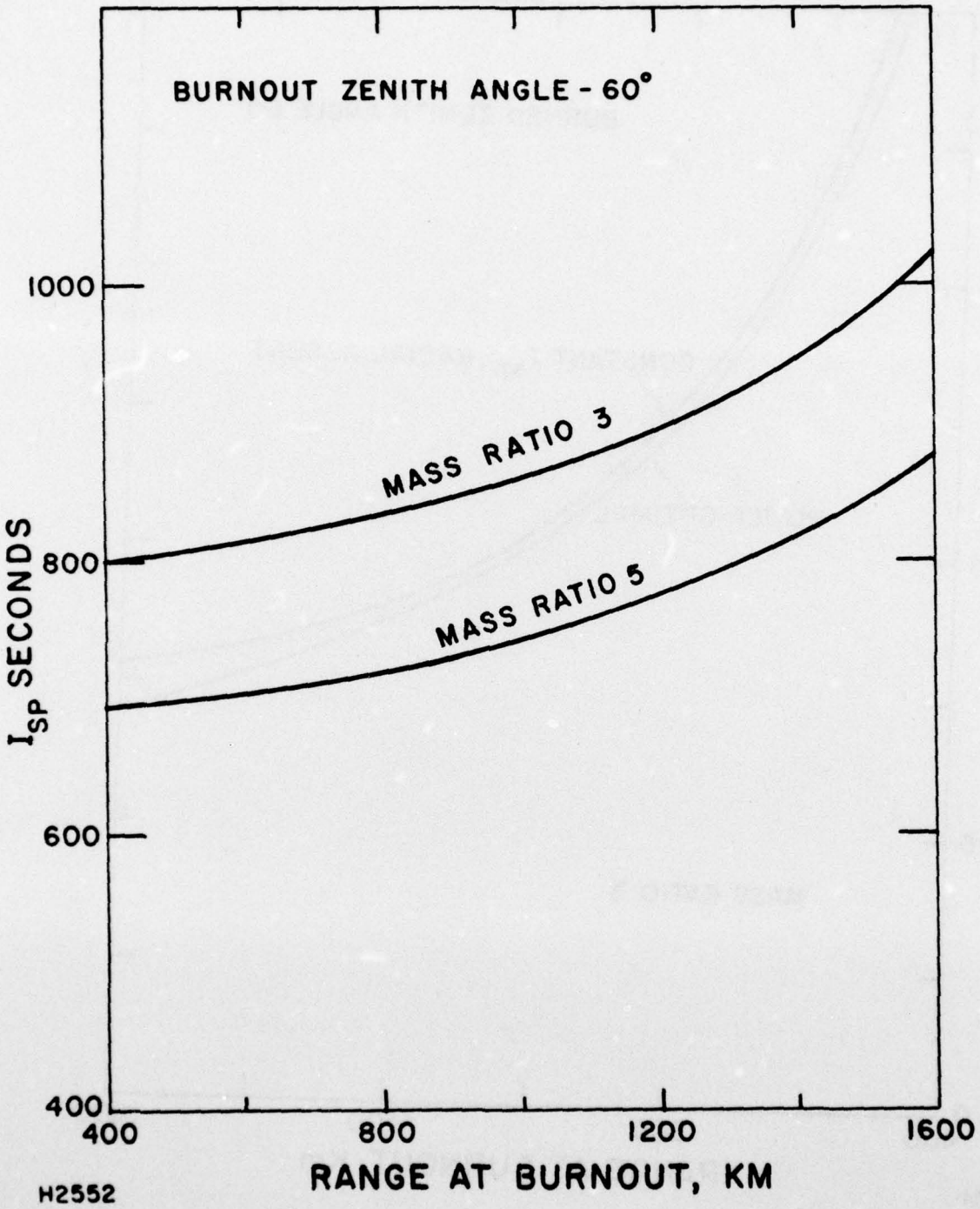

Figure 20 Specific Impulse for Launch to GSO

of 1000 km and zenith angle of 60°. However, it is not expected that the conclusion regarding the optimal mass ratio would vary very much from the field-free case.

It is clear from Figure 19 that the range at burnout should be maximized. For vehicles with payloads, of order one ton, it is probably that a practical upper limit to the range at burnout will be around 1000 km (because of the laser beamspread which may be achieved and the probably physical size of vehicles in this payload class). About 400 MW of exhaust power will be required for every ton injected to the transfer ellipse. After taking into account for the expected engine efficiency and absorption of the laser beam in the atmosphere, about 900 MW of laser output power may be required for each injected ton. The laser output power required for each ton finally in GSO may be up to a factor of two higher, depending on the circularization technique which is used. With a burnout range of 1000 km, in order to give a boost mass ratio of 3, Figure 20 suggest a design specific impulse for the engine of about 850 sec.

7. CONCLUSIONS AND DIRECTIONS FOR FUTURE WORK

The curves showing specific exhaust power requirements for laser-powered launch to high orbit or escape which have been derived in this study provide data needed both in the preliminary technical design of a launching laser and in formulation of economic estimates for the system. These data can be used directly in further tradeoff studies, aimed at determining, for example, the cost-optimum vehicle size in terms of a specified traffic model.

Perhaps the most significant result which has been obtained is the discovery that operation of laser-powered launch vehicles at constant specific

impulse imposes quite small power penalties compared to the power-optimal ascent profile - at least, for the missions which have been examined so far. Furthermore, for these missions, operation at zero beam-thrust angle appears to be feasible.

The particular values obtained of the required specific impulse for these missions (especially launch to GSO) are of immediate importance, providing design goals for near-term laboratory-scale experiments. It is expected that, when radial-thrust launch to escape has been evaluated, it will be found that the specific impulse objective will be below 1000 secs for any reasonable Earth launch mission.

The solution to the power-optimal ascent trajectory problem which has been developed here may readily be extended to other missions, some of which will be described in a later report. It is clear that there are a great many interesting and potentially significant missions for launching lasers which need analysis of the type presented here, in order to evaluate the overall utility of this propulsion technique and to provide priorities amongst goals for laboratory experiments. Some areas of current and future work in mission analysis for launching lasers are the following:

1) More detailed analysis of radial-thrust constant-Isp ascent to a transfer ellipse to GSO, including evaluation of atmospheric drag effects and calculation of angle of attack, aerodynamic stagnation pressure, and laser-beam slew rate histories.
2) Extension of the results obtained so far to radial-thrust launch to escape, in particular to allow calculation of specific impulse vs burnout zenith angle.
3) For ascent to GSO, solution of the problem of choosing the thrust history during boost (and hence the launch trajectory) so as to

minimize the boost exhaust power per unit mass finally established in GSO, as a function of the specific impulse of the circularization kick stage.

4) Comparative evaluation of several techniques for circularization of a transfer ellipse at geosynchronous altitude, including conventional chemical or electric propulsion kick stages, laser-powered kick stages with either the laser or a redirecting mirror in GSO, and the use of small (laser or conventionally powered) tugs which depart GSO to rendezvous and dock with payloads on ascent trajectories.

5) Power-optimal and constant-Isp boost trajectories leading to transfer ellipses to GSO having exoatmospheric perigees, to avoid impacting the EARTH in the event of a failure to circularize at apogee.

6) Extension of these results to derive the minimum specific exhaust power (for given burnout range and zenith angle) required for injection to an elliptical orbit with exoatmospheric perigee, as a function of the apogee radius of the orbit.

7) Power-optimal and constant-Isp, constant beam-thrust angle trajectories for injection to low Earth orbit at the burnout altitude. Effects on such trajectories of aerodynamic constraints such as limits to allowable angles of attack.

8) Energy-optimal rather than power-optimal ascent trajectories. As noted in Section II. 3, energy-optimal trajectories, in addition to minimizing operational costs, also minimize the laser power requirements (and hence capital cost) for a given throughput to orbit, in the high utilization limit.

9) Laser propulsion for transfer from LEO to GSO, with variations depending on whether the laser is located on Earth or in low, intermediate or high orbit, and on whether mirrors in orbit may be used to redirect the laser radiation.

10) Evaluation of laser propulsion for more advanced missions - for example, to power a ferry operating between the lunar surface and lunar orbit.

11) Studies of laser launchers in the context of particular mission models concerned with large-scale military or industrial uses of space.

SECTION III

LASER DRIVEN DETONATION WAVE ROCKET ENGINE

1. INTRODUCTION

A high specific impulse laser propulsion engine must meet a number of stringent conditions. The propellant must absorb the laser energy directly and essentially completely at temperatures that are above the dissociation energy of most molecular absorbers. The hot propellant gas must be efficiently expanded to roughly uniform velocity in a manner that does not exceed the thermal limits of materials. The incident flux needs to be compatible with atmospheric transmission limitations imposed by thermal blooming and aerosol induced plasma breakdown. In addition it is highly desirable that the engine be characterized by economical simplicity and flexibility. The latter virtue would include the ability to operate over a range of specific impulses and power levels, at a variety of beam thrust angles, and with back pressure ranging between atmospheric at launch to hard vacuum at burnout.

This section describes a new repetitively pulsed laser propulsion concept that promises to meet the above requirements. Absorption of the laser radiation is based on the inverse Bremsstrahlung process that occurs in a laser driven detonation wave (LSD). A wide variety of propellant materials may be used without the addition of special absorber seedants. It will be shown that the atomic or molecular weight of the propellant is, to the first order, immaterial to the absorption and subsequent expansion processes and does not affect the resultant specific impulse and efficiency figures. The expansion of the hot gases takes place without benefit of a throat, which is the

point of the most severe thermal loads in conventional rockets. Indeed sufficient data exists from pulsed laser effects studies to predict that thermal loads will pose few problems for this engine.

2. PRINCIPLE OF OPERATION

The basic throatless detonation rocket engine is comprised of a circular thrust disk or base situated at one end of a cylindrical surface which will be termed the "1-D skirt." The thrust disk is suitably perforated to allow the introduction of propellant, or else is formed by the surface of a solid propellant that may be ablated to release propellant gas.

The engine cycle may be divided into two basic phases illustrated in Figure 21. Firstly, propellant is introduced at the thrust disk in a manner such that, at the end of Phase I, a distribution of gaseous propellant extends to a characteristic distance, ℓ_o, from the disk. There are a number of possible methods for introducing the propellant. For instance, a laser pulse could be used to ablate a solid propellant, one end of which forms the thrust disk; or the pulse could evaporate a liquid film introduced through a porous disk. Because of its simplicity and flexibility, laser metering of the propellant will be examined in some detail in Section III.4. Other possible methods of injection not involving a laser pulse include injection of an aerosol, which is organized in Appendix B and self regulating gas phase feed discussed in Section III.5.

The distributed propellant gas is heated to high temperature during the thrust pulse of Phase II. A ground or space based laser beam is aimed at the thrust disk. It is assumed that the propellant gas is initially transparent to the incident pulse so that it strikes the thrust disk before significant absorption occurs in the gas. Experiments have shown that a number

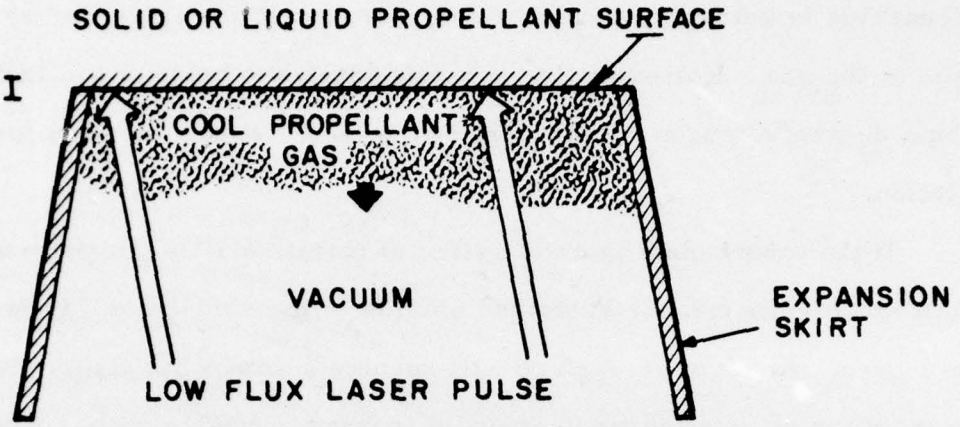

STEP I: A LOW FLUX LASER PULSE ABLATES A MEASURED AMOUNT OF PROPELLANT GAS FROM A SOLID PROPELLANT SURFACE OR FROM A LIQUID FILM ON A POROUS PLATE.

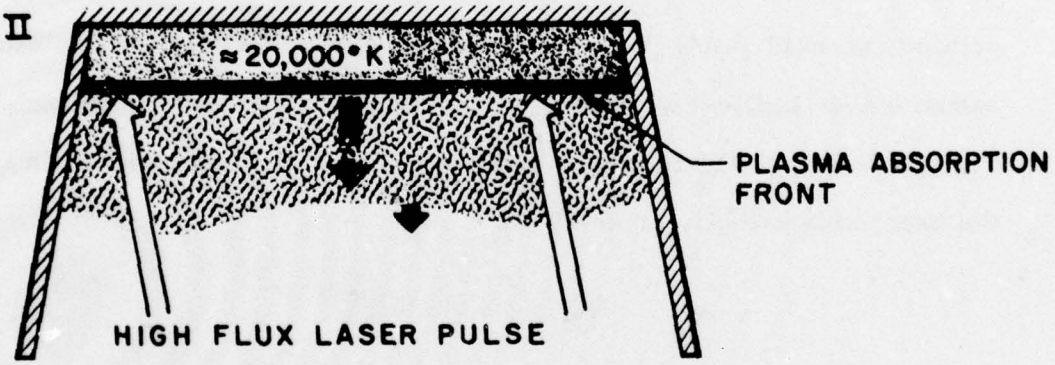

STEP II: A HIGH FLUX PULSE IGNITES A LASER SUSTAINED DETONATION WAVE AT THE SURFACE. A FRONT OF HIGHLY ABSORBING PLASMA, WHICH SHIELDS THE SURFACE FROM FURTHER LASER RADIATION, PROPAGATES BACK TOWARDS THE LASER, HEATING THE GAS PROPELLANT TO ≈ 20,000 °K. THE BEAM IS TURNED OFF WHEN THE FRONT HAS PASSED THROUGH MOST OF THE GAS. THE CYCLE IS REPEATED AFTER THE HOT GASES HAVE EXPANDED.

G9334

Figure 21 Laser Sustained Detonation Wave Rocket Engine

of candidate propellants, such as N_2, will meet this requirement if the incident flux is below the threshold for plasma ignition triggered by particulates in the gas. For example, if particulates are below 5 μm in diameter, normal density nitrogen will transmit up to $\sim 10^8$ W/cm^2 of 10.6 μm radiation.

If the thrust plate is constructed of metal, a 10.6 μm pulse at 10^7 W/cm^2 will ignite a laser sustained plasma at the surface in a time of less than 1 μsec. An ablative surface will require a somewhat higher flux. The threshold for plasma ignition generally increases weakly with increased gas pressure and decreasing wavelength.

The resulting plasma front will propagate through the gas away from plate toward the laser beam source. If the incident flux is above the appropriate threshold value, the plasma is propagated as a Laser Sustained Detonation Wave (LSD) which was first described by Raizer.[1] In such a wave a region of essentially complete inverse Bremsstrahlung absorption travels up the beam at a velocity given by V_D

$$V_D = \left[2(\gamma^2-1)\,\frac{\phi}{\rho}\right]^{1/3} \tag{208}$$

with ϕ denoting the laser flux, ρ the gas density, and γ the effective adiabatic constant [which proves to be ~ 1.2 for the high temperature gases of interest]. In terms of parameter values that will be useful in latter discussions, Eq. (208) is

$$V_D = 4.0 \times 10^5 \left(\frac{\phi_7}{\rho_N}\right)^{1/3} \quad \text{cm/sec} \tag{209}$$

---

(1) Raizer, Y. P., "Heating of a Gas by a Powerful Light Pulse," Sov. Phys. JETP 21, 1009 (1965).

with ϕ_7 denoting the flux units of 10^7 W/cm^2 and ρ_N the density in terms of normal density, 1.2×10^{-3} g/cm^3. The value $\gamma = 1.18$, appropriate for normal density nitrogen, has been used.

For one dimensional laser beams, the threshold for maintenance of a detonation wave at 10.6 μ wavelength has been calculated[2] to be $\sim 5 \times 10^6$ W/cm^2 at standard density. At 1/10 standard density the threshold is below 10^7 W/cm^2. A standard density threshold of 2×10^8 W/cm^2 is predicted at 1.06 μm wavelength, and verified by experiment. If the incident flux is below threshold, a partially absorbing wave may still be propagated, but undesirable strong thermal coupling to the base will occur.

For finite diameter beams, these thresholds are increased to flux levels that give an absorption length on the order of the beam diameter. However, the plasma is contained within the 1-D skirt in this rocket concept, and the fluid dynamics should thus behave as though the beam was of infinite diameter. A more stringent requirement of the flux level demands that the absorption length within the plasma be small compared to the total distance travelled by the detonation wave through the predispersed propellant. This assures not only that the time independent detonation wave is appropriate, but also guards against significant amounts of the laser energy being deposited directly on the rocket base material. A scaling law for the absorption length, L, has been given in Reference 3,

$$L = \frac{5}{\phi_7^4} \left(\frac{\rho_N}{\lambda_{10.6}} \right)^2 \qquad (210)$$

---

(2) Edwards, A., Ferriter, N., Fleck, Jr. J. A., and Winslow, A. M., "A Theoretical Description of the Interaction of a Pulsed Lase, and a Target in an Air Environment," Lawrence Livermore Laboratory, Rept. UCRL - 51489 (1973).

(3) Boni, A. A. and Su, F. Y., "Theoretical Study of Laser Target Interactions," Science Applications Inc. Rept. SA177-567LJ (1977).

for

$$0.4 \leq \phi_7/\rho_N \leq 20 \tag{211}$$

where L is in cm and $\lambda_{10.6}$ is the wavelength normalized to 10.6 μ.

If the incident flux is well above threshold, such that the plasma absorption length is much less than the total detonation wave travel only a small fraction of the incident pulse energy will be absorbed by the thrust plate due to either direct absorption of the flux, reradiation from the plasma, or contact with the hot gas. Experimental measurements using aluminum plates that absorbed 2.5% of a 25 μsec, 10.6 μ beam at low power showed that the thermal coupling drops to 0.7% upon the initiation of a detonation wave in normal air at 2×10^7 W/cm^2. For a rocket operating at 10^9 W and with a 2 m diameter thrust plate, this represents an average thermal loading of 223 W/cm^2 which can readily be handled with feed of propellant through a porous plate. The thermal coupling to ablative plates is expected to be as small. Figure 22 shows a lucite plate that has been irradiated at $\sim 2 \times 10^7$ W/cm^2 for 15 μsec at 10.6 μ giving a fluence of $\sim$330 J/cm^2. The unablated areas are sites of detonation wave ignition which were first shielded from the incoming flux. Since the known threshold for ablation at this pulse length is 3 -4 J/cm^2 only $\sim$1% of the incident fluence was coupled at the ignition sites. The cracks were caused by the pressure impulse. Proper shielding demands a high density of ignition sites which perhaps could be provided by dispersion of a fine metallic powder throughout the solid.

After a time τ_p, when the absorption front has traveled a distance ℓ_o through the propellant gas, the laser pulse is turned off. This leaves a mass of extremely hot gas heated under well controlled and well understood

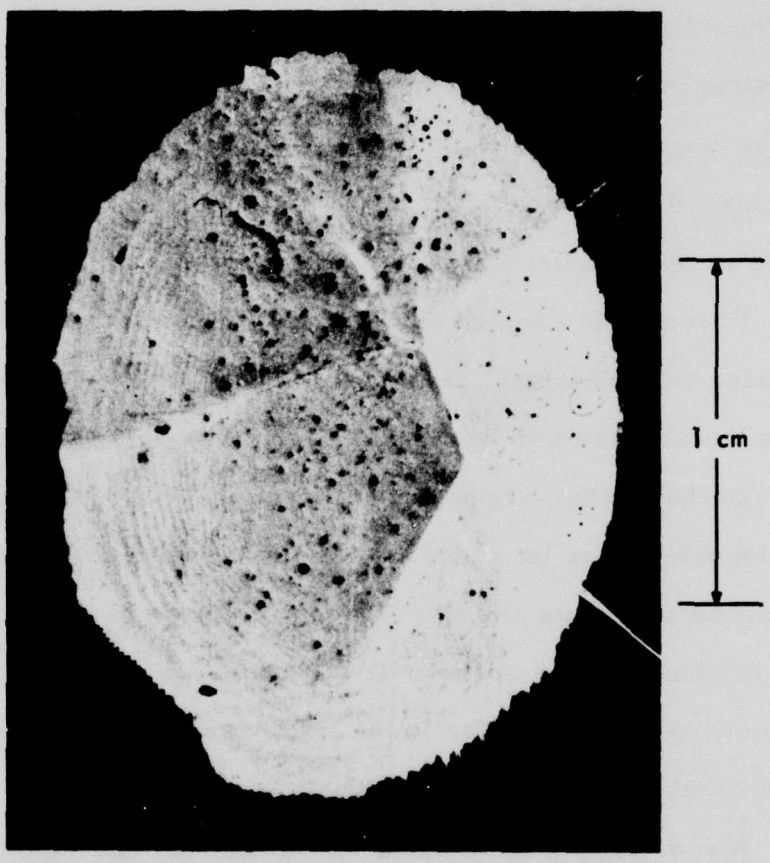

FLUENCE 330 J/cm^2 (15 μsec, 2 x 10^7 w/cm^2)

DAMAGE THRESHOLD 3 – 4J/cm^2

G7102

Figure 22 Plasma Shielded Ignition Sites on Lucite Target

conditions. Since the power absorbed per unit area is ϕ, which is proportional to ρV_D^3 by Eq. (209), and the mass overrun per unit area-time is ρV_D, then the total energy per unit mass initially imparted to the fluid is proportional to V_D^2. This is independent of the atomic mass and other detailed properties of the propellant. Not surprisingly, the effective exhaust velocities will be shown to be on the order of V_D, which is practically obtainable in the 10 km/sec range.

Pressure is exerted on the thrust plate while the laser pulse is on and during the subsequent expansion. The 1-D skirt serves to partially confine the expansion to one dimension, maintaining the pressure for longer times and thus improving the specific impulse and efficiency over what would be obtained in its absence. The velocity of the exhaust products is not constant with time and this is a basic source of inefficiency in comparison with a conventional cw rocket. It will be shown, however, that the dominant source of inefficiency is due to the finite propellant expansion that can be achieved with 1-D skirts of reasonable lengths.

A coasting period follows the expansion. For typical designs this phase is an order of magnitude longer than the sum of the other two phases. The exhaust products are largely dissipated or displaced during this period, allowing for incidence of the next laser pulse without undue absorption in the plume.

3. ANALYSIS OF PERFORMANCE

This section will examine in detail the laser ablation method of providing gaseous atmosphere of propellant at the base of the vehicle. The principle advantage of this technique is that no onboard values, nozzles etc. are required, which results in obvious weight and cost savings. In addition,

the method is quite flexible in that the amount of propellant released, as well as its spatial distribution is simple, varied by changing the characteristics of the ground based laser pulse.

An analysis of the Laser Driven Detonation Rocket may be given with various degrees of sophistication up to large scale fluid codes. In this section a first order approach to the problem is presented. Employing a number of simplifying assumptions, an analytic prediction of performance is given in terms of a nondimensional impulse parameter, f. A numerical calculation based on the method of characteristics for unsteady flow in one dimension is then used to determine the impulse parameter as a function of the 1-D skirt length.

Only operation in vacuum will be described in this section. For earth launch to orbit, typically greater than 90% of the laser thrusting will be effectively under this condition. For simplicity, the initial density will be taken as a constant, ρ_o, across the disk out to a distance, ℓ_o, from the base and zero beyond that. Section III. 4 will show that reasonable approximations to this distribution can be achieved.

The laser thrust pulse will be turned on for a time τ_L, illuminating the rocket base uniformly in space and time at a flux level ϕ_o. A detonation wave is assumed to ignite instantaneously at the thrust plate the moment the laser is turned on. The detonation velocity is constant since ρ and ϕ are constant. The laser is turned off when the wave travels distance $\ell_o = V_D \tau_L$. Initially, the 1-D skirt length will be taken as much longer than ℓ_o so that all the hydrodynamic processes may be treated as one dimensional.

Immediately behind the detonation front the pressure, p_D, and density, ρ_D, according to Raizer, are given by

$$p_D = \frac{\rho_o}{\gamma + 1} V_D^2$$

$$\rho_D = \frac{\gamma + 1}{\gamma} \rho_o \tag{212}$$

Since the thrust plate is neither a source nor sink for gas during the pulse, the fluid velocity must be zero there. It was shown by Pirri, in a study of impulsive laser target effects, that the zero velocity condition implies an expansion fan behind the detonation wave and a reduction in pressure by a factor β

$$\beta = \left(\frac{\gamma + 1}{2\gamma}\right)^{\frac{2\gamma}{\gamma - 1}} \tag{213}$$

This result will be rederived in the next section where a detailed examination of the pressure time history on the base is made. For $\gamma = 1.18$, the value of β is 0.35, and the pressure experienced by the thrust plate, p_{1D}, is given in terms of practical units by

$$p_{1D} = \beta p_D \tag{214}$$

$$= 31.6 \rho_N^{1/3} \phi_7^{2/3} \text{ bar} \tag{215}$$

The pressure on the base is constant at p_{1D} during the laser pulse and remains so until information that the laser has turned off is propagated over a distance ℓ_o from the furthest point of the detonation wave back to the thrust plate. The speed of sound behind the detonation wave is $\sim V_D/2$, so the pressure remains at p_{1D} for a total time of the order $3\tau_L$. One dimensional expansion subsequently causes a decay in base pressure. The impulse per unit area, I/A, can be expressed as

$$I/A = \int p \, dt \tag{216}$$

$$= p_{1D} \tau_L f \tag{217}$$

where f is a nondimensional measure of impulse to be determined. The time integral will be carried over an interpulse time or to whenever effects due a finite 1-D skirt length cause the base pressure to drop to a negligible value.

The mass per unit area of propellant heated by the pulse is simply

$$m/A = \rho_o V_D \tau_L \tag{218}$$

Hence the impulse per unit mass or effective exhaust velocity, c, is from Eqs. (218), (217), (214), (212) and (209).

$$I/m = \frac{\beta f}{\gamma + 1} \tag{219}$$

$$\equiv c \tag{220}$$

Impulse can be written as the product of time averaged thrust times the cycle period, and mass as the product of time averaged mass flow times the cycle period. Thus the time averaged thrust per unit average mass flow is also represented by Eq. (219). As used in the conventional terminology of rocketry engineering, specific impulse is this figure divided by g, the gravitational acceleration.

The energy per unit area deposited in the propellant is

$$E/A = \phi_o \tau_L \tag{221}$$

and, with Eqs. (218) and (209) the deposited energy per unit propellant mass is

$$E/m = \frac{V_D^2}{2(\gamma^2 - 1)} \tag{222}$$

Equations (221) and (222) may be combined to obtain the impulse per unit energy or, equivalently, the time average thrust, T, per time averaged incident power, P.

$$T/P = I/E \tag{223}$$

$$= \frac{2(\gamma^2 - 1)}{\gamma + 1} \frac{\beta f}{V_D} \tag{224}$$

There are a number of possible definitions describing a rocket's efficiency, η. In this paper η represents the power efficiency which is the ratio of the effective exhaust energy $mc^2/2$ to the incident pulse energy

$$\eta \equiv mc^2/2E \tag{225}$$

$$= (\gamma^2 - 1)\left(\frac{\beta f}{\gamma + 1}\right)^2 \tag{226}$$

The impulse per unit energy or thrust per unit power may be expressed in terms of η.

$$\frac{I}{E} = \frac{2\eta}{c} \tag{227}$$

Note that for a given efficiency, the so called coupling coefficient, I/E, necessarily decreases with specific impulse. As an example, in Eq. (227) a 1000 sec I_{sp} at 100% efficiency implies a coupling coefficient of 20 dyne sec/J or, equivalently, 20 metric ton/GW. With $\gamma = 1.2$ a 100% efficient rocket would have a normalized impulse $f = f_{max} = 9.86$ derived from setting the left side of Eq. (227) to unity. The efficiency is sensitive to f in that it depends on the square.

$$f_{max} = \frac{\gamma + 1}{\beta\sqrt{\gamma^2 - 1}} \tag{228}$$

$$\eta = (f/f_{max})^2$$

The laser powers required to perform a given mission must be divided by η to obtain the actual power necessary when real imperfect rockets are employed.

It is also interesting to compare the effective exhaust velocity c to the ideal exhaust velocity $\hat{c}$. With the ideal rocket all the exhaust gas molecules are given the same exhaust velocity $\hat{c}$, and no energy is lost in terms of frozen chemistry.

$$\hat{c} \equiv \sqrt{2\,E/m} \tag{229}$$

$$= \frac{V_D}{\sqrt{\gamma^2 - 1}} \tag{230}$$

The last line makes use of Eq. (222). The ratio of effective to ideal velocity is

$$\frac{c}{\hat{c}} = \frac{\beta f \sqrt{\gamma^2 - 1}}{\gamma + 1} \tag{231}$$

and this ratio is unity if f is again 9.86, the maximum possible value.

All of the important performance figures are now specified in terms of a single unknown parameter, the normalized impulse, f. A numerical determination of this quantity will be given by application of the method of characteristics in one dimension for unsteady flow. In the discussion to follow it will be assumed that the reader is generally familiar with the technique and only the specifics as applied to this problem will be treated.

Construction of an x-t diagram of the propellant heating and subsequent expansion will employ the laser pulse length, τ_L, as the unit of time, velocity will be measured in terms of the detonation velocity, V_D, and distance in the natural units $V_D\tau_L$. Thus the detonation wave propagating through the cold propellant is represented in these coordinates by a line with slope of unity for $0 \leq x/V_D\tau_L \leq 1$, as shown in Figure 23.

All the gas dynamic processes taking place behind the detonation wave for $t/\tau_L < 1$ and over all space for $t/T_L > 1$ will, by the absence of derived

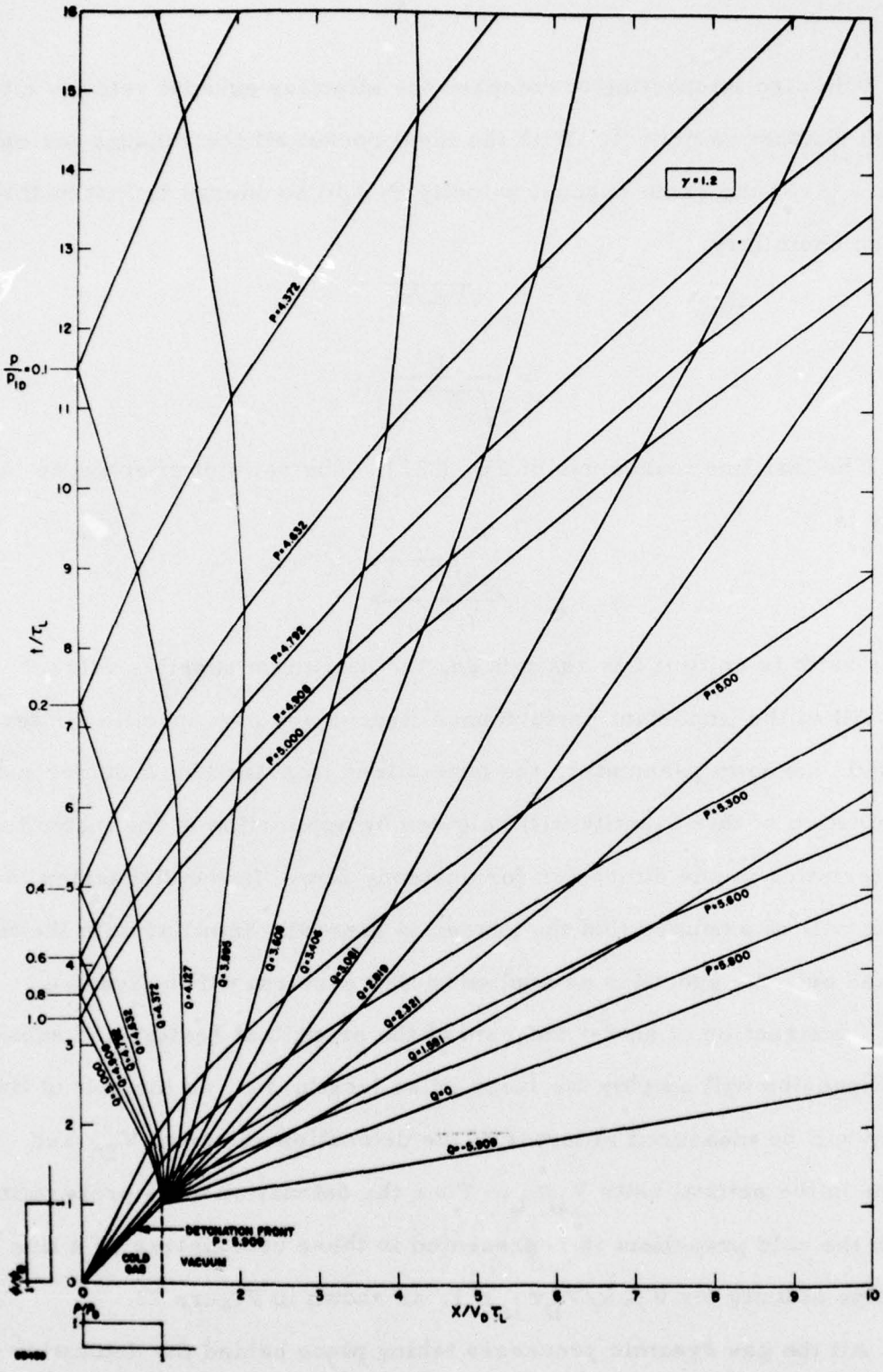

Figure 23 One-Dimensional x-t Diagram for $\gamma = 1.2$ Gas

shock waves, prove to be isentropic. This is a direct result of the assumption of uniform cold propellant density, uniform laser flux, and the heating of all the propellant by the detonation wave. By avoiding shock waves with strength dependent jump conditions, a single x-t diagram at a given value of γ will serve to describe any physically realistic combination of ρ_o, ϕ_o, and τ_L.

The local flow velocity in the gas will be given by u, and the local sound speed by a. Two characteristic quantities, P and Q, defined by

$$P = \left[\frac{2}{\gamma - 1} a + u\right] \frac{1}{V_D} \tag{232}$$

$$Q = \left[\frac{2}{\gamma - 1} a - u\right] \frac{1}{V_D} \tag{233}$$

are propagated without change in isentropic flow along x-t trajectories with slope u + a and u - a respectively. Once the values of u and a are known along suitable boundaries, the values of P and Q can be found along that boundary and the trajectories of constant P and Q may be plotted to any desired accuracy.

Immediately behind the detonation wave, the so called Chapman-Jouget conditions hold, and the flow velocity in the detonation wave frame of reference is sonic at the value

$$a_D = \frac{\gamma}{\gamma + 1} V_D \tag{234}$$

In the rocket reference frame, the gas velocity is

$$u_D = V_D - a_D \tag{235}$$

$$= \frac{V_D}{\gamma + 1} \tag{236}$$

The value of Q directly behind the front is obtained from Eqs. (233), (234), and (236),

$$Q_D = \frac{1}{\gamma - 1} \tag{237}$$

and it is constant all along the front. By virtue of the Chapman-Jouget condition, $u - a = -V_D(\gamma - 1)/(\gamma + 1)$ at the front, and lines of constant $Q = Q_D$ are propagated from the front towards the base at all points along the front. The entire region behind the detonation is filled with characteristics at constant Q making for a "simple wave" process. The fluid velocity must be zero at the base, which implies that the Q characteristics have a slope $-V_D/a_{base}$. Setting Eq. (237) equal to Eq. (233) with $u = 0$ and $a = a_{base}$ yields $a_{base} = V_D/2$. Hence the Q_D characteristics bend over to the left in a manner to be determined.

The P characteristics form a centered rarefraction fan behind the detonation front. Lines of constant P emanate from the origin and follow straight trajectories given by

$$\frac{x}{t} = a + u \tag{238}$$

The trajectories are straight since $a = a(P, Q)$ and $u = u(P, Q)$ by Eqs. (232) and (233), Q is a constant, Q_D, to the left of the detonation, and P is a constant by definition along a trajectory of constant P.

Elimination of the sound speed between Eqs. (233), (237), and (238) gives the flow velocity in terms of position and time.

$$u = \frac{2V_D}{\gamma + 1}\left(\frac{x}{V_D t} - \frac{1}{2}\right) \tag{239}$$

with limits

$$u_D = \frac{V_D}{\gamma + 1}, \quad x = V_D t \tag{240}$$

$$u_T = 0, \quad x = \frac{V_D t}{2} \tag{241}$$

That is, the "tail" of the expansion fan moves at one half the detonation velocity. Similarly, elimination of the flow velocity gives the sound speed

$$a = \frac{V_D}{\gamma + 1} \left[1 + (\gamma - 1) \frac{x}{V_D t}\right] \tag{242}$$

with limits

$$a_D = \frac{\gamma}{\gamma + 1} V_D, \quad x = V_D t \tag{243}$$

$$= \frac{V_D}{2}, \qquad x = \frac{V_D t}{2} \tag{244}$$

The values of P in the fan are then

$$P = \frac{3 - \gamma}{(\gamma - 1)(\gamma + 1)} + \frac{4}{\gamma + 1} \frac{x}{V_D t} \tag{245}$$

with limits

$$P_D = \frac{3\gamma - 1}{(\gamma - 1)(\gamma + 1)}, \quad x = V_D t \tag{246}$$

$$P_T = \frac{V_D}{\gamma - 1} = Q_D, \quad x = \frac{V_D t}{2} \tag{247}$$

To the left of the tail P is a constant, P_T, equal to Q_D, and the velocity u is zero.

In Figure 23 only the Q_D characteristic emanating from the $t/\tau_L = 1$, $x/V_D\tau_L = 1$ point is drawn. The space between this curve, the time axis, and the detonation trajectory is filled with parallel Q_D waves. Similarly the space to the left of the "tail" P_T characteristic is filled with parallel P_T waves up to the point where the drawn Q_D characteristic intersects the time axis.

For isentropic flow, the pressure at any two points is related in terms of the corresponding sound speeds by

$$\frac{p'}{p} = \left(\frac{a'}{a}\right)^{\frac{2\gamma}{\gamma - 1}} \tag{248}$$

where one of the points has been denoted by a prime. Substituting the sound speed behind the detonation wave from Eq. (234) and the sound speed at the tail of the expansion fan from Eq. (244), Pirri's result, Eqs. (213) and (214), for the initial base pressure is recovered.

When the laser is suddenly turned off at $t = \tau_L$, that information is propagated from the site of disturbance as a Q wave centered expansion fan. To the right, i.e., the vacuum side of Figure 23, the maximum expansion velocity will take place at the hydrodynamic limiting value. The density and sound speed are both zero at the vacuum fluid boundary and by Eqs. (232) and (233) $Q_V = - P_V$, where the subscript V refers to that boundary. The boundary P_V characteristic has the same value as P_D. Thus the vacuum expansion velocity, by Eqs. (232) and (244), is

$$u_V = \frac{3\gamma - 1}{(\gamma - 1)(\gamma + 1)} V_D \tag{249}$$

Within the fan, the value of Q varies continuously between Q_D and Q_V.

The one remaining boundary condition on the problem is that the fluid velocity is always zero at the base, which implies that P and Q be equal there.

$$Q_{base} = P_{base} \tag{250}$$

Construction of Figure 23 was carried out by calculating the values of a and u from Eqs. (232) and (233) at the intersection of each P and Q characteristic and extending each characteristic at the new slope $(u + a)^{-1}$ or $(u - a)^{-1}$ respectively without iterative or interpolative corrections. Sample higher order corrections showed that the characteristics net was fine enough to give accuracy sufficient for present purposes.

The pressure time history at the base is obtained by noting the time of intersection of a characteristic with the base and the relationship

$$P_{base} = [(\gamma - 1)\, Q_{base}]^{\frac{2\gamma}{\gamma - 1}}\, P_{1D} \qquad (251)$$

which is derived from Eqs. (250), (248), and (233). The base pressures are shown at the left edge of Figure 23.

The effect of finite 1-D skirt length may be approximated on the conservative side by assuming that the base pressure drops to zero immediately upon arrival at the base of expansion waves due to the skirt cut off. These waves can only propagate upstream against subsonic flow. In the x-t diagram, the flow is supersonic everywhere that the slope of the Q waves is positive. For a given 1-D skirt length, the flow at the lip does not become sonic until the first Q wave, Q_S, becomes vertical at that point. The information is then transmitted to the base when that same Q wave reaches the base.

For example, if the 1-D skirt length was $\sim 1.3\, V_D \tau_L$, the flow at the lip becomes sonic at $t \sim 3\, \tau_L$ and the $Q = Q_S = 4.127$ characteristic carries the expansion to the base by time $t \sim 11.5 \tau_L$. The base pressure is then $0.1\, P_{1D}$ and the normalized impulse f, from numerical integration of the pressure up to that time, is ~ 5.6.

Contributions to the base impulse after the arrival at the base of the Q_S characteristic are of relatively greater importance if the 1-D skirt length is short. A more accurate procedure imposes sonic flow boundary conditions at the 1-D skirt exit for all times greater than the time, t_s, at which the Q_S characteristic reached the end of the skirt. Application of Eqs. (232) and (233) with a = u yields

$$Q = \frac{3 - \gamma}{\gamma + 1}\, P \qquad (252)$$

Every P characteristic reaching the end of the skirt at times $t > t_s$ reflects as a Q wave with value given by Eq. (252). The subsequent propagation of these Q waves to the base and their reflection there as P waves is followed as before.

The boundary condition imposed here is only accurate in the limit of the 1-D skirt length much greater than the diameter of the base. In that limit the flow in the tube is indeed one dimensional and the sonic surface effectively will be at the end of the skirt. The sonic surface will be roughly located at the end of the skirt around the periphery, but it will extend well beyond the end of the skirt at the axial position. These two dimensional phenomena are such as to make the one dimensional calculations of impulse an underestimate.

A computer program has been constructed to carry out these characteristic calculations. A given characteristic is propagated forward in time at a slope $V_D/(u \pm a)$ that is derived from the average of the properties at the last intersection point and the next intersection point. This leads to noticeable greater accuracy than obtained in the computation of Figure 23. The behavior of base pressure with time for a number of 1-D skirt lengths is presented in Figure 24. As anticipated, the pressure remains at a constant value, P_{1D}, for $t \sim 3\tau_L$ before decaying initially at a rate faster than $\sim t^{-2}$, and later as $\sim t^{-\gamma}$ until the effects of finite 1-D skirt length are felt.

The areas under the pressure curves have been integrated numerically to give the normalized impulse f. Calculations were done for $\gamma = 1.18$ and $\gamma = 1.2$ and they show, Figure 25, little sensitivity to this parameter. The efficiencies are also shown. Although both values of γ give the same efficiency for an infinite length skirt, there are noticeable differences for finite

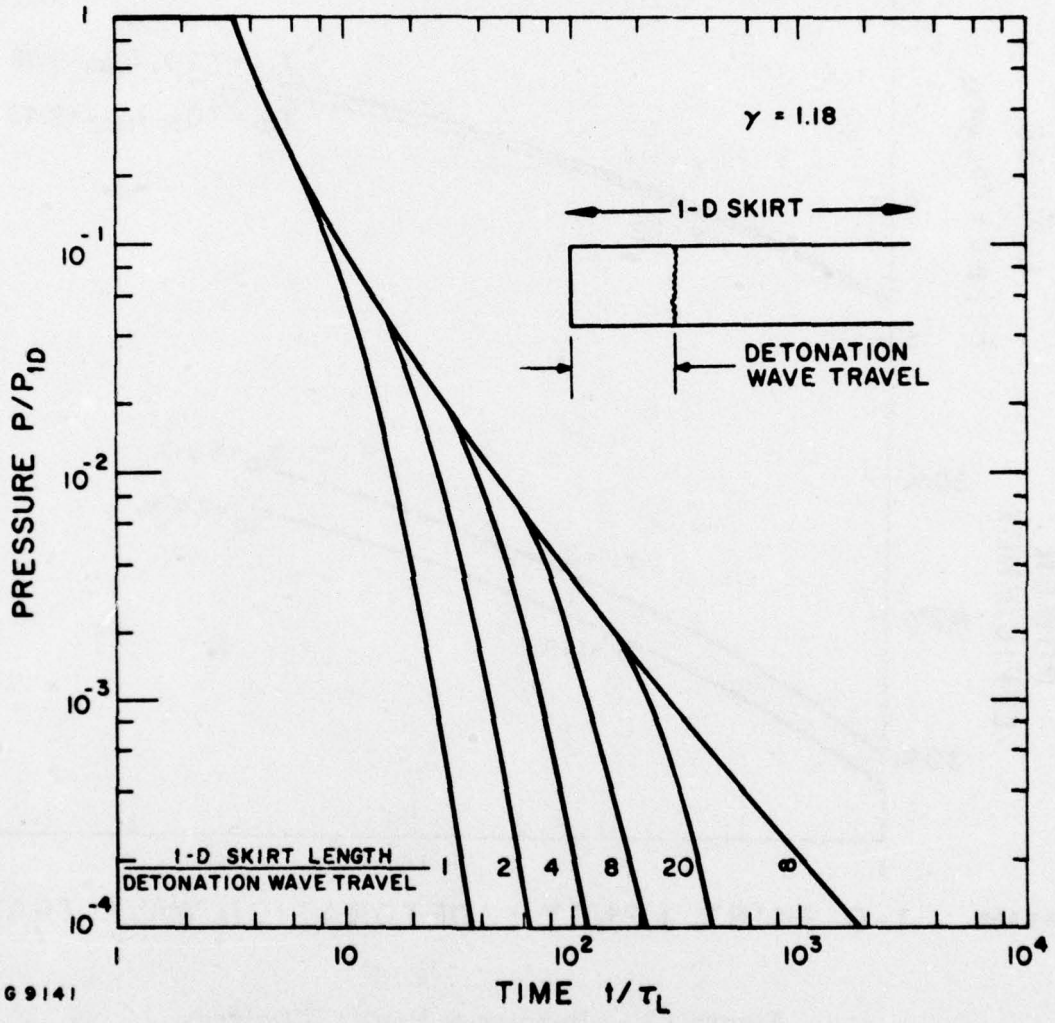

Figure 24 Pressure vs Time Variable 1-D Skirt Length

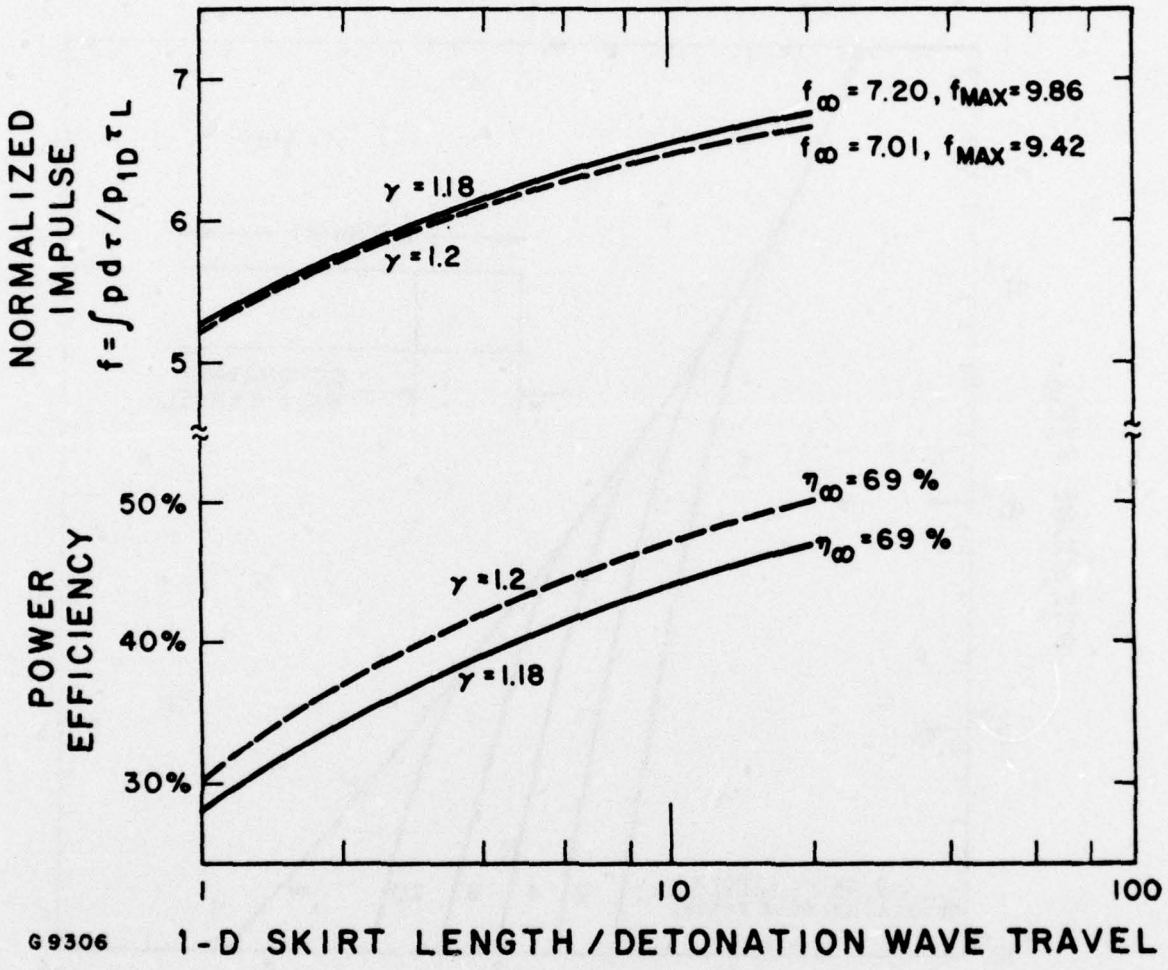

Figure 25 Impulse & Power Efficiency

skirts. It is to be expected physically that for fixed degree of expansion, a gas with a lower γ will have more energy tied up in internal modes and will hence have less efficiency.

When the 1-D skirt is infinite in length, the expansion of the gas is complete and the 31% departures from 100% efficiency represents the loss due to inhomogeneity in the exhaust velocity distribution. For finite length skirts the decreased efficiency results from ejection of the gas at non zero enthalpy with contributions from ionization, dissociation, and random motion. A constant γ calculation does not directly identify the components of internal energy, but their effects on isentropic gas dynamics are roughly included as long as the expansion rates are not so fast as to result in frozen flow. Preliminary calculations show that over a range of parameters of interest nitrogen propellant would not be ionized, but would still be significantly dissociated and that the ionization and dissociation recombination rates are fast enough to preclude frozen flow. Further work on possible losses due to real gas effects and phenomenal such as radiative and wall friction losses is in order.

As a specific example of the parameters that result from the preceding calculations, consider the example of a rocket designed to operate at a specific impulse of 800 sec with a 1-D skirt length of 10 $V_D \tau_L$. From Figure 25 the efficiency and normalized impulse would be, respectively, $\eta = 44\%$ and $f = 6.5$. The effective exhaust velocity is 7.8×10^5 cm/sec and (219) gives $V_D = 7.4 \times 10^6$ cm/sec, slightly less than c. A 10 μsec pulse would give 7 cm of detonation wave travel and the 1-D skirt would be 74 cm in length. The energy per unit mass is 70 kJ/gm and the coupling coefficient is 11 dyne sec/J or, 11 metric ton/GW.

4. PROPELLANT METERING PULSE

The propellant surface is assumed to be perfectly absorbing to the incident radiation, over an absorption length short compared to any other scale of interest to the problem. On the other hand, the evolving vapor is taken as being perfectly transparent to the radiation. As an example of these conditions, a film of water absorbs 10.6 μ radiation in a scale of ~ 1 wavelength, yet steam, at $\sim 100^{\circ}C$ and 10^{-3} g/cm^3 has an absorption length of ~ 600 cm. The incident flux will be taken as uniform over the base of the vehicle and constant in time at the level ϕ_a for a time τ_a. Before the pulse is turned on vacuum conditions are assumed. The degree to which this is realized in practice will depend on the repetition rate and the altitude of the rocket.

The effective energy per unit mass necessary to ablate the propellant in the absence of heat conduction losses is taken as a constant, Q^*. The ablation velocity, u_c, is given in terms of the incident flux, ϕ_a, and the condensed phase density, ρ_c,

$$u_c = \frac{\phi_a}{\rho_c Q^*} \tag{253}$$

For times longer than χ/u_c^2, where χ is the material thermal diffusivity, the ablation depth exceeds the thermal penetration depth. In practical cases of interest this time will prove short compared to the evaporation pulse length, and heat conduction in the condensed phase can be ignored. Also, the ablation velocity will proved to be small compared to molecular velocity of particles leaving the surface, and the effects of finite surface recession velocity can be neglected. Under these assumptions the surface jumps to a constant temperature T_c when the metering pulse is turned on, since an energy balance is established between incoming radiation and ablation.

In the free molecular limit, for which there is no backscattering to the surface, the mass and energy flux are computed from a half Maxwellian characterized by the temperature, T_c, of the condensed phase and the corresponding saturated vapor density, ρ_s. This gives a mass flux of $\rho_s u_s$ and a kinetic energy flux of $2 RT_c \rho_s u_s$, where $u_s = \sqrt{RT_c/2\pi}$, and R is the gas constant per unit vapor mass.

Backscattering due to collisions will reduce this mass flux if particles are readsorbed. Even if all backscattered particles reflect from the surface, the energy flux could be altered if the reflected particles accommodate to the surface temperature. In the interest of simplicity it will be assumed that perfect reflection with no accommodation takes place. That is, the free molecular limit for energy and mass flux will be used. Most of the proposed propellant materials are molecular and, in contrast to the situation with monatomic metal vapor, there is some justification in assuming no readsorption.

The flow at the surface will generally be subsonic, but, with surface pressures much greater than ambient, the flow will accelerate to supersonic values within a few mean free paths. This can occur without area change and without heat addition due to either conduction or direct absorption of the laser flux. The process is driven by the entropy production which results from collisional relaxation of the original nonequilibrium velocity distribution. The flow velocity, u_*, and density, ρ_*, at the sonic surface, as will be shown, are the only parameters necessary to characterize the hydrodynamics beyond that surface. However, they must be related to conditions at the surface for a complete solution.

At the sonic surface complete thermal equilibrium is assumed. That is, the velocity distribution is Maxwellized at temperature T_* which will also be the temperature of the internal degrees of freedom. If the energy flux at the sonic surface is equated to the energy flux at the condensed phase surface, the following equation results,

$$\left[\frac{\gamma}{\gamma - 1} RT_* + \frac{u_*^2}{2}\right] \rho_* u_* = \left[\frac{n}{2} + 2\right] RT_c \rho_s u_s \tag{254}$$

On the right hand side the energy transport due to internal molecular energy in equilibrium with the surface, $nRT_c/2$, has been added to the kinetic energy contribution. The number of degrees of freedom can be expressed as $n = (5-3\gamma)/(\gamma - 1)$. In the interest of simplicity, the specific heat ratio at the surface has been taken equal to that at the sonic station. When more accurate results are desired the assumption should be dropped. Making use of mass conservation, $\rho_* u_* = \rho_s u_s$, and the sonic condition $u_* = \sqrt{\gamma RT_*}$ the sonic parameters are related to the surface conditions.

$$T_* = T_c/\gamma \tag{254a}$$

$$u_* = \sqrt{RT_c} \tag{254b}$$

$$= \sqrt{2\pi}\, u_s$$

$$\rho_* = \rho_s/\sqrt{2\pi} \tag{254c}$$

The method of characteristics will be used to deduce the flowfield beyond the sonic surface. Since the initial mean free path is generally short compared to other dimensions of interest, the sonic surface is taken as coincident with condensed propellant surface at $x = 0$. In constructing the x-t diagram, Figure 26, time will be normalized to τ_a and distance to $a_* \tau_a$ where $a_* = u_*$ is the sound speed at the sonic surface. By assuming the ablation takes place into a perfect vacuum, shock waves are avoided.

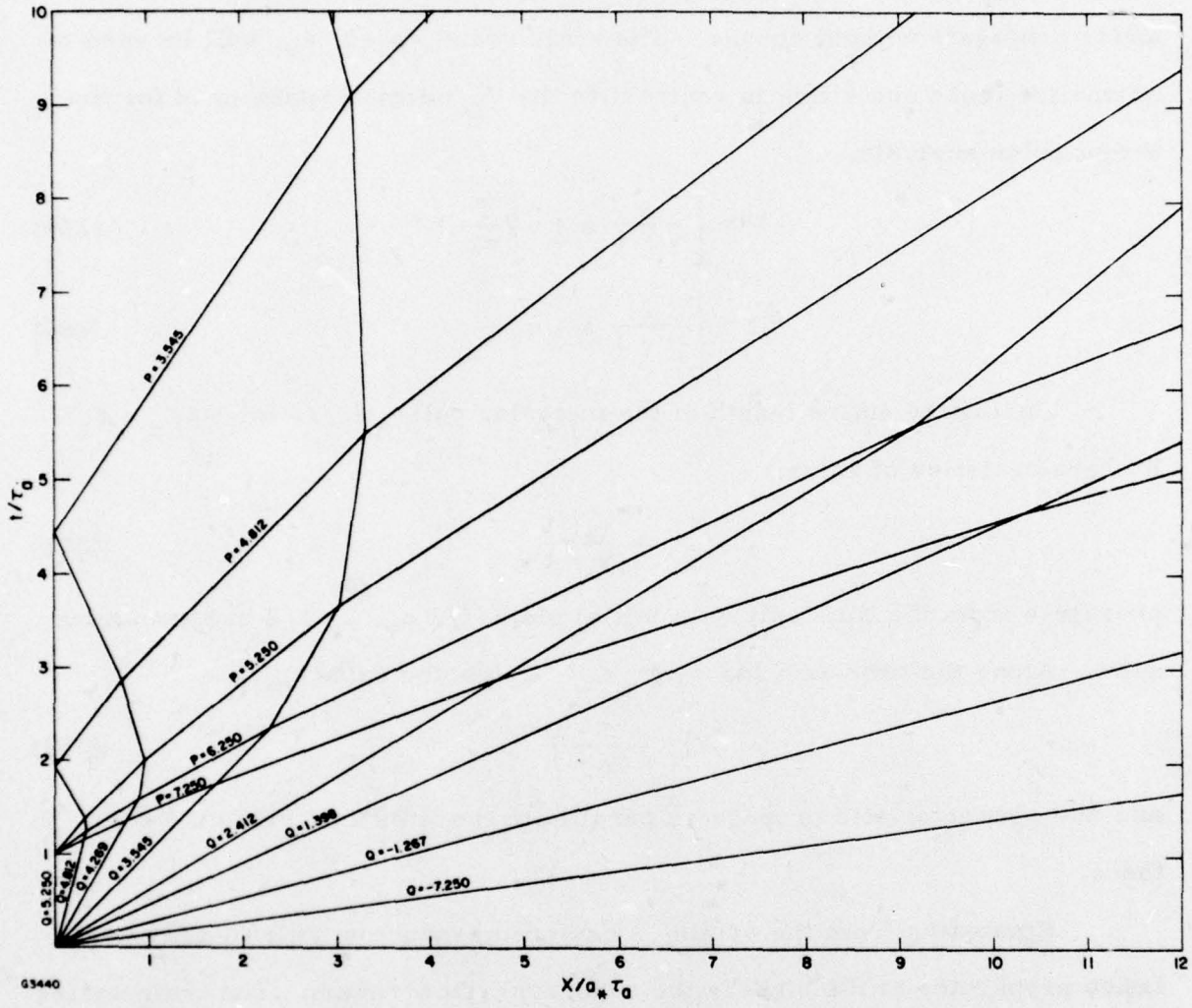

Figure 26 XT Diagram for Propellent Metering Process

This, together with the fact that the vapor is transparent to the metering pulse, means that the flow is isentropic, and the characteristic quantities P and Q propagate without change. The sonic sound speed, a_*, will be used to normalize these quantities in contrast to the V_D normalization used for the thrust pulse analysis.

$$P = \left[\frac{2}{\gamma - 1}\, a + u\right] \frac{1}{a_*} \tag{255}$$

$$Q = \left[\frac{2}{\gamma - 1}\, a - u\right] \frac{1}{a_*} \tag{256}$$

During the entire length of the metering pulse, i.e., for $\tau/\tau_a < 1$, P characteristics of value,

$$P_* = \frac{\gamma + 1}{\gamma - 1} \tag{257}$$

propagate from the time axis with initial slope $1/2\ a_*$, or 1/2 in normalized units. Along the time axis for $\tau/\tau_a < 1$, Q has the value Q_*

$$Q_* = \frac{3 - \gamma}{\gamma - 1} \tag{258}$$

and that characteristic propagates parallel to the time axis since $u - a = 0$ there.

Emanating from the origin, a centered expansion fan of Q characteristics propagates to the right in the supersonic flow region. The trajectories are straight lines since they traverse a region of constant P.

The sound speed decreases through this "starting fan," reaching a minimum of zero at the hydrodynamic limit of the vacuum fluid interface. By definition, P has the value

$$P_v = u_v/a_* \tag{259}$$

along the interface, where u_v is the velocity of the interface (and the zero density fluid there). However, it has been argued that P is a constant, P_*. This gives the boundary velocity as a constant,

$$u_v = \frac{\gamma + 1}{\gamma - 1} a_* \tag{260}$$

The value of Q varies through the starting fan, decreasing from Q_* to Q_v,

$$Q_v = \frac{\gamma + 1}{\gamma - 1} \tag{261}$$

which is equal to $- P_v$, and the slope is $1/u_v$. The P characteristic that emanates from the origin is coincident with the Q_v characteristic, and those emanating at later times tend to become parallel at large x. Only the P_* characteristic emanating from the $t/\tau_a = 1$ point is explicitly drawn on Figure 26.

When the metering pulse is suddenly terminated at $t/\tau_a = 1$, that information is propagated into flowfield by another expansion fan, the "termination" fan. This fan is comprised of P characteristics since the flow in the fan is subsonic. The trajectories are not straight lines since they interact with varying Q characteristics of the starting fan. The limiting characteristic to the right is the previously discussed P_* trajectory from $t/\tau_a = 1$. At the termination point the flow velocity decreases from u_* to zero since the condensed phase is no longer a source for particles and it is assumed that the surface reflection coefficient is unity. Hence the value of P decreases through the fan to the limiting value of

$$P_* = \frac{2}{\gamma - 1} \frac{a_t}{a_*} \tag{262}$$

and that characteristic propagates initially at a slope of a_*/a_t. The sound speed at the termination point is obtained from noting that $Q = Q_t$ still has the value Q^* and, by Eq. (255) with u = 0, that $Q_t = P_t$. The sound speed is then given by

$$a_t = \frac{3 - \gamma}{2} a_*$$

For values of γ greater than unity this represents a sudden decrease from a_*.

The densities at two points in isentropic flow are related to the corresponding sound speeds by

$$\frac{\rho}{\rho'} = \left(\frac{a}{a'}\right)^{\frac{2}{\gamma - 1}} \tag{263}$$

Thus the density at the termination point must undergo a sudden drop of

$$\frac{\rho_t}{\rho_*} = \left(\frac{3 - \gamma}{2}\right)^{\frac{2}{\gamma - 1}} \tag{264}$$

which varies between 0.30 at $\gamma = 5/3$ and $e^{-1} = 0.37$ at limit of $\gamma = 1$.

For times greater than $t/\tau_a = 1$ the surface velocity remains zero and $P = Q$ at $x = 0$. The values of Q are, of course, determined from the intersection of Q characteristics with the surface after "refraction" in the termination fan.

This completes the discussion of boundary conditions. The characteristic trajectories in the region $x,\ t \neq 0$ were determined by the same method as described in the section on the thrust pulse analysis. The x-t diagram presented in Figure 26 uses $\gamma = 1.32$, the value for water vapor at $100^{\circ}C$. The general features are not expected to be a sensitive function of γ.

Density profiles at various times may be obtained by substituting

$$\frac{a}{a^*} = \frac{\gamma - 1}{4} (P + Q) \tag{265}$$

from Eqs. (255) and (256) into Eq. (263). Values of P and Q along a line of constant time are interpolated between the plotted characteristics. These results are presented in Figure 27 for $\gamma = 1.32$. Note the constant surface density and self similar profile while the metering laser is on. The drop in surface density when the laser is turned off is readily apparent at $t/\tau_a = 1.5$, and it results in a density peak that moves away at roughly twice the sonic speed a_*. The relative magnitude of this peak decreases with time.

The results shown in Figure 27 have been replotted in Figure 28 with the density normalized to the peak density and distance normalized to $a_* t$ rather than $a_* \tau_a$. This allows easy comparison of the general features of the profiles at different times. Note that by time $t/\tau_a = 5$ a relatively rectangular distribution has developed despite the fast expansion of the tail. It is on the basis of this distribution that the constant density assumption was made for the thrust pulse analysis.

The foregoing material may be applied to the determination of the required metering pulse characteristics necessary for setting up a "rectangular" distribution of density ρ_o and length $\ell_o = V_D \tau_L$ for the thrust pulse. The desired density, ρ_o, is a fraction of ϵ of the sonic plane density ρ_*. The value of ϵ is somewhat arbitrary and depends on the chosen mass distribution. If the distribution with $t/\tau_a = 3$ is taken, $\epsilon \approx 0.15$ from Figure 27. With $t/\tau_a \approx 5$, $\epsilon \approx 0.09$. The saturation density is, from Eq. (254c):

$$\rho_s = \frac{\sqrt{2\pi}}{\epsilon} \rho_o \tag{266}$$

Using ρ_s, the material surface temperature can be determined by reference to thermodynamic tables relating temperature to saturation

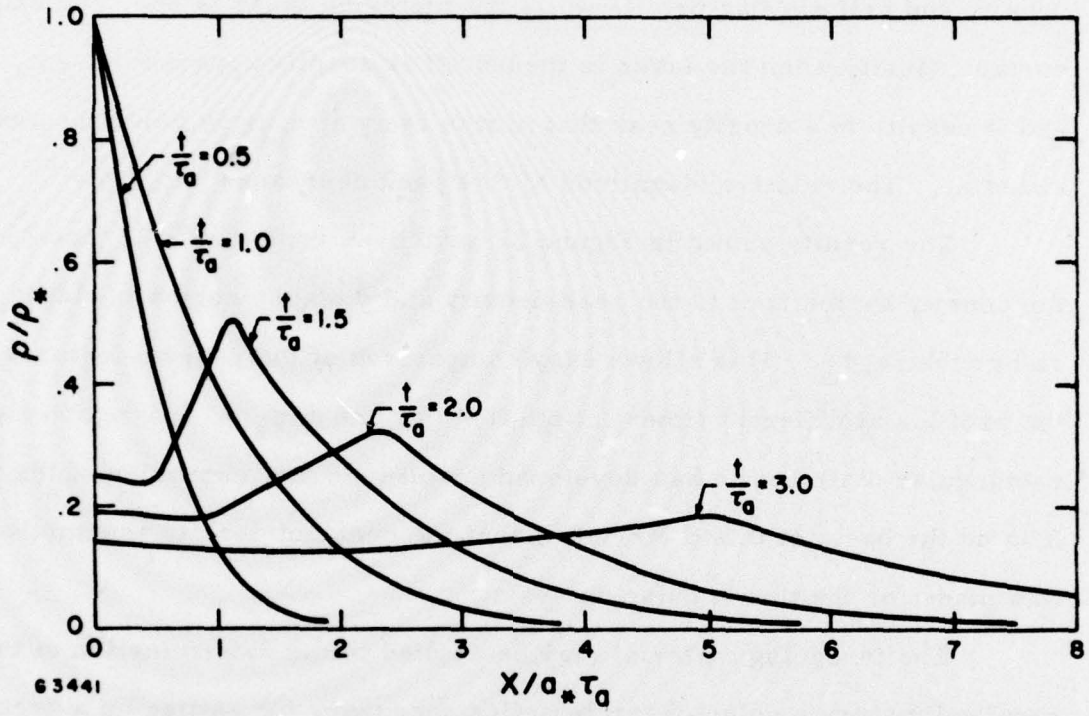

Figure 27 Vacuum Evaporation Density Profile

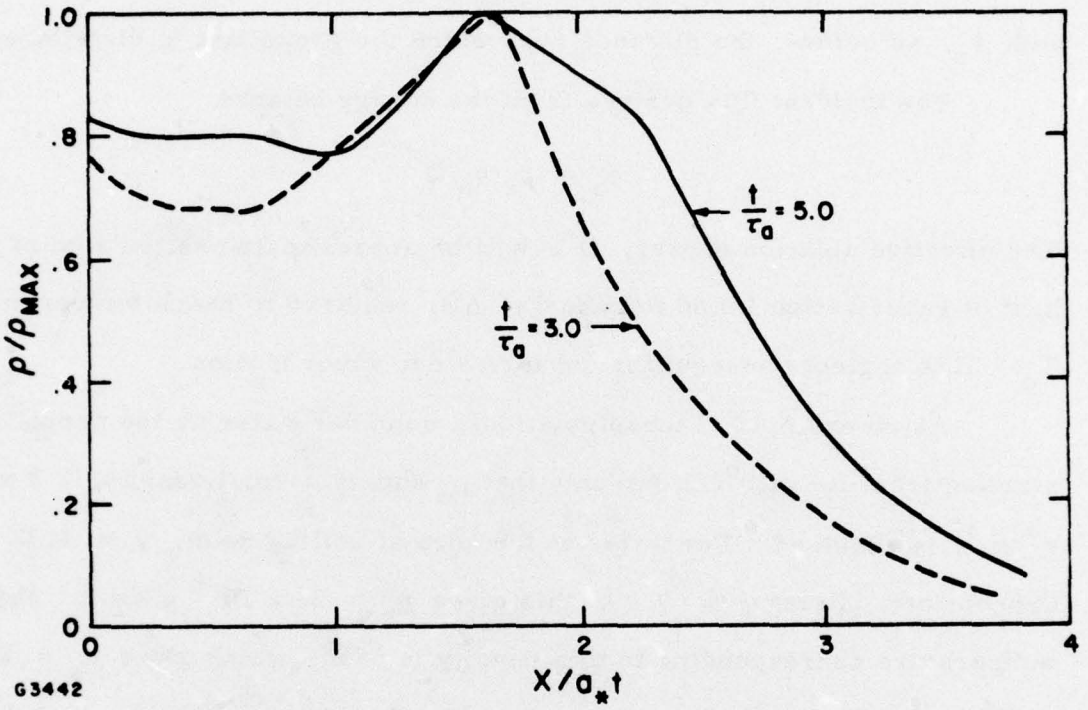

Figure 28 Vacuum Evaporation Density Profile

properties. And given T_c, u_s can be calculated. The pulse time is then obtained from conservation of mass

$$\tau_a = \frac{\rho_o \ell_o}{\rho_s u_s} \tag{267}$$

with ℓ_o, as before, the distance over which the propellant is distributed.

The incident flux derives from the energy balance

$$\phi_a = \rho_s u_s Q^* \tag{268}$$

The effective ablation energy, Q^*, will be approximated as the sum of the heat of vaporization L and the energy, ΔH, required to reach temperature T_c. This neglects nonequilibrium terms due vapor motion.

As an example of these relations, consider water as the propellant starting from ice at 0^oC. Assume that ρ_o equals normal density, 1.2×10^{-3} g/cm^3, is required. For water at the normal boiling point, $\gamma = 1.32$ is appropriate. Using $\epsilon = 0.09$, this gives $\rho_s = 33 \times 10^{-3}$ g/cm^3. The temperature corresponding to this density is 553^oK which gives $u_s = 2.0 \times 10^4$ cm/sec. Hence the evaporation pulse has the duration $\tau_a = 1.3 \times \ell_o$ μsec, with ℓ_o in units of cm. Since the chosen distribution with $\epsilon = 0.09$ is obtained at time $\tau/\tau_a \approx 5$, the thrust pulse should start at $\sim 9 \times \ell_o$ μsec after the start of the metering pulse. At 553^oK the heat of vaporization is 1544 J/g and the energy to reach that temperature is 1569 J/g. Kinetic energy $\sim u_s^2/2 = 20$ J/g is small and its neglect is justified. The incident flux necessary to maintain the 660 g/cm^2-sec rate of ablation is $\phi_a = 2 \times 10^6$ W/cm^2. Neglect of surface recession velocity and thermal conductivity is shown to be appropriate since $u_c = 680$ cm/sec $\ll u_s$ and $\chi/u_c^2 \approx 20$ nsec $\ll \tau_a$.

5. FLUX CONCENTRATORS

A roughly conical reflector can be affixed to the base of the rocket to collect laser flux from an area greater than the base itself. There are a number of advantages and disadvantages to using such a scheme. Some of these will be listed here but no attempt will be made at a systems tradeoff. It will also be demonstrated that practical optical solutions exist.

For a given incident beam (fixed beam divergence, pulse power, average power) and fixed rocket base diameter and flux, it is obvious that a collector allows a vehicle to go to a greater range before power is lost due to diffraction spreading. One payoff is greater final mass per unit laser power. For fixed flux on the base, the flux incident at the collector aperture decreases as the square of the base to collector diameter ratio. Hence, modest concentration ratios can insure that nowhere in the atmosphere outside the engine does the flux exceed known particle breakdown fluxes, even when base fluxes are well above the detonation wave ignition flux. For example, a base flux of 4×10^7 derived from a 16/1 concentrator would require 2.5×10^6 at the aperture, below the 3×10^6 W/cm^2 large particle threshold.

Alternately, for fixed beam divergence, pulse time, average power, and flux collection area (i. e., fixed maximum range) a concentrator allows the base diameter to be decreased at constant base flux. This gives a decrease in the required pulse energy, an advantage with some laser systems. Average power would be maintained by an increase in the repetition rate. As before, the advantage of low peak fluxes in the atmosphere is maintained. The mass of the 1-D skirt and the thrust plate (for nonsolid propellant systems) would reduce as the square of the reduced base diameter. The peak acceleration of the system would be reduced by the same factor giving

savings in structure weight and shock absorber mass. In addition, sufficiently high repetition rates could be achieved to allow self regulating gas phase propellant feeding, in which gaseous propellant is admitted from a plenum through holes in the base plate when the base pressure drops below a given level.

Another advantage of the system is that nonuniform incident flux profiles may be transformed into uniform flux profiles at the base. It is expected that the highest power efficiencies will be obtained with uniform flux profiles such as were assumed in the one dimensional thrust pulse analysis. It is clear that an adaptive optics system that has a 1 m Airy disk diameter at 1000 km can give a good representation of uniform flux over a 2 m base diameter at close range and only a fair one at 1000 km. Assume instead that the adoptive optics were continually adjusted during ascent to give the same flux profile as the best one obtainable at 1000 km. Then a fixed concentrator optical design could maintain an excellent approximation to constant base flux throughout the range.

The optical concentrators to be described preserve the ability to vary the flux profile across the base in the metering and/or thrust pulse and hence develop control torques without onboard variable thrusters. If the flux collection area is maintained constant, the control torque moment arm decreases, as the base diameter is decreased.

Finally, the efficiency of the rocket engine is improved if the reflector also serves as an expansion nozzle. This will occur as long as the turning angle of gas flow is not too large. Computer calculations with the methods of characteristics code were performed for the cases with exit area equal to ten and one hundred times the base area. The length was held fixed

at ten times the detonation wave travel and γ was 1.18. The efficiency as a function of exit area to base area is given in Figure 29. The results are fitted by a power law. $\eta \propto [\text{area ratio}]^{0.11}$. This is a slow dependence, but practical benefits still are to be attained. For instance, a sixteen to one area ratio improves the efficiency from 44% to 60%.

On the negative side, the concentrator introduces a number of complexities that are solved either directly at cost or through weight, which ultimately reflects in cost. There is also a loss of flexibility, in that fixed off axis operation (thrust axis not parallel to laser axis) is difficult, and variable off axis operation is probably impractical. The choice of possible propellant materials will also be limited.

As will be shown the surface area is larger than the aperture area. This structure must be supported against forces due to aerodynamic drag, average accelerations to ~10 g's and higher peak accelerations, and impulsive internal pressures.

The surface must be highly reflective. Optical coatings that survive the exhaust environment may be impossible from an engineering standpoint or prohibitively expensive. Metallic surfaces, such as copper for 10.6 μ radiation, have the advantage of not being susceptible to catastrophic damage resulting from pin hole defects. However, the resulting ~1% absorption of 10^9 watts incident flux cannot be dissipated by reradiation at realistic temperatures. Hence, active cooling is required, which increases the weight of the reflector, supports, and all the auxiliary pumping systems. This also rules out the use of solid propellants which cannot be circulated.

The incident energy per unit propellant mass for a 50% efficient 800 sec I_{sp} rocket is, ~61 kJ/g. If 1% of this energy is absorbed by the

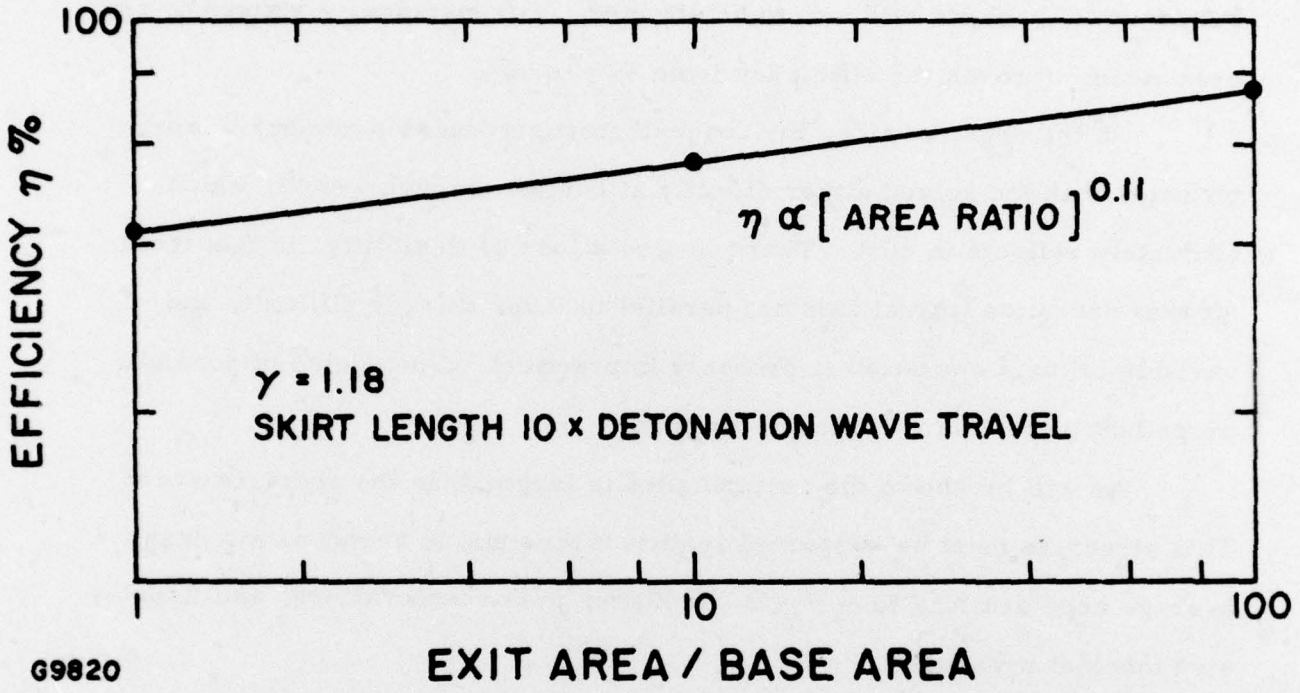

Figure 29 Detonation Rocket Efficiency vs Area Ratio

reflector, the propellant coolant must carry away 615 J/g. Water propellant stored as ice at 0°C, has 753 J/g available for cooling without a gas phase transition. Propellants such as liquid nitrogen or argon would of necessity be vaporized, and a gaseous propellant injection system would be necessary.

The basic optical function of the flux concentrator is to transform an axially symmetric flux distribution $\phi(R)$, at the entrance aperture into a uniform flux, ϕ_o, greater than the average value of $\phi(R)$. Referring to Figure 30, let R be the radius at which a ray strikes the reflective surface at distance x from the base. The radius at which that same ray strikes the base on the opposite side of the axis will be designated as r. By convention, r is negative if the ray strikes the base on the same side of the axis. The angle between the ray and the axis is α.

$$\alpha = \tan^{-1} \frac{r + R}{x} \tag{269}$$

The required shape of the concentrator is obtained by simultaneous integration of the equations

$$dR = \frac{\phi_o - \phi(r)}{\phi(R)} \frac{r}{R} dr \tag{270}$$

$$dx = \frac{dR}{\tan \alpha/2} \tag{271}$$

The first equation simply conserves flux lines and the second equation is determined by equality of the angle of incidence and the angle of reflection.

There are several classes of solution, some of which are illustrated in Figure 31 for a fixed 2 m diameter opening and a 16x concentration ratio. In what will be called type I, the ray from the maximum R crosses the axis to the maximum r. Rays from the minimum R meet the base at the axis.

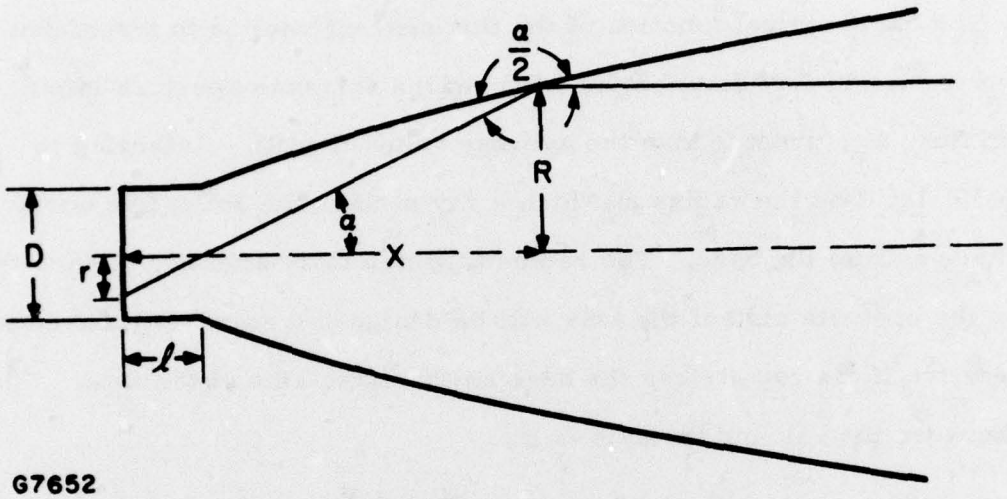

Figure 30 Flux Concentrator Geometry

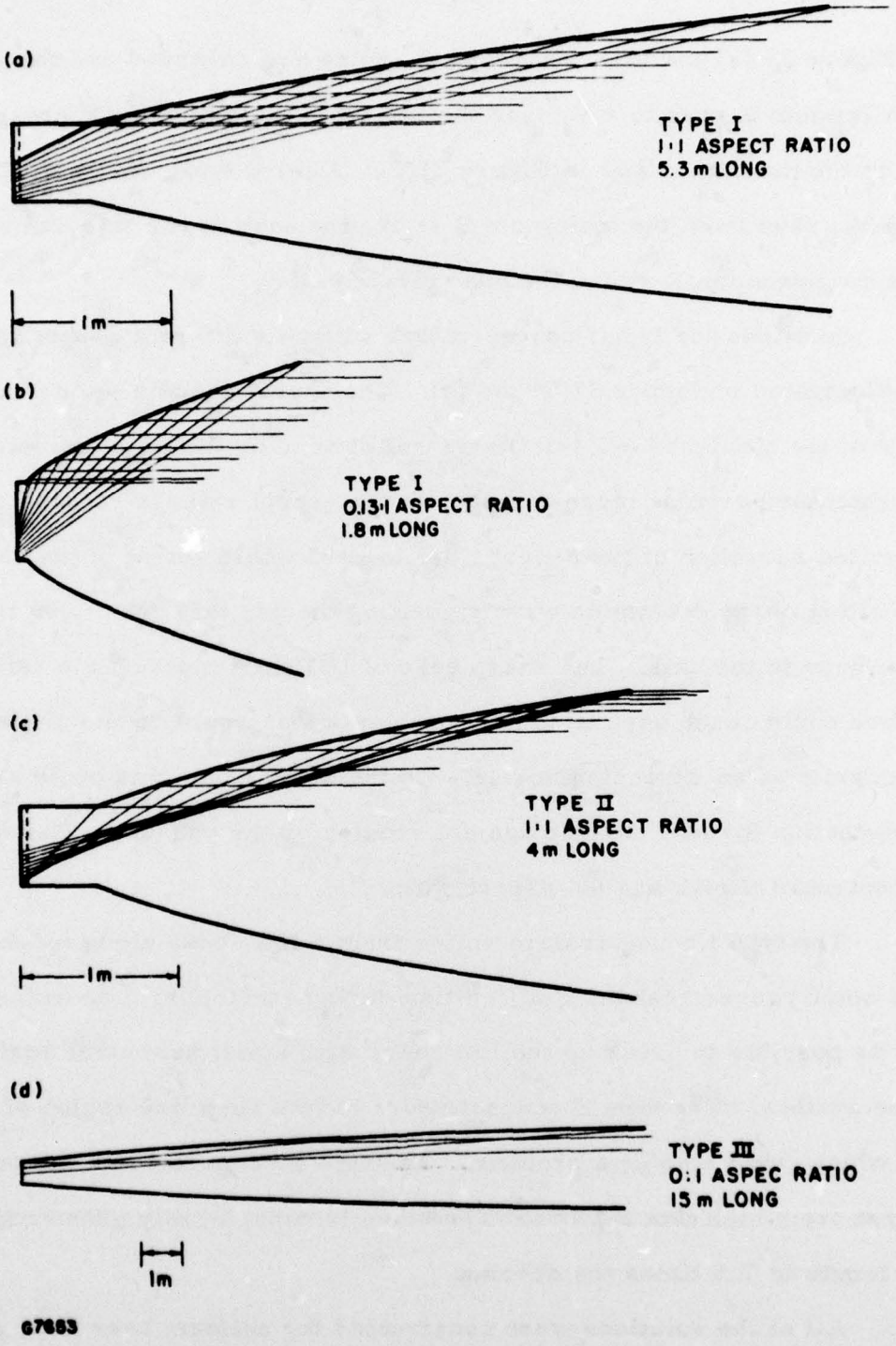

Figure 31 16X Concentrator Designs with 16 to 1 Concentration Ratio

See Figure 31 (a) and (b). With type II, roles are reversed and the ray from the maximum R goes to r = 0 and the ray from the minimum R crosses the axis to the maximum r as in Figure 31(c). A third type, shown in Figure 31(d) has rays from the maximum R strike the base at the axis and rays from the minimum R strike the base directly.

Solutions for type I concentrators with two different aspect ratios are illustrated in Figure 31(a) and (b). The aspect ratio is defined as the length of the straight (1-D skirt) segment divided by the base diameter. The concentrator becomes more compact as the aspect ratio is reduced. Unlimited reduction of the aspect ratio to zero would result in the undesirable effect of the detonation wave vignetting the ray that goes from the edge of the base to the axis. The sharp edge of I-D skirt meeting the reflector surface could cause separated flow problems that would reduce the efficiency of the skirt as an expansion nozzle. On the other hand, this could also act as protection for this surface against erosion by the exhaust. The type III concentrator always has 0:1 aspect ratio.

The type I concentrators suffer from a line focus along the axis. This could cause breakdown difficulties during atmospheric operation. It may be possible to break up the line focus with small azimuthal variations in the surface. The type II concentrators have a cusp like region of high flux which could also be a problem. The type III concentrator appears to be free from high flux regions. The price is considerably greater bulk. The length is 7. 5 times the opening.

All of the solutions were constructed for uniform base flux, given uniform flux at the entrance. If the incoming flux tapers off with radius, the shape of the concentrators will be changed. Since the type II and III

concentrators take rays from large R and displace them to small r, their shapes will be relatively insensitive to an incident profile that decreases with R.

There undoubtedly remains a good deal of room for innovation with regard to these concentrators. For instance a more compact design with many of the advantages of the type III concentrator may be achieved by starting from the base with the type III concept and then switching to a type I or type II design. More sophisticated computation of their hydrodynamic performance will demand 2-D numerical methods.

SECTION IV

LASER AND INITIAL LAUNCH FACILITY

1. LASER

Initial design studies of the laser driven detonation wave rocket have identified the factors determining the required pulsed laser characteristics. The longer IR wavelengths are favored because of their short inverse bremsstrahlung absorption lengths at moderate fluxes. The pulse length is bounded on the short side by thermal transfer to the base during wave ignition and on the long side by the size of the structure necessary to maintain one dimensional performance. A lower limit on peak pulse power is determined from the desired specific impulse, the lowest propellant density giving adequate absorption, and the smallest base area compatible with range and flux concentrator design limitation.

A detailed description of possible laser facilities would be premature at this stage of laser propulsion studies. However it will be useful to show that any of a number of requirements can be met using a design based on modular laser amplifiers. Indeed it would be practical to construct a 10^9 watt average power laser using some existing repetitively pulsed lasers as the basic building block.

The beam from a master oscillator laser can be split so as to drive a number of amplifier lasers coherently. Each amplifier output can in turn drive another group of amplifiers and so on until the total power output of the amplifiers is the requisite value. Precautions must be taken against the spontaneous emission from an amplifier feeding back to the previous stages. Geometric flux falloff with element separation and saturable

absorbers have been applied to this end. If the ray paths from oscillator to the various output amplifiers are maintained within a coherence length of each other the phases at the outputs will have a fixed relationship to each other.

The amplifier output apertures, which in general will be separated from each other for mechanical reasons, may be arranged in a number of ways such that their beams fall on an array of contiguous flat mirror facets. The facets in turn are oriented so that the reflected beams are parallel and contiguous. (A familiar reverse analogy of this was found in an old time ballroom decoration. A spot light beam was reflected from a chandelier in the form of a ball covered with small mirrors.) The reflected beam proceeds from the "Chandel" beam combines to a beam director whose variable orientation allows gross tracking of the rocket vehicle.

One possible layout for such a large scale laser launch facility is illustrated in Figure 32. The lasers are stacked in bays and their beams are directed horizontally through the open side of the building to the corresponding elements of the Chandel.

Only in the near field, where geometric optics dominates, do the phase relations between the individual segments remain unimportant. For rocket burnout ranges on the order of 10^3 km and spot sizes on the order of 1 meter, i.e. ~1μm radian beam divergence, diffraction limited performance is called for. This not only minimizes the physical size of the output aperture, ~ 25m at 10.6 μm, but it also maximizes the near field peak flux. The latter is an advantage from the standpoint of reducing atmospheric CO_2, absorption at 10.6 μm.

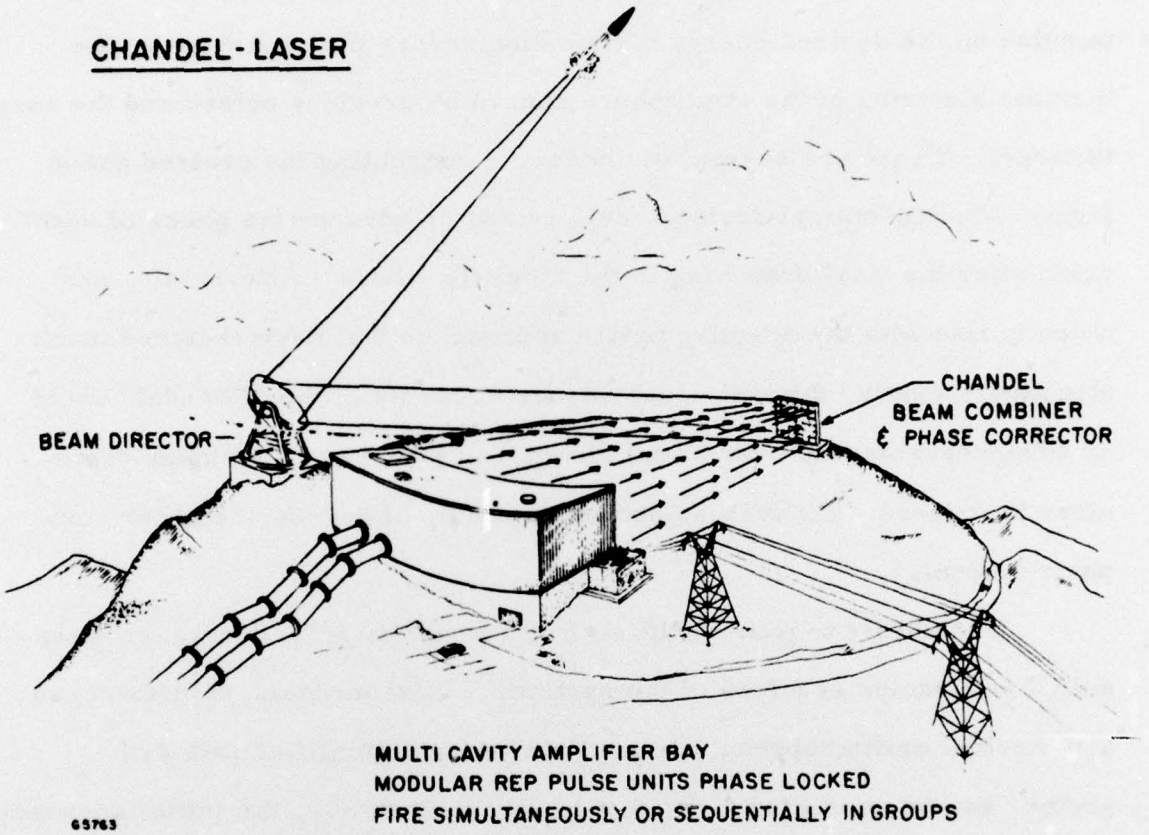

Figure 32 Conceptual Layout of Laser Propulsion Launch Site. Rocket would be introduced into the beam at a few hundred meters altitude by means of a pneumatic tube (not shown)

Decent diffraction limited capability demands control of the phase across the output aperture with respect to an ideal profile to within some fraction of 2π. The ideal profile in a given situation will depend from pulse to pulse on the desired energy distribution across the rocket base, the thermal blooming of the atmosphere caused by previous pulses and the range to target. There are several methods of constructing the desired phase front. Electro-optical devices could retard or advance the phase of each beam after the final branching in the amplifier chain. Alternately, and more in line with the adaptive optics approaches that have received much attention recently, the individual mirror elements of the "Chandel" could be advanced-retarded over small distances as well as tilted using piezo-electric drivers. All such adjustments would, of course, be under computer control.

The ability to phase shift each beam significantly decreases mechanical accuracies required of the system. Initial mechanical differences and thermal drifts between one oscillator-output amplifier path and another can be corrected from shot to shot. Similarly, the initial accuracy of the large beam director mirror can be relaxed. Indeed it can be made of segments. Thermal and gravitational (due to changing orientation) distortions can be corrected. This control also allows the beam director to be a gross pointing device with the accurate directional pointing trimmed from shot to shot by element phase adjustment.

It has been suggested that the beam director be dispensed with by mounting each element of the Chandel on its own large excursion beam director. The difficulty is that beam super positive then results in certain orientations; to avoid this the elements must be separated, which increases diffraction losses.

With respect to this latter point, it is well known that resolution increases if elements of an aperture are separated. Radio astronomy frequently takes advantage of this with long baselines between dish receiving antennae. This is fine for receivers, but an array of separated sending elements can never give a greater intensity at the far field than a single circular element of area equal to the sum of the element areas. At equal power the array can at most put the same peak intensity as the circular aperture on a central order disk; but the diameter is smaller, and the rest of the power is wasted in side orders.

Two strong advantages of the Chandel laser concept are its redundancy and flexibility. Given hundreds or more laser units, failure of a few during a launch would not seriously degrade system performance. Or, spares could be brought on line with proper phase correction to account for their different location.

The facility allows a range of repetition rates and pulse times at constant power that is well beyond the range of the individual elements. For instance, by dividing the back into nine groups with each group having a compact contiguous grouping of reflectors at the Chandel, the repetition rate can be increased by a factor of nine if separate oscillators are provided. The range at which a given spot size can be achieved will, of course, decrease a factor of three in the example. As discussed in the section on launch phase, the higher repetition rate may be an advantage early in the launch when loss of resolution is no problem.

2. LAUNCH

The initial insertion of the rocket engine and load into a position suitable for laser propulsion may be accomplished in a number of ways.

The initial trajectory problem is that the rocket plume will degrade the surface of the mirror, leading to surface breakdown and catastrophic beam loss. The rocket engine must therefore be introduced into the laser beam at a sufficiently large distance from the mirror system. It has been suggested that a large gantry should be used with the rocket at the top and the laser mirror-director underneath. Such an arrangement would need to be taller than the average near-sea-level plume length in order to avoid beam interference. For the typical rocket engine discussed in Section III, the plume at sea level would be ~100 meters long (see Section VI). The rocket vehicle should therefore be introduced into the beam at least this distance from the mirror, which requires an extremely large gantry, and high repetitive rates will introduce considerable complexities.

A second method is to use a recoverable chemical booster to initialize launch. The rocket would be launched some distance away from the laser site, and maneuvered into the beam. The chemical booster would then drop off and be parachuted to safety, and laser propulsion would take over. Problems with this approach include design of a truly recoverable booster, and the added complexity of the launching control system.

A third method consists of using a pneumatic launch system, similar to that designed for missile launch. The rocket would be contained in a pneumatic gun, which would project it to an altitude of, say, 1/2 km. At this point the laser would acquire the engine and laser propulsion would take over. In principle this system could be very simple, providing a rapid rocket handling capacity more easily envisaged than in the other cases.

The equation of motion of an unpowered rocket of cross-sectional area A and mass m travelling vertically upward through air of density ρ is

$$m\ddot{x} = -\rho C_D \dot{x}^2 A - mg. \tag{272}$$

Ignoring changes of ρ with x and writing $a = \frac{\rho C_D A}{m}$, the position of the rocket will be

$$x = \frac{1}{a} \ell n \left\{ \frac{\cos C - \sqrt{agt}}{\cos C} \right\}, \tag{273}$$

where

$$\tan C = V_o \sqrt{\frac{a}{g}}; \tag{274}$$

and we obtain the maximum height attained as:

$$x_{max} = \frac{1}{2a} \ell n \left(1 + \frac{aV_o^2}{g} \right). \tag{275}$$

where V_o is initial velocity.

Thus the initial velocity required to reach altitude x_{max} will be

$$V_o = \sqrt{\frac{gm}{\rho C_D A}} \left[e^{2\rho C_D A x_{max}/m} - 1 \right]^{1/2} \tag{276}$$

Taking typical values, $A = 4 \times 10^4 cm^2$, $\rho = 1.3 \times 10^{-3}$, $C_D \sim 1$, $m \sim 5 \times 10^6 g$, for $x_{max} = 1/2$ km we obtain $V_o \sim 1.3 \times 10^4$ cm/sec, which indicates that the effect of air resistance is to increase the vacuum value of V_o by 30%.

In order to attain this initial velocity, and accepting accelerations of Gg on the vehicle, the length of the pneumatic gun is $\frac{860}{G}$ m. For a vehicle 10 m long, an acceleration of G = 20 gives a gun 43 meters long. The gas pressure required will be $-mg + \mathbb{P}A = m Gg$, or $\mathbb{P} = \frac{mg}{A}(G + 1)$. The case above required $\mathbb{P}$ = 2.6 atm. on the rocket engine base. This appears to be a relatively simple requirement

REFERENCES

1. Raizer, Y. P., "Heating of a Gas by a Powerful Light Pulse," Sov. Phys. JETP 21, 1009 (1965).

2. Edwards, A., Ferriter, N., Fleck, Jr. J. A., and Winslow, A. M., "A Theoretical Description of the Interaction of a Pulsed Lase, and a Target in an Air Environment," Lawrence Livermore Laboratory, Rept. UCRL - 51489 (1973).

3. Boni, A. A. and Su, F. Y., "Theoretical Study of Laser Target Interactions," Science Applications Inc. Rept. SA177-567LJ (1977).